Targeted Delivery of Chemotherapeutic Drugs Using Human Serum Albumin for the Treatment of Cancer

THESIS

Submitted in partial fulfillment

of the requirements for the degree of

DOCTOR OF PHILOSOPHY

by

NAGESWARA RAO VYSYARAJU

ID. No. 2015PHXF0516H

Under the Supervision of

Prof. Swati Biswas

BIRLA INSTITUTE OF TECHNOLOGY AND SCIENCE, PILANI

2024

BIRLA INSTITUTE OF TECHNOLOGY AND SCIENCE, PILANI

CERTIFICATE

This is to certify that the thesis titled **"Targeted Delivery of Chemotherapeutic Drugs using Human Serum Albumin for the Treatment of Cancer"** submitted by **Nageswara Rao Vysyaraju**, ID No. **2015PHXF0516H**, for an award of a Ph.D. from the Institute, embodies original work done by him under my supervision.

Signature of the Supervisor:

Name in capital letters: SWATI BISWAS

Designation : Professor

Date : 14th March 2024

DECLARATION

I declare that this thesis has been composed solely by myself and that it has not been submitted, in whole or in part, in any previous application for a degree. The content of the thesis is original and is the outcome of my research work. Any relevant material taken from the open literature has been referred to and cited, as per established ethical norms and practices.

Nageswara Rao Vysyaraju

ACKNOWLEDGEMENT

The satisfaction, which accompanies the successful completion of any task, is incomplete without the mention of the names of those people who made it possible in time with their blessings, guidance, support, instrumental help, and/or revitalizing tasks.

First and foremost, I would like to thank the almighty Supreme Soul for providing me with the patience and strength to undertake this research.

I would like to express my gratitude to my esteemed guide, Prof. Swati Biswas, for taking me under her tutelage and allowing me to pursue a Ph.D. degree under her guidance. Respected Ma'am, it was a pleasure knowing you and learning from you many things, both said and unsaid, which I will cherish throughout my lifetime. Thank you for your guidance, encouragement, and support throughout the course of my study. Your endless optimism, enthusiasm, and infectious energy toward breakthrough research will always be a source of inspiration for me.

I would like to say specials thanks to my industry colleagues and supporters like Dr. Harshal P Bhagwatar, Dr. Mayur Sankalia, Mr. Bhushan S Yeola, Dr. Sridhar Desikan, and Dr. Reddy's Laboratories Ltd team for supporting me in the completion of doing my Ph.D.

I am wholeheartedly thankful to Prof. Balaram Ghosh, Department of Pharmacy, BITS-Pilani, Hyderabad campus, who acted as a Doctoral Advisory Committee (DAC) member from the department of Pharmacy.

I am wholeheartedly thankful to Prof. V. V. Vamsi Krishna, Department of Pharmacy, BITS-Pilani, Hyderabad campus who acted as a Doctoral Advisory Committee (DAC) member from the Department of Pharmacy.

I express my profound gratitude to Prof. Sajeli Begum, Professor, and Head of the Department of Pharmacy, for her support and for extending the facilities to work at the institute.

I have to express my sincere thanks to the Chancellor, BITS-Pilani, for providing the necessary infrastructural support to carry out my research work. I am sincerely thankful to Prof. G. Sundar, Director; Prof. V. Ramgopal Rao, Vice-Chancellor; Prof. Venkata Vamsi Krishna Venuganti, Dean, Academic- Graduate Studies and Research; and Prof. P Yogeeswari, General Administration for facilitating my research work at the institute.

I would like to thank the central analytical laboratory of BITS-Pilani, Hyderabad Campus, for providing me with a scientific platform to excel in my career.

I am fortunate to have met nice colleagues and lab mates in BITS, where I got an opportunity to work with them on various occasions. I am grateful to Mr. Sanjay, Mr. Milan, Mr. Asif, Mrs. Sri Ganga, Dr. Soniya, Mr. Ganesh, Mr. Praful, Mrs. Sravani, Mr. Tarun, and Ms. Himaja. Thanks, all of you, for your remembrance and for being a source of happiness.

I express my sincere thanks to seniors Dr. Omkara Swami, Dr. Preeti Kumari, Dr. Vishnu Kiran, Dr. Himanshu Bhatt, and Dr. Yamini Bobde, who were very supportive; their attention and timely concern for my Ph.D. gave me a lot of enthusiasm.

I am thankful to Mrs. Sarita, Mrs. Rekha, Mrs. Sunita, Mr. Rajesh, Mr. Upalaiah, Mr. Mallesh, Mr. Kumar, Mr. Narsimha, and Mr. Tirumalaiah for their kind co-operation during the lab in the entire tenure of my Ph.D.

I would like to thank everybody important for the successful completion of this research work that I may have inadvertently failed to mention.

I owe my loving thanks to my father, Mr. Ganapati Raju Vysyaraju, my mother, Mrs. Hymavathi, and my other family members; without their encouragement and understanding, it would have been impossible for me to finish this work.

My special gratitude to a very special person, my wife, Gnana Deepika Narayanasetty, for her continued and unfailing love, support, and understanding during my pursuit of a Ph. D degree that made the completion of my thesis possible.

Nageswara Rao Vysyaraju

ABSTRACT

Cancer is highly prevalent and can be attributed to a multitude of causes, often stemming from genetic and epigenetic abnormalities. Nanomedicines exhibit exceptional attributes, making them an optimal choice for targeted drug delivery to specific sites in the body. Human Serum Albumin nanoparticles represent an exemplary nanocarrier system characterized by remarkable ligand binding capacity. Human Serum Albumin (HSA) employs endothelial transcytosis to facilitate drug transfer, allowing it to reach tumor tissues through the Enhanced Permeability and Retention (EPR) effect. HSA nanoparticles specifically bind to the 60-kDa glycoprotein (gp60) receptor, also known as albondin. This interaction leads to the subsequent binding of gp60 to caveolin-1, an intracellular protein, resulting in the formation of caveolae. These transcytosis vesicles actively target intracellular localization within the tumor, enabling precise drug delivery.

The commercially available human serum albumin formulation of paclitaxel is Abraxane® using the nab-technology, where the drug reaches the tumor site and accumulates through the EPR effect through the leaky vasculature of the cancer cells. Many cancer drugs are under development and at different stages of the clinical studies with Human Serum Albumin as a drug delivery system, e.g., nab-docetaxel and nab-rapamycin. In my current research, human serum albumin has been used as a drug carrier system that has been explored for the delivery of anticancer drugs, Olaparib, and oxaliplatin for treating triple-negative breast cancer (TNBC). TNBC is a type of breast cancer that lacks the expression of HER-2, ER, and PR. Olaparib was approved by the FDA for the treatment of triple-negative breast cancer under the brand name Lynparza® from the company AstraZeneca which has side effects due to its non-specificity of the drug delivery.

In our study, Olaparib was physically entrapped within human serum albumin nanoparticles. The nanoparticles are formed using a cross-linking agent Glutaraldehyde (Ola@HSA nanoparticles). The preparation process was optimized using the design of experiments using

the central composite design. The variables selected for the optimization process were polymer ratio and Glutaraldehyde concentration, and the responses evaluated were particle size, %DL and %Entrapment efficiency.

Nanoparticles were characterized for the physicochemical parameters like particle size, surface charge, %drug loading, %entrapment efficiency, morphology, kinetic stability of the prepared nanoparticle formulation, x-ray diffraction analysis, differential scanning calorimetry analysis, FTIR analysis, x-ray photon correlation spectroscopic analysis, protein conformation using SDS-PAGE, circular dichroism spectroscopy study, *in vitro* drug release, and haemolysis assay. Further, Olaparib@HSA NPs were evaluated for their *in vitro* evaluation studies like cell viability by MTT assay, cellular uptake studies, Annexin-V assay, nuclear staining assay, DNA fragmentation, mitochondrial membrane potential, ROS detection assay, spheroid study, growth inhibition/live-dead cells assay in spheroids in triple-negative breast cancer cell-lines like MDA MB-231 and 4T1 cell lines. The optimized formulation shows the physicochemical parameters like particle sizes of 143.5±0.43 nm and zeta potential of −11.27 ± 3.25 mV for OLA@HSA NPs, entrapment efficiency (% EE) is 76.01 ± 2.53% and % DL is 6.76 ± 0.22. kinetic stability was good for the prepared nanoparticles at refrigerated conditions of 4°C compared to the controlled room temperature of 15-25°C studied for a period of 30 days, from the *in vitro* drug release data, it was observed that the highest amount of the drug release was observed at pH 5.5, compared to the other pH 6.5 and pH 7.4. X-ray diffraction analysis conforms that the prepared nanoparticles were amorphous. The gel-chromatography study by SDS-PAGE analysis indicates that OLA@HSA NPs band width matches with the human serum albumin band width of 66KDa. percent haemolysis was proportional to the drug concentration, and the highest 5.1% was observed with the nanoparticles prepared on 250µg/mL of the concentration.

The *in vitro* cell viability study indicated OLA@HSA nanoparticle shows a cell viability of 21.21 ± 3.85% compared to the viability of the free Olaparib of 30.25 ± 3.42% in 48hours in 4T1 cells at the drug concentration (100µg/mL). The IC50 values of OLA@HSA NPs towards 4T1 were calculated as 6.54 µM in 48 hours of treatment compared to 11.47 µM for free Olaparib treatment. The cell viability studies indicate that NPs reached the target site internalized in cancer cells with time. The level of the drug increases in the cancer cell line with time observed a higher level of expression marker phosphatidylserine was in OLA@HSA NPs-treated compared to free Olaparib and then to the control sample, which is untreated. From the *in vivo* studies data, it was observed that there was significant suppression of the tumor volume with OLA@HSA NPs compared to free Olaparib and control samples without drug treatment. The isolated tumors after the OLA@HSA NPs-treatment showed an increased expression of a proliferative marker, Ki-67, p53, and ROS, and PARP-1 expression reduction indicating a strong apoptotic response.

The second drug which was studied for the treatment of triple-negative breast cancer was Oxaliplatin and its combination with Olaparib. Combination drug delivery systems have an efficient synergistic approach for cancer treatment compared to individual drug treatment.

Here in the current research of the second objective, Oxaliplatin was conjugated with Human Serum Albumin to form HSA(OXA) NPs, which was further used to prepare nanoparticles to load Olaparib. To prepare the OLA@HSA(OXA) NPs used BAC as a cross-linking agent. The prepared combination nanoparticle formulation system was characterized for its physicochemical evaluation compared against the OLA@ HSA(OXA) NPs in-terms of all the physical parameters like morphology, surface charge by measuring zeta potential, % entrapment efficiency, % drug loading, particle size, kinetic stability, protein conformation studies using SDS-PAGE, CD spectroscopy, In vitro drug release studies and haemolysis assay. Further, all three formulations of Olaparib@HSA NPs, HSA(OXA) NPs, and

OLA@HSA(OXA) NPs, were evaluated for their efficacy with each other by performing the in-vitro cell viability studies and i*n vivo* performance in mouse model.

The drug-loaded nanoparticles were used for the measurement of the particle size, which is 115 ± 2.3 nm, 125 ± 2.3 nm, and 138.32± 6.3 nm, respectively, for OLA@HSA NPs, HSA(OXA) NPs, and OLA@HSA(OXA) NPs with a very narrow polydispersity index (PDI) (0.178, 0.124, 0.181). The Zeta potential of the formulation of OLA@HSA NPs, HSA(OXA) NPs, and OLA@HSA(OXA) NPs showed a negative ζ-potential and the respective values of the zeta potential is −12.1 ± 3.2 mV, - 10.1 ± 3.2 mV, -17.2± 3.2 mV respectively. The DL% of OLA@HSA NPs, HSA(OXA) NPs, and OLA@HSA(OXA) NPs was 10.5%, 11.2 % and 12.3% and the EE% of OLA@HSA NPs, HSA(OXA) NPs, and OLA@HSA(OXA) NPs was 80.3%, 78% and 84% respectively. The scanning electron microscopy images of the OLA@HSA NPs, HSA(OXA) NPs, and OLA@HSA(OXA) NPs indicated uniform spherical particles with particle size 120.32±2.5 nm, 125.32±2.5 nm, and 140.47±3.4 nm. All these physical parameters of the formulation, like particle size, zeta potentials, %DL, %EE and particle size by SEM analysis, are comparable with each other between the formulations. The protein conformation studies using SDS-PAGE observed to be a uniformly thick band around 66,500 Da for HSA, OLA@HSA NPs, HSA(OXA) NPs, and OLA@HSA(OXA) NPs indicating that all three drug was entrapped into the protein human serum albumin NPs.

From the *in vitro* studies, it was demonstrated that a combination formulation of OLA@HSA(OXA) nanoparticles showed the highest cytotoxicity in cancer cell-line studies, which was done using the 4T1 and MDAMB-231 cell lines and shows the synergistic effect with the combination drug delivery of Olaparib with Oxaliplatin delivery using the Human serum albumin as a drug carrier. OLA@HSA(OXA) NPs showed an IC50 of 7.38 µg/mL compared to free OXA, which had an IC50 of 10.73 µg/mL in the MDA MB 231 cell line for a treatment period of 24 hours. Combination indices (CI) provide insight into the synergistic,

additive, or antagonistic response of the combination therapy. A CI value less than 1 indicates synergism, 1 represents an additive effect, while a value above 1 is projected as an antagonistic therapeutic response. It was observed that only optimal OLA@HSA(OXA) NPs formulation with a loaded drug ratio of 50:50 (OLA: OXA) showed synergism with all Fa (fraction affected) values below 1 in MDA-MB-231 cells for both 24 h and 48 h.

Higher cell cycle arrest (G2/M phase) and apoptosis, significant cell death, and highest reduction of tumor volume were seen in combination drug delivery formulation that is with OLA@HSA(OXA) NPs compared to the free drug, blank sample, and the individual formulations of OLA@HSA and OXA(HSA) NPs.

TABLE OF CONTENTS

LIST OF TABLES

LIST OF FIGURES

LIST OF ABBREVIATIONS AND SYMBOLS

ACN	Acetonitrile
CCD	Central composite design
CD	Circular dichroism
$CDCl_3$	Deuterated chloroform
DAPI	4′,6-Diamidino-2-phenylindole dihydrochloride
DCFH-DA	2,7-dichlorodihydrofluorescein diacetate
DL	Drug loading
DLS	Dynamic light scattering
DMSO	Dimethyl sulphoxide
DOE	Design of experiment
DSC	Differential scanning calorimetry
DTP	Drug: polymer
EE	Encapsulation efficiency
EDC	N-(3Dimethylaminopropyl)-N′-ethyl carbodiimide hydrochloride
EPR	Enhanced Permeability and Retention
FITC	Fluorescein isothiocyanate
FTIR	Fourier transform infrared spectroscopy
GPC	Gel permeation chromatography
H & E	Hematoxylin and eosin

HPLC	High-performance liquid chromatography
HSA	Human serum albumin
^{1}H NMR	Proton Nuclear Magnetic Resonance
IC_{50}	Half maximal inhibitory concentration
IVIS	*In vivo* imaging system
JC 1	5,5′,6,6′-Tetrachloro-1,1′,3,3′ tetraethylbenzimidazolocarbocyanine iodide
MCF-7	Human breast cancer cell line
MEM	Minimum essential medium eagles
MOC2	Mouse oral squamous cell carcinoma
mPEG	Methoxy polyethylene glycol
MTT	3-(4,5-dimethylthiazol-2-yl)-2,5-di-phenyltetrazolium bromide
MWCO	Molecular weight cut-off
mg	Milligram
min	Minute
mL	Millilitre
mm	Millimetre
mmol	Millimole
NHS	N-hydroxysuccinimide
NPs	Nano-particles

nm	Nanometer
OLA	Olaparib
OXA	Oxaliplatin
PBS	Phosphate buffered saline
PDI	Polydispersity Index
PI	Propidium iodide
PLA	Polylactic acid
ROS	Reactive oxygen species
RT	Room temperature
SD	Standard deviation
SEM	Scanning electron microscope
SOSG	Singlet oxygen sensor green
TEA	Triethylamine
THF	Tetrahydrofuran
TUNEL	Terminal deoxynucleotidyl transferase-mediated nick-End labeling
XRD	X-Ray Diffraction
4T1	Murine mammary carcinoma
µg	Microgram
µL	Microlitre
µM	Micromolar

Chapter 1

Introduction

1. Cancer

Breast cancer (BC) is an extremely prevalent form of cancer that affects a lot of women all over the globe, with an estimated yearly effect of ~2-2.5 million people. Around 627,000 women died, according to figures, as a result of the BC in only 2018 alone. Invasive BC will affect around 12.5% of American women eventually in their life (1). The prevalence of BC among women has continuously been the highest of all malignancies in both developed nations like the United States and developing nations like China (2) (**Fig1.1**). In India, BC is the most prevalent kind of cancer among women. The WHO figured that over 170,000 Indian women are afflicted by BC, an increase of 14% above the country's overall cancer incidence rate (1). Over 2.05 million new instances of BC were reported by GLOBOCAN in 2018, placing it second among all cancer types (3)**.** Based on distinct features, BC is divided into many molecular subtypes, such as progesterone receptor (PR)/estrogen (ER) positive, luminal (A and B), and human epidermal growth factor receptor 2 (HER2) type (4). The subtypes of BC that are positive for the progesterone receptors (PR) and estrogen (ER), two of the recognized subtypes, account for around 70 % of all reported instances. Triple-negative BC (TNBC) is a subtype of BC that only occurs in around 20 % of cases and lacks the expression of HER-2, ER, and PR (5). TNBC has an aggressive phenotype and a greater risk of metastasis, comparable to basal-like BC (which occurs in roughly 75% of TNBC cases). Multiple tumor suppressor genes may have undergone genetic changes and genomic instability, which would explain the higher risk of metastasis (6). Around the world, the proportion of TNBC cases ranged from 7 to 28%, with India having the highest occurrence (7).

TNBC nevertheless exhibits a variety of clinical, morphological, and biochemical characteristics while sharing certain common pathological and clinical markers (8). when administered to individuals with advanced cancer (metastatic stage), chemotherapy typically lacks specificity and effectiveness, possibly leading to patient death (9). About 80–90% of

fatalities from BC are caused by metastasis. Even though substantial developments in surgical procedures, hormone therapy, radiation treatment, and chemotherapy have decreased mortality and boosted survival rates, between 20–30% of patients initially diagnosed at an early stage continue to develop metastatic illness (10,11). Environmental deterioration and lifestyle choices that lead to the disturbance of estrogen homeostasis are linked to the rising prevalence of BC. BC risk is increased for women between the ages of 40 and 55, especially when there is a family history of the illness (12,13). Numerous studies have shown that post-menopausal women's chance of developing cancer is increased by an increase in body mass index (14). In addition, consuming too much fat might change the amounts of circulating estrogens, which can cause hormonally dependent BC (15). A woman's chance of tumor development is further heightened. If she possesses a familial background of breast cancer or has been exposed to ionizing radiation. Early ionizing radiation exposure, especially, may raise the risk of BC development (16). BC may develop due to many factors, including environmental, behavioral, hormonal, genetic, and nutritional ones. Oral contraceptive usage and post-menopausal hormone treatment have also been connected to a rise in the condition (17). BC stem cells (BCSCs) and tumor microenvironments are examples of tumor heterogeneity, which plays a crucial role in chemotherapy failure and drug resistance in BC/TNBC. It is consequently difficult to manage TNBC and BC. The growth of nanotechnology, however, offers an alternative perspective on therapeutic strategies. Nanotechnology is distinct because of its ability to modify surfaces, entrap more drugs, and have nano-metric size and longer circulation half-lives. It also provides both active and passive targeting options. These attributes represent a paradigm change in the way BC and TNBC are treated.

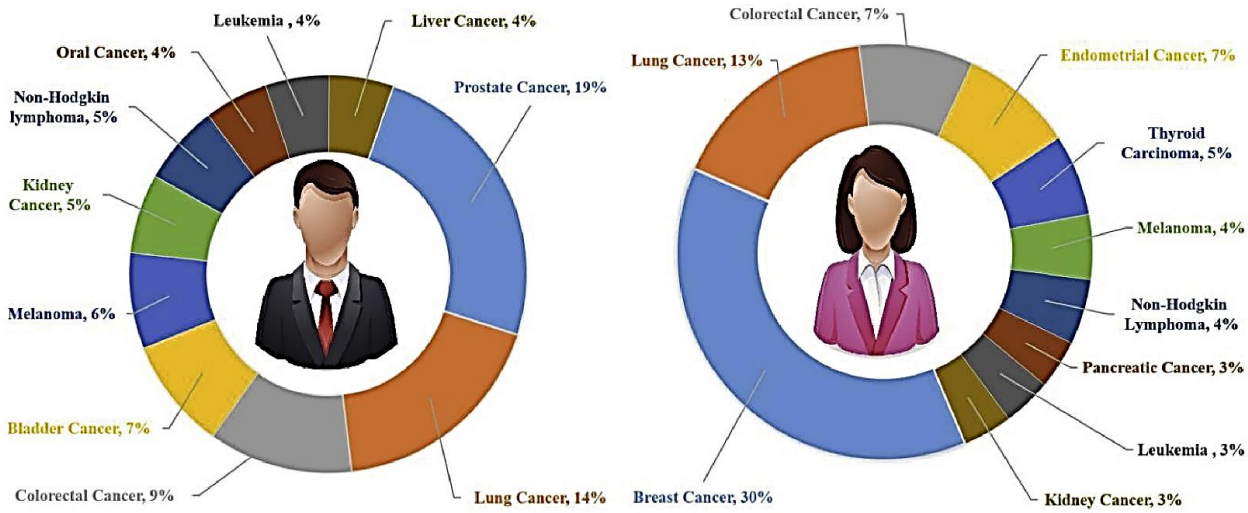

Figure 1.1. Cancer incidence in the US in 2018. Adapted with permission from ref. (2).

1.1.Pathogenesis

Breast tumors typically initiate from the hyperproliferation of the ductal tissue, which subsequently progresses into either metastatic carcinomas or benign tumors upon continued exposure to diverse carcinogenic stimuli. The microenvironments surrounding tumors, such as stromal factors and macrophages, have significant impacts on the development and advancement of BC. In rats, exposure to carcinogens solely in the stromal tissue and not in the extracellular matrix or the epithelium could induce neoplastic growth in the mammary gland (18,19). Macrophages are capable of producing an inflammatory microenvironment with mutagenic properties that facilitate angiogenesis and aid cancer cells in evading immune surveillance (20,21). The observation of distinct DNA methylation patterns between tumor-associated and normal microenvironments suggests that epigenetic alterations occurring within the cancer microenvironment may have a role in the growth of cancer (22,23). Cancer stem cells (CSCs) have recently been recognized as a distinct subset of cells within cancer, and CSCs have been implicated in tumor initiation, evasion, and relapse. The aforementioned cells possess the potential to differentiate into either progenitor cells or stem cells originating from regular tissue. Additionally, they exhibit the capacity for self-renewal and demonstrate resistance towards conventional therapeutic interventions such as radiation and chemotherapy

(24,25). The identification of BC stem cells (bCSCs) was first reported by (26), which can initiate new tumors in immunocompromised mice even with a small number of just 100 bCSCs. It is anticipated that the origin of these cells is luminal epithelial progenitors rather than basal stem cells (27). Several signaling pathways, such as p53, Notch, Wnt, Hedgehog, HIF, and PI3K, are involved in the invasion, proliferation, and self-renewal of bCSCs (28). However, additional investigation is necessary to gain a comprehensive understanding of bCSCs and to develop innovative strategies for their direct elimination.

There exist two theoretical frameworks for the onset and advancement of BC: the cancer stem cell theory and the stochastic theory (22,29). According to the cancer stem cell theory, the origin of all tumor subtypes can be traced back to a small subset of cells known as progenitor cells or cancer stem cells. The development of different tumor phenotypes is attributed to acquired epigenetic and genetic mutations in these cells. The proposition put forth by this theory posits that the targeting of cancer stem cells may prove to be a viable and efficacious approach in the treatment of diverse forms of neoplastic growths. The stochastic hypothesis, on the other hand, contends that each tumor subtype develops from a singular type of cell, which may be a progenitor cell, stem cell, or differentiated cell. Any breast cell may progressively acquire sporadic mutations; once a sufficient number of mutations have amassed, the breast cell can convert into a tumor cell. Despite the factual support for both hypotheses, none of the existing theories provide a comprehensive explanation for the genesis of human BC.

1.2.Risk Factors of Breast Cancer

The multiple risk factors that are implicated in the BC are depicted in a schematic diagram given below.

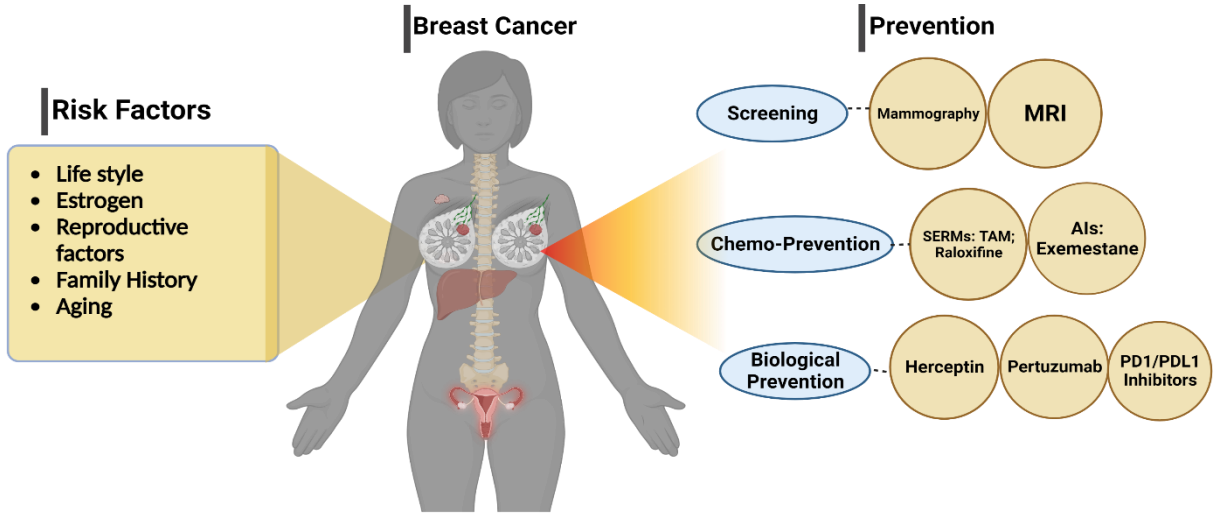

Figure 1.2. A diagrammatic representation illustrating the risk factors and preventative measures for BC.

1.3.1. Aging

Apart from gender, aging represents a significant contributing factor in the susceptibility to BC, as the occurrence of this disease is strongly associated with advancing age. In the year 2016, almost all BC-related deaths in the United States, amounting to 99.3%, were observed in females who were above the age of 40, with 71.2% occurring in women aged 60 or above (30). Hence, it is imperative to schedule mammography screenings in advance for women aged 40 or older.

1.3.2. Family history

According to (31), family factors account for around 25% of BC cases. Women with a familial predisposition to BC, particularly those who have a mother or sister who has the illness, are more likely to have it. The findings of a cohort study conducted in the United Kingdom, which involved a sample size of more than 113,000 women, revealed that those who had a first-degree

relative diagnosed with BC had a 1.75-fold higher likelihood of developing the same disease relative to those who did not have any affected relatives. Women with two or more first-degree relatives who have been diagnosed with BC are subject to an elevated risk of the ailment by a factor of 2.5 or greater (31). Mutations in BC-related genes, such as BRCA1 and BRCA2, help to explain the hereditary predisposition to the disease.

1.3.3. Reproductive factors

Reproductive variables, including early onset of menstruation, delayed onset of menopause, delayed age of first pregnancy, and low parity, are known to enhance the risk of BC. The incidence of breast cancer exhibits a 3% elevation in risk for each year of delayed onset of menopause, while the risk decreases by 5% or 10% for each year of delayed onset of menstruation or each additional birth, respectively. A hazard ratio of 1.54 was observed in a recent cohort study conducted in Norway. The findings suggest a higher susceptibility for individuals who gave birth to their first child at an advanced age (≥35 years) in comparison to those who gave birth at a younger age (<20 years). The reproductive factors, parity, and age at first birth exhibit a robust correlation with the estrogen receptor (ER) status, with varied odds ratios (OR) observed for ER+ and ER- BC. Parity displayed OR of 0.7 and 0.9 for ≥3 births and nulliparae, respectively. The study found that age at first birth had OR of 1.6 and 1.2 for individuals aged 30 years or older and under 25 years, respectively, for both ER- and ER+ BC (32).

1.3.4. Estrogen

BC risk is associated with both endogenous and exogenous estrogens. Premenopausal women's ovaries generate the majority of endogenous estrogen, which may be lowered with ovariectomy to lessen the risk of BC (33). Exogenous estrogen sources include hormone replacement therapy (HRT) and oral contraceptives. Despite improvements in oral contraceptive formulations to reduce harmful effects, nonetheless, women of Iranian and African American

descent continue to face a higher risk of developing BC (34). A decrease in risk was observed among women who discontinued the use of oral contraceptives for a period exceeding ten years. Studies have indicated that HRT, which involves administering exogenous estrogen or other hormones to women who are postmenopausal or menopausal, may increase the risk of developing BC. HRT users had a 1.66 relative risk of BC compared to non-users, according to the Million Women Study carried out in the UK (35). A study was conducted on a cohort of 22,929 Asian women to examine the potential influence of HRT on the risk of developing BC. According to the study, the hazard ratios for breast cancer were 1.48 and 1.95 after 4 and 8 years of HRT use, respectively (36). However, the risk of BC significantly decreased after stopping HRT for two years. The hazard ratio for developing a new breast tumor among BC survivors who use HRT is 3.6, indicating a high risk of recurrence (37). The incidence rate of BC in the United States has decreased by approximately 7% following the disclosure of the adverse effects of HRT in the Women's Health Initiative randomized controlled trial in 2003, which resulted in a decline in HRT usage (38).

1.3.5. Lifestyle

Contemporary lifestyles, marked by overindulgence in alcohol consumption and high consumption of dietary fat, may have the propensity to elevate the risk of developing BC. Alcohol consumption has been found to elevate estrogen-related hormones in the bloodstream, thereby inducing the activation of estrogen receptor pathways. Based on a meta-analysis of 53 epidemiological studies, it has been determined that the ingestion of 35-44 g of alcohol per day can increase the vulnerability to BC by 32%. Additionally, the risk ratio of breast cancer escalates by 7.1% with each additional intake of 10 g of alcohol per day (39,40). The current Western diet is characterized by a high abundance of fats, particularly saturated fats. Consuming excessive amounts of fat has been linked to increased mortality (RR=1.3) and un-favorable outcomes in patients with BC (41). The potential correlation between smoking and

the risk of developing breast cancer remains a topic of discussion. However, it has been observed that mutagens found in cigarette smoke have been identified in the breast fluid of non-lactating women. Furthermore, the probability of developing BC is greater in women who both smoke and consume alcohol (RR=1.54) (42). Contemporary evidence suggests that smoking, particularly during adolescence and early adulthood, entails a higher risk of BC incidence (43,44).

Significant progress has been achieved in clinical and theoretical investigations related to BC, as evidenced by **Fig 1.2**. Current prevention strategies, such as screening, chemoprevention, and biological prevention, have demonstrated higher precision and efficacy compared to historical approaches. Despite the reduction in BC mortality rates, it remains the primary cause of cancer-related deaths among women aged 20-59 years.

1.3.6. Genes related to BC

Many genes that are connected to BC have been discovered. As demonstrated in **Table 1**, oncogenes and anti-oncogenes both exhibit mutations and abnormal amplification, which are essential for the processes of tumor initiation and development.

Table 1.1 Genes linked to the development of breast cancer.

Function	**Location**	**Gene**	**Breast cancer abnormality**	**Ref.**
oncogene	11q13	CCND1 (Cyclin D1)	50% of breast tumors exhibit overexpression.	(45)
	3q26.3	PIK3CA	Mutations are present in 37% of HR+/HER2- metastatic BC and 40% of early BC cases.	(46)
	17q12	HER2	Around 20% of primary BCs show detection of HER2 overexpression.	(28)

Anti-oncogenes	17q21 and 13q12	BRCA1/2	BRCA1/2 mutations cause around 20-25% of inherited BCs and 5-10% of all BCs.	(28)
Tumor suppressor gene	18q21.33	Maspin	Maspin expression is present in 20-80% of invasive BCs.	(47)
	3p14.2	FHIT	FHIT hyper-methylation rate is 8.4 times higher in BC than in normal breast tissues.	(48)
	16q22.1	CDH1 (E-cadherin	85% of lobular breast carcinomas exhibit CDH1 inactivation.	(49)
	11q22-q23	ATM	ATM mutation generally increases the risk by 2-3 times, and in women under 50 years, the risk is raised by 5-9 times.	(50)
	10q23.3	PTEN	Up to 33% of BCs experience loss of PTEN protein expression.	(51)
	13q14.2	RB1	20-35% of BCs exhibit Rb1 inactivation.	(52)
	17q21.3	NME1	SNP of the NME1 gene is linked to a greater risk of BC-specific mortality (HR=1.4) and early-stage cancer patients (HR=1.7).	(53)
	17p13.1	P53	30% of BCs have mutations.	(54)

1.4. Nanomedicine-based approaches for breast cancer

Nanotechnology offers diverse methodologies for the visualization, monitoring, diagnosis, and delivery of chemotherapeutic agents to the tumor site. The utilization of nanoparticles has demonstrated enhanced drug delivery effectiveness and decreased toxicity, and they can also

surmount biological barriers, thereby enhancing their anticancer activity. Nanomedicine represents a confluence of diverse fields, including information technology, molecular biology, engineering, medicine, pharmaceutics, and material science. The amalgamation of nanoscience and medicine provides a powerful tool to probe the intricacies of biological systems and gain insights into their underlying mechanisms. Nanocarriers have the ability to traverse the cellular membrane and other obstructions, thereby enhancing drug permeation and transportation. To ensure their clinical viability, it is crucial to address key factors such as biocompatibility, circulation duration, and stability, which can be effectively achieved through the use of nanomedicine. Nanoparticles used in nanomedicine, such as drug-encapsulated micelles, liposomes, and NPs, exhibit distinctive properties that enable them to breach the biological membrane and transport the enclosed drug into cells (**Figure 1.3**). The parameters that dictate elimination mechanisms, biodistribution, and cellular absorption, include particle size, morphology, and surface characteristics. The predominant nanoparticles employed in BC therapy include gold nanoparticles, polymeric nanoparticles, micelles, solid lipid nanoparticles, and liposomes, among a range of other nanoparticle types.

1.4.1. Liposomes

In 1964, Bangham and Horne introduced liposomes as spherical vesicles composed of an aqueous core surrounded by a phospholipid outer layer, with a size range of approximately 50 to 200 nm. The utilization of liposomes in the precise administration of therapeutic agents, encompassing both hydrophobic and hydrophilic drugs, is attributed to their phospholipid bilayers comprising biodegradable, biocompatible, and non-immunogenic constituents (55). Their minute dimensions facilitate their infiltration through vascular pores, leading to tumor localization. Additionally, it has been recorded that P-glycoprotein (P-gp) inhibition was achieved by employing anionic membrane lipids, wherein liposomes were utilized for the transportation of rhodamine 123 as a substrate for P-gp. As a result, the retention of rhodamine

123 within MCF-7/P-gp cells was found to increase, providing evidence for the functional transfer of its substrate by P-gp (56). In 1965, the FDA granted its initial approval to Doxil®, a liposomal formulation

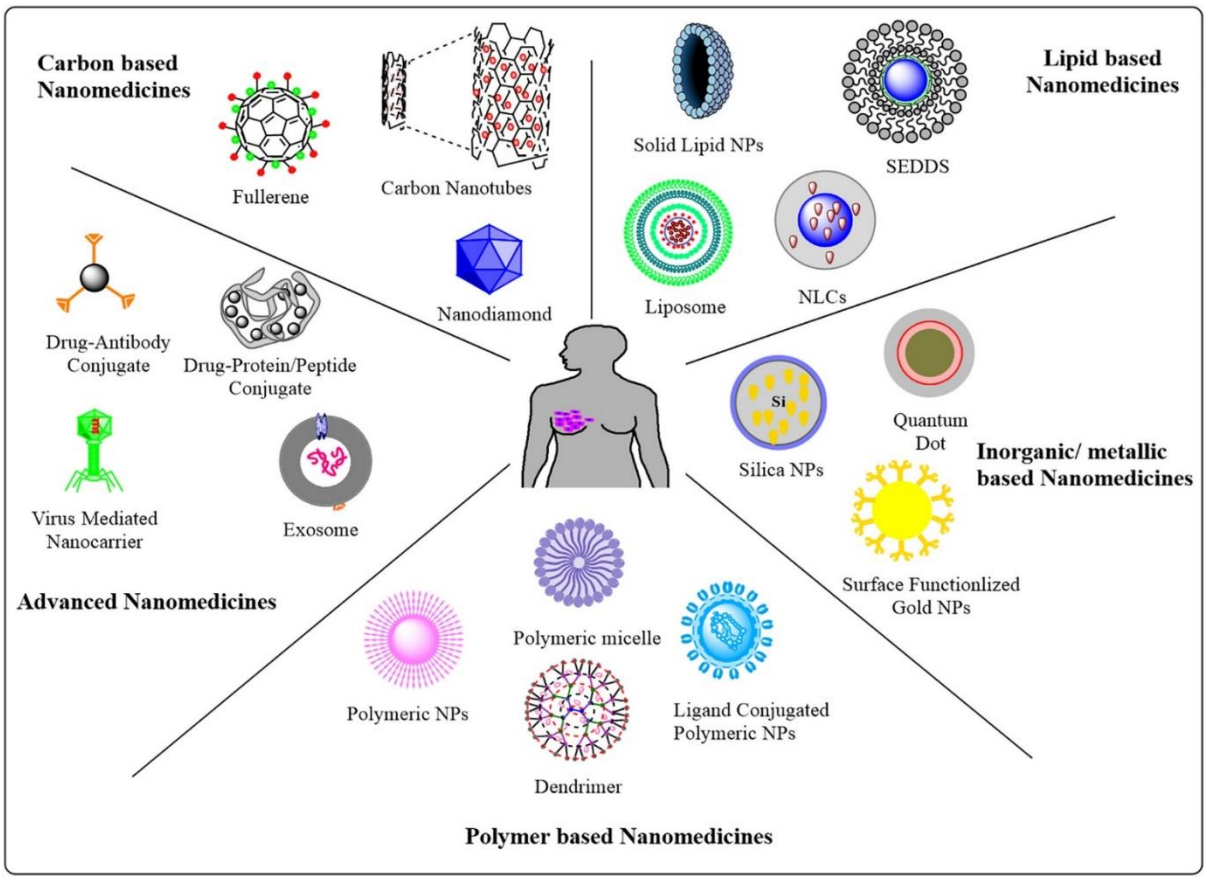

Figure 1.3. Nanomedicines utilized for BC therapy. Reprinted with permission from Ref. (57).

Of doxorubicin for the treatment of AIDS-related Kaposi's sarcoma, ovarian cancer, and multiple myeloma (U.S. FDA, 1995). In 2016, the drug received further approval for the treatment of breast cancer (58). In a study, (59) reported the development of liposomes for targeted BC therapy. The liposomes were functionalized using AS1411, a DNA aptamer with a high affinity for nucleolin, and Doxorubicin was incorporated as a payload. The functionalization of liposomes with AS1411 aptamer resulted in increased cellular uptake and cytotoxicity in MCF-7 BC cells, as compared to liposomes that were not targeted. Furthermore, the utilization of liposomes specifically designed for doxorubicin delivery demonstrated

enhanced infiltration into tumor tissue, leading to superior antineoplastic efficacy against xenograft MCF-7 breast cancer cells in immuno-deficient nude mice. The study exhibits that liposomes functionalized with AS1411 aptamer have the potential to detect nucleolin overexpression on the surface of MCF-7 cells, thereby enabling targeted drug delivery with high selectivity (59). In another study, Haiqiang Cao *et al*. reported the envelopment of a liposomal drug carrier with an isolated macrophage membrane to enhance targeted transport to metastatic regions. The enhancement of the macrophage membrane resulted in an increase in the uptake of emtansine liposome by metastatic 4T1 breast cancer cells while also exhibiting inhibitory effects on cellular viability. *In vivo*, the liposome was facilitated in its ability to target metastatic cells and exert a significant inhibitory effect on lung metastasis of BC through its association with the macrophage membrane. The findings suggested a biomimetic approach that utilizes the biological characteristics of macrophages to improve the therapeutic efficacy of nanoparticles *in vivo* for the treatment of cancer metastasis (60). In addition, a variety of liposomes that are selectively modified with arginine8–glycine–aspartic acid (R8GD) have been developed to encapsulate daunorubicin and emodin individually. The synergistic effect of the two specific liposomes demonstrated pronounced cytotoxicity against MDA-MB-435S cells, leading to a significant inhibition of vasculogenic mimicry (VM) formation and subsequent tumor cell metastasis. According to the research findings, the utilization of targeted liposomes led to the selective accumulation of chemotherapeutic agents at the tumor site, thereby inducing a noticeable antitumor response (61).

1.4.2. Micelles

Micelles are self-assembled structures composed of amphiphilic molecules which possess hydrophilic heads and hydrophobic tails. These structures exhibit a particle size distribution within the range of 10 to 100 nanometers. Micelles offer various benefits, such as extended circulation periods in the bloodstream, minimal toxicity, and increased accumulation in tumors.

In addition, they are frequently employed for delivering anticancer drugs with limited water solubility. Pluronic block copolymers, comprising poly (ethylene oxide) and poly (propylene oxide) in a triblock configuration, are extensively employed for the formulation of drug delivery micelles. Micelles have been utilized for delivering numerous anticancer drugs, specifically to BC cells. (62) has investigated the potential benefits of utilizing chitosan/vitamin E conjugate micelles (OXPt@Ch/VES Ms) as a delivery system for Oxaliplatin to improve its efficacy and ability to reverse multidrug resistance (MDR) in BC. The results showed a lower IC50 against both sensitive and resistant MCF-7 and MDA-MB-231 cells compared to OXPt alone. Treatment with OXPt@Ch/VES Ms induced G2/M cell cycle arrest, apoptosis, significant DNA damage, and mitochondrial depolarization. Furthermore, OXPt@Ch/VES Ms treatment led to decreased nephrotoxicity, reduced tumor growth, and prolonged survival compared to OXPt alone. These findings suggest that OXPt@Ch/VES Ms has the potential to serve as an effective nanomedicine for overcoming conventional OXPt-mediated drug resistance and nephrotoxicity in BC. In another study, (63) devised a bimodal therapeutic strategy that employed stable micelles altered with fibronectin-specific CREKA peptides. This approach effectively packed two hydrophobic chemotherapeutic agents, vinorelbine (V) and doxorubicin (D), in an aqueous solution. The designation of C-DVM was assigned to this newly developed construct in the novel. According to their findings, the utilization of small C-DVM micelles proved to be an effective strategy for the co-delivery of drugs into 4T1 cells while also inducing the disruption of microtubule structures. Additionally, C-DVM displayed a potent capacity to eliminate and hinder the invasion of 4T1 cells. Furthermore, a pharmacokinetic study conducted *in vivo* demonstrated that C-DVM extended the half-life of drug circulation and resulted in higher drug accumulation in lung metastatic foci after 24 hours. Moreover, The anticancer studies in mice harboring tumors showed that the C-DVM

effectively reduced tumor development and decreased lung metastasis. The developed nano platform could be a promising treatment option for metastatic breast cancer. (63).

1.4.3. Polymeric Nanoparticles

Polymeric nanoparticles (NPs) are tiny particles with a size between 1 and 1000 nm with the ability to load drugs within or on to the surface-adsorbed onto the polymeric core. These nanoparticles can accommodate anticancer drugs through various methods, such as dissolution, entrapment, encapsulation, or adsorption within the polymer matrix. The selection of polymers for the fabrication of nanoparticles can encompass natural polymers, such as gelatin, alginate, cellulose, and chitosan, as well as synthetic polymers like poly (lactic-co-glycolic acid) (PLGA), polylactide (PLA), and poly-ε-caprolactone (PCL). Moreover, they are frequently employed for delivering anticancer drugs in BC therapy. In a study, Katiyar *et al*. developed polymeric NPs for BC therapy using a combination of Piperine and rapamycin (PIP and RPM). PLGA was chosen as the polymer due to its moderate ability to reverse MDR, which may confer supplementary advantages. The nanoparticles that were prepared demonstrated consistent drug release *in vitro* for several weeks. The initial release pattern followed a zero-order kinetics with non-Fickian transport, after which it shifted to Higuchi kinetics with Fickian diffusion. The findings indicate that the introduction of a chemosensitizer has led to enhanced uptake of the RPM, which is a P-gp substrate. The pharmacokinetic analysis demonstrated a more favourable absorption profile of RPM when delivered through polymeric nanoparticles in comparison to its suspension form. Furthermore, the bioavailability of RPM was significantly improved by 4.8 times when administered in combination with the chemosensitizer. Based on an *in vitro* study using cell lines, it has been observed that the efficacy of nanoparticles is superior to that of free drug solutions. The findings suggest that the utilization of a blend of PIP and RPM nanoparticles could be a potentially promising strategy in the management of BC (64). Biodegradable PCEC nanoparticles were developed and

evaluated by Xiong *et al.* for their potential to carry both curcumin and paclitaxel at once. The study investigated the efficacy of the drug delivery system (PTX-CUR-NPs) in inhibiting BC growth through *in vitro* and *in vivo* experiments. The study findings revealed a gradual and sustained release pattern of paclitaxel and curcumin from the drug delivery system, with no initial burst effect. Moreover, the PTX-CUR-NPs exhibited a dose-dependent cytotoxic effect against MCF-7 cells, with a higher rate of apoptosis than the free drugs (PTX + CUR). The results of the cellular uptake study demonstrated that the PCEC polymeric nanoparticles loaded with the drugs were more efficiently taken up by tumor cells *in vitro*. *In vivo*, studies demonstrated noteworthy impediments of neoplasm proliferation, prolonged viability, and decreased adverse reactions compared to the free PTX + CUR drugs. Additionally, treatment with PTX-CUR-NPs brought about reduced Ki67 expression and heightened TUNEL positivity indicative of increased apoptosis in tumor cells, signifying the therapeutic potential of the drug delivery system (65).

1.4.4. Solid lipid nanoparticles (SLNs)

Solid lipid nanoparticles (SLNs) are a type of nanoparticle that is composed of solid lipids. The utilization of SLNs, which were first introduced in 1991, presents a superior and alternative carrier system compared to conventional colloidal carriers like liposomes, polymeric nano and microparticles, and emulsions. SLNs were first introduced as a promising drug delivery system for oral administration (66). Since then, SLNs have garnered significant interest in the field of cancer treatment due to their favourable characteristics, such as physical stability, high drug capacity, biocompatibility, and desirable drug release profile. SLNs are a promising area of research in the field of nanotechnology, offering numerous potential applications in clinical medicine, drug delivery, and scientific research across various disciplines. Geeta et al. reported the development of transferrin-targeted SLNs for BC therapy. In the present study, transferrin-conjugated solid lipid nanoparticles (SLNs) were created to improve the localization of

tamoxifen citrate in breast cancer. The proposed formulations demonstrated a higher cytotoxic effect on MCF-7 BC cells than free drugs in a concentration and time-dependent manner. For cellular internalization, both Confocal microscopy and Flow cytometry analysis has been performed and demonstrated higher uptake of SLN in MCF-7 cells than the free drug. The Results suggested that the developed nano-formulation can be a promising targeted nanomedicine for BC therapy.

1.4.5. **Gold Nanoparticles**

Gold nanoparticles, characterized by a gold core and a size of less than 150 nm, possess inert and non-toxic properties, as reported by Manju and Sreenivasan (2010). Because of their biocompatibility, gold nanoparticles have gained attention as promising carriers for anticancer agents, as highlighted by Singh et al. (2017). Arvizo et al. (2010) have reported various benefits of gold nanoparticles, including radio-sensitization and photothermal therapy. Furthermore, García Calavia et al. conducted a study demonstrating the use of a lactose derivative for stabilizing and dispersing phthalocyanine-functionalized gold nanoparticles in aqueous solutions. In a 2018 work, Garcia Calavia et al. produced and modified gold nanoparticles with a mixed monolayer composed of zinc phthalocyanine and a lactose derivative. The phthalocyanine-gold nanoparticles were coated with lactose, which led to the production of water-dispersible nanoparticles that could produce singlet oxygen and cause cell death when exposed to radiation. The *in vitro* targeting efficacy of lactose-functionalized gold nanoparticles carrying lactose phthalocyanine towards the galectin-1 receptor located on the surface of SK-BR-3 and MDA-MB-231 BC cells was investigated. The results indicate that lactose has significant potential as a selective targeting agent for galactose-binding receptors that are upregulated in breast cancer cells. Previous studies have reported the ability of gold nanoparticles to bind with antibodies that are specific to tumor cell surface antigens that are overexpressed (Lim et al., 2011). Multiple scientific investigations have demonstrated that gold

nanoparticles (AuNPs) have the potential to increase the availability of drugs at specific sites, improve the effectiveness of cancer treatments such as chemotherapy, radiotherapy, photothermal therapy (PTT), and photodynamic therapy (PDT), and influence gene expression. *In vitro* and *in vivo* studies have verified the ability of AuNPs to impede the growth, progression, and spread of triple-negative BC (TNBC) cells. These mechanistic properties of AuNPs represent an attractive avenue for developing drugs with improved therapeutic effectiveness against TNBC. Consequently, utilizing AuNPs for TNBC therapeutics may represent a promising approach (67).

The current work was carried out using the **polymeric-based nano-particles of Olaparib with Human serum albumin,** which will have a targeted drug delivery to the cancer organs.

1.5. Human Serum Albumin as Nano-carrier:

Human Serum albumin is a biologically available protein with a molecular weight of 66.5 kDa and consists of 585 amino acids. HSA contains three structurally similar domains, and each domain contains two sub-domains. Like the first domain is subdivided into IA and IB, the second one is subdivided into IIA and IIB, and the third one is subdivided into IIIA and IIIB. HSA represents about 60% of the total protein content of the blood serum, which helps regulate the osmotic pressure of the body. HSA also helps in the binding and transport of molecules, as well as anti-oxidant and anti-inflammatory actions (68)

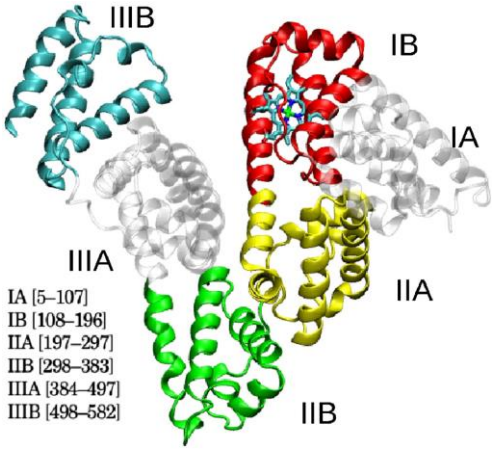

Figure1.4: HSA structure

HSA binds with many substances like fatty acids, porphyrins, and many varieties of drugs. Drug pharmacokinetics/pharmacodynamics depends on the degree of interaction between the drug and Human serum albumin. The affinity of the interaction can be determined using different techniques like fluorescence, circular dichroism, and spectroscopic techniques (69);. Two main binding sites have very high affinity for different substances, known as Sudlows's sites. The first one is located in the core of the IIA subdomain, and the second is in the IIIA subdomain. (70). Human Serum Albumin has many free amino and carboxylic groups, which allows it to have covalent or non-covalent interaction by hydrophobic adsorption, amide condensation, and ionic interaction. (71)

Albumin has good stability in the pH range of 4 to 9 as well as relative thermal stability (stable until 10 h at 60°C), which makes it an excellent nanomaterial for the designing of dosage forms with a variety of therapeutic agents upto concentrations of 5–20% (72)

Human Serum Albumin is one of the agents for targeted drug delivery to cancer cells. HSA has a good binding ability to bind with the cell-surface receptor, that's is, gp60 receptors (60 KDa glycoprotein), further this binding activates the intracellular protein caveolin-1 leading to the formation of the transcytosis vesicle, caveolae. As albumin has a specific mechanism to bind with gp60 receptors, which were over-expressed in the cancer cells, this was one of the reasons for albumin as a drug carrier in cancer treatment. Albumin is also known to bind with osteonectin, known as secreted protein acid rich in cysteine (SPARC) due to its sequence homology with gp60. SPARC is also overexpressed in tumor cells. SPARC present in the tumor cells increases the drug delivery to the tumor cell by sequestering the albumin-bound drugs enhancing the delivery of paclitaxel into the tumor microenvironment.

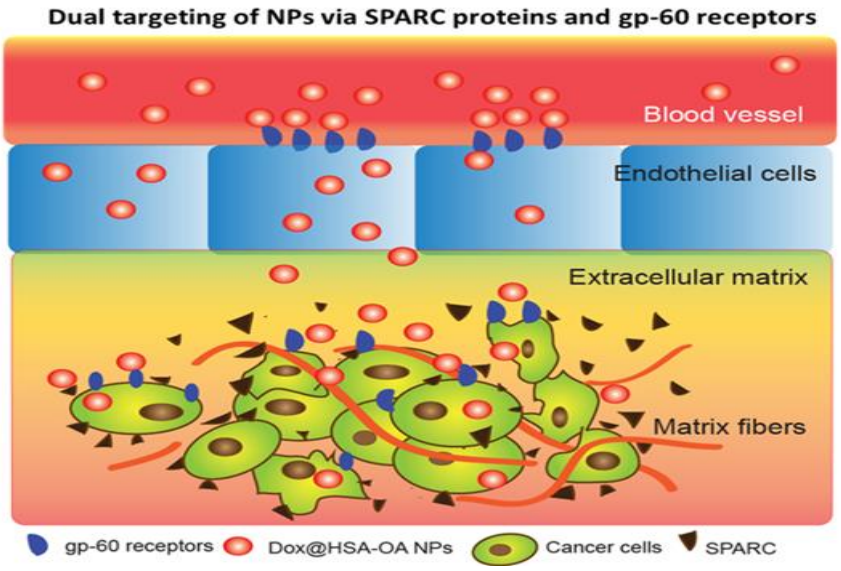

Figure 1.5: Active targeting of albumin NPs via SPARC proteins and gp-60 receptors. Adapted with permission.

1.6. Techniques for the preparation of albumin Nano-particles:

The different techniques for the preparation of the nanoparticles are categorized as physical and chemical methods. The physical method uses heat or pressure or a combination of heat and pressure; the chemical method involves chemical agents such as solvents, crosslinking agents, or the agents to induce self-assembly.

- De-solvation (coacervation)
- Emulsification
- Nanoparticle albumin-bound technology (NAB-technology)
- Thermal gelation
- Formation of NPs by self-assembly
- Microfluidic Technology
- Nano Spray Drying

1.6.1. De-solvation (coacervation):

De-solvation process contains two steps that are preparation of the aqueous solution and the preparation of the organic solution. Organic solutions can be varied based on the solubility of the drug solution, and that can be ethanol, acetone, or any other de-solvating agent.

The drug dissolved in the organic solvent will be added to the aqueous human serum albumin solution or protein solution under constant stirring at a controlled rate or manual addition, which will turn the aqueous solution into turbid.

During this de-solvation process protein's tertiary structure will be exposed, and the inner hydrophobic moieties will interact with the other protein inner structures and forms the generation of small aggregated nanoparticles via non-covalent interactions, which ultimately leads to the formation of the sub-micron nano-particles particles.

For these sub-micron nano-particles, a cross-linker like glutaraldehyde or EDC will help in cross-linking and form stable sub-micron nano particles.

In some instances, the reduction of some of the disulfide bridges or cysteine-cysteine interactions between different HSA molecules could produce nano-particle formulations formation without the use of toxic crosslinking agents, such as glutaraldehyde.

The different factors which will influence the formation of nanoparticles using the de-solvation technique are concentrations of protein, cross-linker in the solution, amount of de-solvating agent, the buffer used, and stirring time and speed, which play critical roles in nanoparticle characterization, including particle size, drug loading, entrapment efficiency, and polydispersity (73)

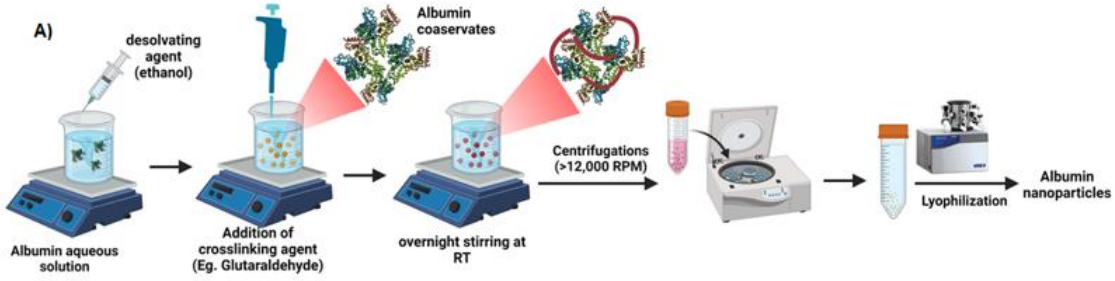

Figure1.6: Preparation of the nanoparticles using the de-solvation technique

1.6.2. Emulsification:

Emulsification techniques involve the preparation of the oil phase or organic phase and the preparation of the Aqueous phase, followed by the preparation of crude emulsion. The crude emulsion will be prepared by adding the oil/organic phase to the aqueous phase by stirring or high-shear homogenization.

The prepared crude emulsion will be subjected to high-pressure homogenization for the formation of O/W nano-emulsion. Further, the formed nanoparticles will be stabilized by heating >120 °C or chemical crosslinking with a cross-linking agent like glutaraldehyde.

A recent publication states that hydrophobic ionic liquid agents like 1-butyl-3-methylimidazolium hexafluorophosphate (BmimPF6) were used as oil components in place of oils (castor oil, olive oil, etc.) and/or conventional organic solvents (cyclohexane, dichloromethane, etc.) to protect from the environment.\ as a green synthesis approach. The work used the hydrophobic ionic liquid, 1-butyl-3-methylimidazolium hexafluorophosphate ($BminPF_6$).

Different factors will influence the emulsion process; the homogenization speed, glutaraldehyde/surfactant concentrations, and the compositional fractions (surfactant/ionic liquid ratio) are important process parameters affecting particle size.

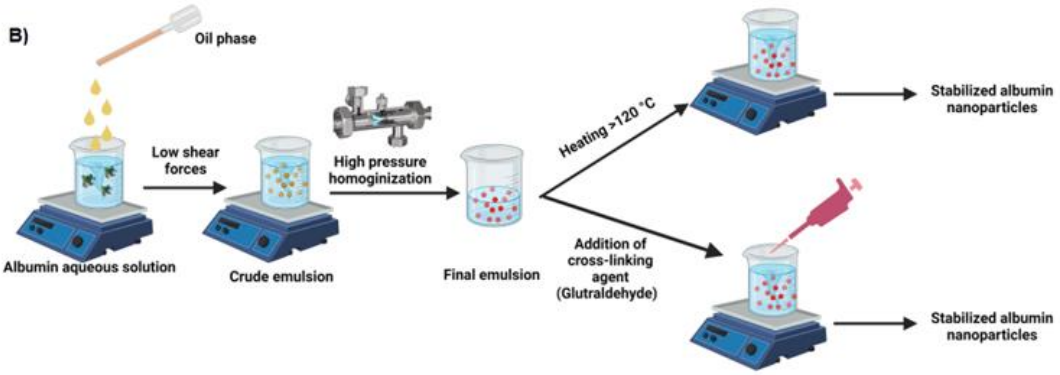

Figure 1.7: Preparation of the nanoparticles using the emulsification technique.

There are many other methods reported in the literature for the emulsification process Phase inversion temperature (PIT), which is a low-energy emulsification method; phase inversion can be induced by either modification of temperature or change of composition. (74)

1.6.3. Nanoparticle albumin-bound technology (NAB-technology)

NAB technology is clinically translated to prepare albumin nanoparticles of Paclitaxel (ABI-007) was the first product approved by USFDA using this technology.

The process involves a modified emulsification technique, where a crude emulsion is formed initially by gradually adding the oil phase containing the drug to the aqueous phase containing human/bovine serum albumin (pre-saturated with 1 % chloroform), followed by mild homogenization using the high shear homogenizers, further the crude emulsion is subjected to high-pressure homogenization.

The organic phase containing the drug will be surrounded by the albumin particles and forms the nano-emulsion (O/W) with high pressure; further, the solvent will be removed by rotary evaporation. Further, it will be filtered through 0.22 µm for sterilization, followed by lyophilization to obtain the solid lyophilized product.

The unique advantage of nab-technology is the absence of the use of any other excipients, including crosslinking agents for nanoparticle stabilization, and the final product is free from

organic solvents. The particle size of albumin-bound nano-paclitaxel formulations prepared following Nab-technology is 130 nm, posing no capillary obstruction risk (75). Moreover, the NPs size is optimal for the eventual accumulation of tumor tissue by the Enhanced Permeability and Retention (EPR) effect.

1.6.4. Formation of Nano-particles by self-assembly:

Nano-particle will be self-assembled by the conjugating process that conjugates the hydrophobic moiety to the albumin using the different cross-linking agents, usually the combination of ethyl (dimethyl aminopropyl) carbodiimide and N-hydroxy succinimide.

The process involves the breaking of disulfide bonds using β-mercaptoethanol increases hydrophobicity and allows thiol-mediated conjugation; the process can be the interaction between the amine group and the acidic moiety via acid-amine coupling reaction.

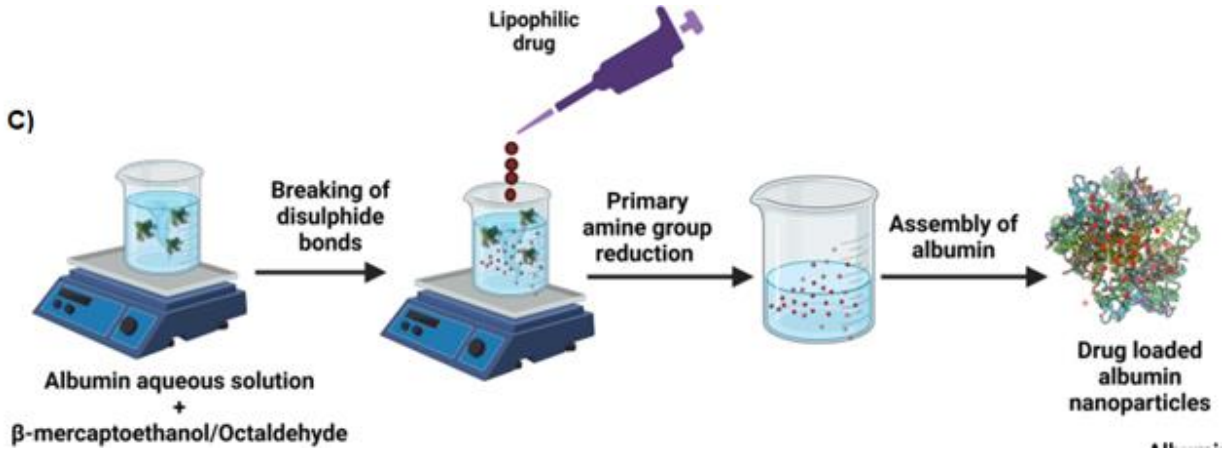

Figure 1.8: Preparation of the nanoparticles by self-assembly technique.

1.6.5. Thermal gelation:

Thermal gelation is a heat-induced process where the protein solution undergoes heating. During the heating of the protein/albumin solution, there is a conformational change of protein tertiary structure that is unfolding and followed by protein− protein interactions. This

interaction between proteins will occur due to the formation of hydrogen bonds, electrostatic, hydrophobic interactions, and disulfide-sulfhydryl interchange reactions.

The different parameters which will affect the conditions of the process are pH, protein, concentration, and ionic strength. The final matrix which formed will depend on the balance of repulsive and attractive forces between the protein molecules(76)

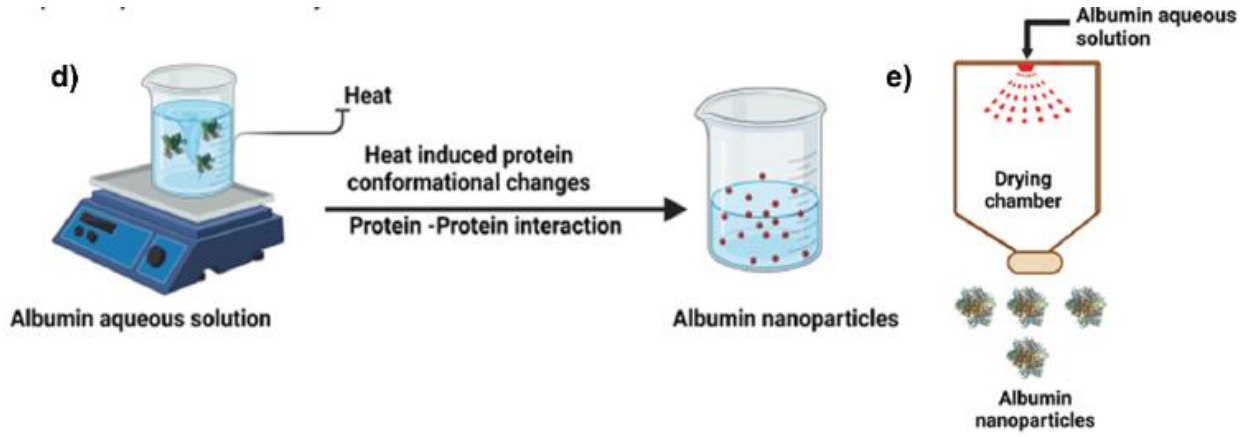

Figure 1.9: Preparation of the nanoparticles using the thermal gelation technique.

1.7.0. OLAPARIB-HUMAN SERUM ALBUMIN NANO-PARTICLES:

The current research talks about the advantages of the PARP-inhibitor Olaparib as a Nano drug delivery system by using the Huma Serum Albumin (HSA) as a career for drug delivery for the treatment of triple-negative breast cancer.

Nano-particles reach the tumor micro-environment, through the leaky vasculature of the tumor cells, and thereby release the chemotherapeutic moiety. On the other side, the Nano-particles are usually unable to permeate across the body's normal organs and tissues; hence the toxicity is very limited with the nano-particles. Encapsulated nano-particles will have the targeted release to the cancer cells.

Olaparib is the current formulation as the tablet dosage forms, and delivering PARP inhibitors without modulation often leads to a toxic effect; therefore, a delivery vehicle is essential to encapsulate them.

1.7.1. Nano-formulations for Delivery of Olaparib using Human Serum Albumin for Triple-negative breast cancer Treatment:

Nanomedicine is a new technology and platform for the treatment of cancer

Nanotechnology remains a novel platform for cancer therapeutics. Nano-mediated drug and protein delivery has been widely investigated in cancer treatment. Cancer drugs have certain limitations like an encapsulation of anticancer moiety, low water solubility, immediate drug release, short circulation life, and low safety index; some of these issues were addressed using nano-technology. Apart from this, nano-medicines have a great impact on the Pharmaco-kinetics and pharmacodynamics of the drugs, and targeted drug delivery to the cancer cells has the advantage of low side effects.

Olaparib is the PARP inhibitor that induces DNA damage in cancer cells, and the therapeutic activity can be augmented when combined with a chemotherapeutic agent.

Currently, the FDA approved Olaparib tablet dosage and its limitations and side-effect on cancer patients:

- Olaparib undergoes first-pass metabolism.
- Limitations of Bio-availability due to its poor solubility
- Off-targeted toxicity

Major warning indications for the usage of Olaparib oral treatment for TNBC treatment were Myelodysplastic Syndrome/Acute Myeloid Leukemia (MDS/AML) in 1.5% of the patients, Pneumonitis occurred in 0.8% of the patients, Venous thromboembolism (VTE) in 8% of the patients and also reported Embryo-Fetal Toxicity.

The most common side effects of Olaparib are the following with the Olaparib oral tablet dosage form nausea or vomiting, tiredness or weakness, low red blood cell counts, diarrhea, loss of appetite, headache, changes in the way food tastes, cough, low white blood cell counts, shortness of breath, dizziness, indigestion or heartburn and low platelet counts.

Current research work involves the preparation of the Olaparib-Human Serum Albumin nanoparticles is a unique platform for drug delivery. They have been extensively investigated for their potential use in anticancer drug delivery and the treatment of triple-negative breast cancer.

NPs can be fabricated in a variety of ways to increase the drug encapsulation capacity at the inner core, and they can also be equipped with multiple functions on the outer core to improve the drug activity in the target environment. Besides, Olaparib-Human Serum Albumin Nanoparticles have the potential to deliver poorly water-soluble drugs and provide a sustained releasing profile to prolong the blood circulation time.

Olaparib with Human Serum Albumin nanoparticles will have improved blood half-life, *in vivo* uptake, and pharmacodynamics. Olaparib has advanced the treatment of ovarian cancer by providing patients with an effective and molecularly targeted maintenance therapy.

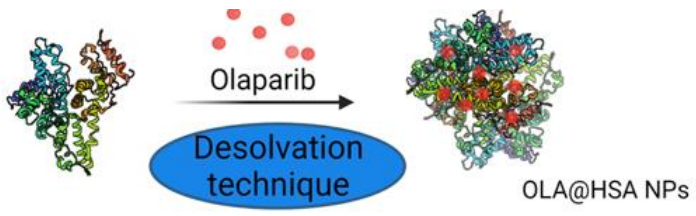

Figure1.10: Preparation of the Olaparib- Human Serum Albumin nanoparticles by de-solvation technique.

1.8. Olaparib

Olaparib is a poly (ADP-ribose) polymerase inhibitor and made available as an oral capsule dosage form approved by the FDA and developed by AstraZeneca. Initially, when Olaparib was introduced into the market, it was indicated for BRCA mutation-positive ovarian cancer, and later it was identified for the treatment of triple-negative breast cancer where negative for human epidermal growth factor receptor (HER) 2, negative for estrogen, and negative for progesterone receptors. Olaparib was proved to be effective in combination therapy with other chemotherapeutic agents. Olaparib has undergone with different clinical trials either in combination therapy or as monotherapy for different cancer treatments are Ovarian Cancer, breast cancer, uterine cancer, Prostate cancer, Pancreatic cancer, Gastric cancer, Non-small cell lung cancer, and Colorectal cancer. As the currently approved dosage form is the oral dosage and due to its lack of specificity, it has many side effects during usage, are Myelodysplastic Syndrome/Acute Myeloid Leukaemia, Pneumonitis, Venous thromboembolism (VTE) and Embryo-fetal Toxicity.

1.8.1 Physicochemical properties of Olaparib:

Olaparib is a pure water-soluble ($C_{24}H_{23}FN_4O_3$, molecular weight: 435.08 g/mol), and it is classified as a BCS class-II drug indicated for the treatment of triple-negative breast cancer. It has a very low water solubility of 0.0601 mg/mL and a log P value of 2.72 (https://go.drugbank.com/drugs/DB09074), and it has UV absorption maxima at 207 nm. The chemical structure of oleanolic acid is shown in **Figure 1.11 (** https://pubchem.ncbi.nlm.nih.gov/compound/Olaparib, Id no- 23725625). The melting point of 198°C (safety data sheet of Olaparib from Thermo Fischer).

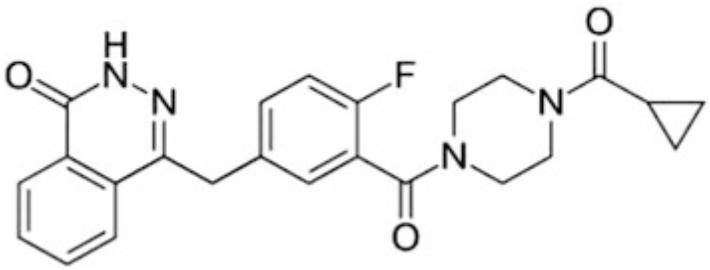

Figure 1.11: Chemical structure of Olaparib

IUPAC Name: chemically as 4-[[3-[4-(cyclopropanecarbonyl) piperazine-1-carbonyl]-4-fluorophenyl] methyl]-2H-phthalazin-1-one.

Molecular formula= C24H23FN4O3

Molecular weight = 435.08 g/mol

1.8.2 Oxaliplatin

Oxaliplatin is a platinum-based chemotherapeutic compound, and it will be used for the treatment of meta-static colorectal cancer. Oxaliplatin has an off-label indication in the treatment of triple-negative breast cancer, biliary adenocarcinoma, and lymphocytic leukemia. This drug is from the family of platinum-based chemotherapeutic agents used in combination with fluorouracil and leucovorin for the treatment of colorectal cancer. The platinum-containing compounds attach to the DNA and form a cross-link, and this cross-linking will help in inhibiting the DNA replication, transcription, and arrest of the cell cycle replication and results in cell death.

1.8.3 Physicochemical properties of Oxaliplatin

Oxaliplatin has a water solubility of 27.5mg/mL and a log p of -0.47. Oxaliplatin has limited solubility in water and is less insoluble in methanol, and acetone is slightly soluble in water.

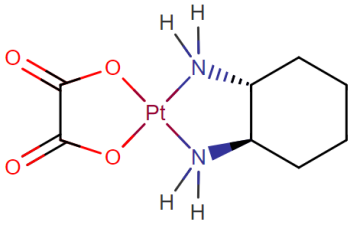

Figure 1.12: Chemical structure of Oxaliplatin

IPUPAC-Name:(3aR,7aR)-octahydro-2',5'-dioxaspiro[cyclohexa[d]1,3-diaza-2-platinacyclopentane-2,1'-cyclopentane]-3',4'-dione

Molecular Formula: C8H14N2O4Pt

Molecular weight: 397.294

1.8.4 Objectives

Our aim for the study is to develop human serum albumin-bound Olaparib nanoparticles as sustained drug-releasing tumor-targeting of nanomedicine to inhibit growth and metastasis in the mouse model for the treatment of triple-negative breast cancer. We have developed nano-particles of Olaparib HSA nanoparticles by using glutaraldehyde as a cross-linking agent through the formation of CO-NH bonding.

Objective 1: To prepare the Olaparib human serum albumin nanoparticles by de-solvation technique and using the Glutaraldehyde as a crosslinking agent to the treatment of triple-negative breast cancer

Specific aims:

(i) To prepare Olaparib containing human serum albumin nanoparticles and cross-linking with glutaraldehyde.

(ii) To Optimize the nano-particles preparation process using the central composite screening design to understand the factors influencing the nano-particles preparation process.

(ii) To characterize the prepared nano-particles using the different physicochemical methods size, surface charge, %Entrapment Efficiency, %Drug loading, morphology, kinetic stability, x-ray diffraction, Differential scanning calorimetry, FTIR analysis, X-ray photon electron microscopy, protein confirmation studies using SDS-PAGE and Circular dichroism spectroscopy, *in vitro* drug release, and Haemolysis assay

(iii) *In vitro* studies of the prepared nanoparticles using the *In vitro* cell-based assays in monolayer- MTT Assay, Annexin-V assay, cell cycle analysis, nuclear staining assay, DNA fragmentation assay, Mitochondrial membrane potential assay, ROS detection assay, spheroid study, and Growth inhibition/live-dead cells assay in spheroids.

(iv) *In vivo* studies of the prepared Olaparib-human serum albumin nanoparticles using Tumour inhibition study, Tunel assay/detection of Ki-67, ROS generation in tumor tissue, and H & E staining.

Objective 2: To prepare Olaparib and Oxaliplatin containing human serum albumin nano-particles as a combination therapy for the treatment of triple-negative breast cancer in a mouse model.

Specific aims:

(i) To prepare Olaparib and Oxaliplatin containing human serum albumin nanoparticles and the usage of the BAC as a conjugating agent for the Oxaliplatin and N, N-bis acryloyl

cystamine (BAC) as a cross-linking agent for the Olaparib loading and to check the impact of combination drug delivery.

(ii) To characterize the prepared nano-particles using the different physicochemical methods size, surface charge, %Entrapment Efficiency, %Drug loading, morphology, kinetic stability, protein confirmation studies using SDS-PAGE and Circular dichroism spectroscopy, *in vitro* drug release, and Haemolysis assay

(iii) *In vitro* studies of the prepared nanoparticles using the *In vitro* cell-based assays in monolayer- MTT Assay, Annexin-V assay, Cell cycle analysis, nuclear staining assay, DNA fragmentation assay, Mitochondrial membrane potential assay, ROS detection assay, spheroid study, and Growth inhibition/live-dead cells assay in spheroids.

(iv) *In vivo* studies of the prepared nanoparticles using Tumour inhibition study, Tunel assay/detection of Ki-67, ROS generation in tumor tissue, and H & E staining.

Chapter 2

Preparation, In vitro Characterization, In vitro studies, and in vivo studies of the Olaparib-Human Serum Albumin Nano-particles

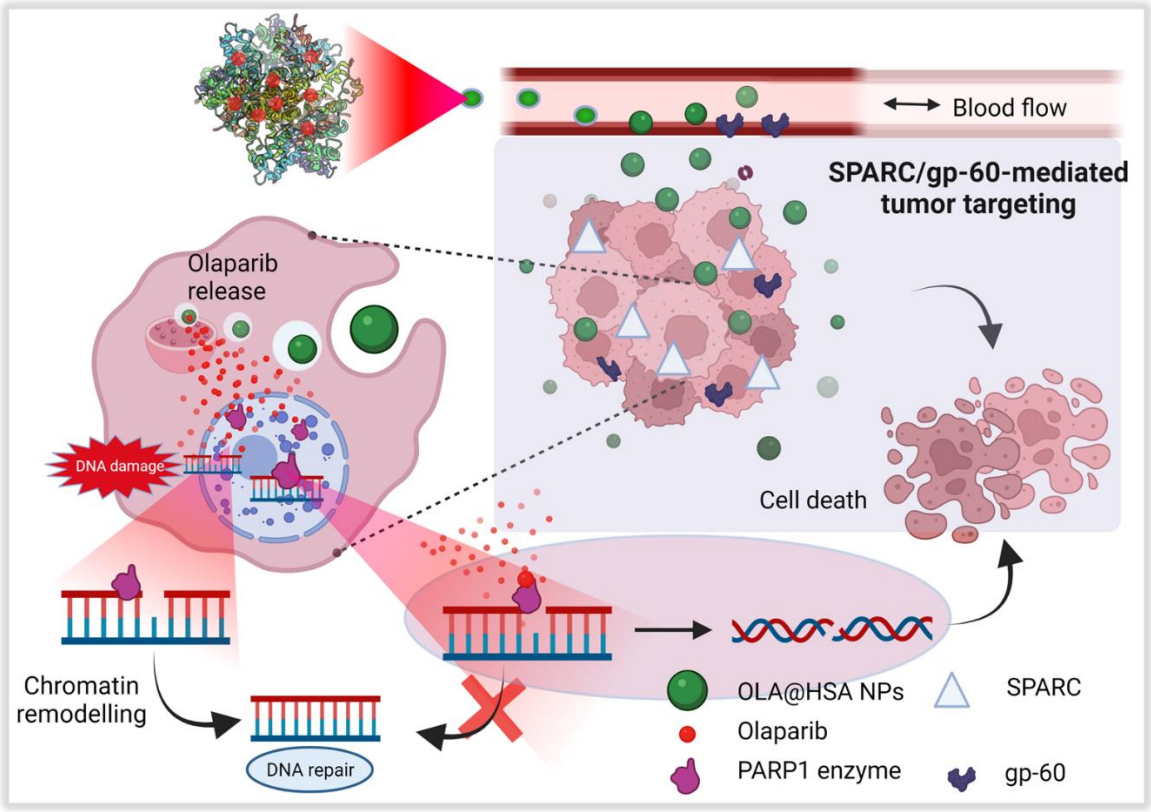

2.1 Introduction

Triple-negative breast cancer (TNBC) is the most lethal breast cancer subtype affecting the younger women population (below 40) that lacks the expression of three significant breast cancer markers, estrogen (ER), progesterone (PR), and human epidermal growth factor (HER-2) receptors. TNBC encounters a poor prognosis and a high relapse rate due to this cancer's invasiveness and metastatic potential(77). Approximately 15-20 % of breast cancer patients are triple-negative, indicated by the immunohistochemical staining(78). Moreover, approximately 5 % of randomly selected breast cancer patients possess germline deleterious breast cancer gene (BRCA) mutation(79). BRCA1 and BRCA 2, located on chromosomes 17 and 13, are tumor-suppressor genes involved in the homologous recombination (HR) repair mechanism to rectify double-stranded DNA damage in the proliferating cancer cells(80). The gene repair re-establishes the genetic sequence for normal cell functioning. However, the mutation in BRCA1 and BRCA2 genes impairs the HR mechanism resulting in the activation of oncogenes, which predisposes the individual to a high risk for breast cancer occurrence(81). Majorly, patients with BRCA1 mutations are inclined to be affected by TNBC(82).

Poly(adenosine diphosphate-ribose) polymerase (PARP) family of proteins is vital to repair breaks in DNA single strands(83). The BRCA-mutated cells activate PARP enzymes, which enhance the process of ADP ribosylation. The repaired single-strands replicate, leading to the survival of the cells. PARPi inhibits PARP enzyme activity and forms many ssDNA (single-stranded DNA), which eventually causes the dsDNA (double-stranded DNA) breakage at the replication fork(84). However, the exact mechanism of enzyme inhibition by the small molecule PARP inhibitors is still unclear(85). The BRCA1/2-mutated cells are sensitive to PARP inhibition to a much greater extent than the other breast cancer cells undergoing the BRCA-mediated HR mechanism for DNA repair(86). Likewise, PARP-inhibition enhances the

effectiveness of radiation therapy by inactivating the repair procedure of damaged DNAs accumulated following radiation treatment (87).

Olaparib is a PARP inhibitor (PARPi), first approved by USFDA (United States Food and Drug Administration) to treat patients with recurrent BRCA-mutated ovarian and breast cancers. Olaparib demonstrated therapeutic benefits in phase III clinical trials (Olympia AD study) in patients with BRCA1/2-mutated HER2 negative BCs(88-90). Olaparib was approved by USFDA as a first-line treatment to treat BRCA1/2-mutated/HER-2/neu negative breast cancer in January 2018 (oral dose/tablet. 300 mg, twice daily). In the Olympia AD Phase III trial, a statistically significant progression-free survival rate was achieved with Olaparib compared to other standard chemotherapeutic treatments(89). Olaparib is therapeutically effective in metastatic TNBC with fewer side effects than other chemotherapeutic agents, including capecitabine, eribulin, and vinorelbine (90, 91)

However, sequential or combination treatment of this drug with other anticancer agents is yet to be explored. Further research unraveled that Olaparib was effective in BRCA-mutated tumors of other organs (92).

The BCS (Biopharmaceutical Classification System) class IV drug, Olaparib, suffers from low aqueous solubility and permeability. The reason for Olaparib's less sensitivity towards the growth inhibition of wild-type BRCA tumors could be its poor bioavailability (93). Moreover, Olaparib treatment is associated with several side effects, including anemia, nausea, myelodysplastic syndrome, acute myeloid leukemia, and pneumonitis (90, 94). The existing marketed formulations are tablets and capsules, which require more dosing to overcome the poor bioavailability and has severe adverse effect of hematological toxicity. The Olaparib oral formulation (Lynparza) has limited success against triple-negative breast cancer, primarily due to its insufficient localization to the tumor. Due to all these drawbacks, there is a need for the development of nano-formulations that can maintain adequate drug concentration and extend

the release of the drug. Various Olaparib-nanoparticles systems have been developed recently to improve the pharmacokinetic properties of the drug, tumor-targeting, and improve radio sensitization (92, 95-97). Nano-formulation of Olaparib, a lipid-based injectable system, enhanced the PARP inhibition and radio sensitivity of specific prostate cancer cells (95). A PEG-poly(caprolactone) NPs system loaded with Olaparib improved the therapeutic effect of radiotherapy compared to the free drug in lung cancer (96). Several combination therapies using Olaparib and other chemotherapeutic agents were studied recently and proven to have sensitized the cancer cells towards treatment in various tested cancers, including the brain, pancreatic (BRCA-mutated), and breast cancers (98-100).

In our study, Olaparib was physically entrapped in human serum albumin (HSA) NPs to prepare OLA@HSA NPs via a de-solvation technique using ethanol (de-solvating agent) and glutaraldehyde (crosslinker). Albumin NPs possess unique features beneficial to be used as a drug delivery system in cancer (101). They are nano-size, biocompatible, non-immunogenic, and can carry hydrophobic drugs. Albumin NPs display tumor targetability via passive [Enhanced Permeability and Retention (EPR effect)] and active targeting mediated by the binding with secreted protein acidic and rich in cysteine (SPARC) and gp60 receptors, over-expressed on the cancer cell/cancer cell linked endothelial cells surface (102). The study, for the first time, fabricated albumin-bound nano-Olaparib and investigated its therapeutic efficacy and lung metastasis-inhibitory potential in triple-negative breast cancer. The NPs were physiochemically characterized thoroughly for particle size, zeta potential, drug loading, entrapment efficiency, stability, and biocompatibility. The anticancer activity was judged *in vitro* using murine and human TNBC cells in monolayers and human TNBC cell spheroids. Further, the therapeutic efficacy and anti-metastatic ability were evaluated *in vivo*.

2.2 MATERIALS AND METHODS

2.2.1 Materials

Human serum albumin was purchased from Baxter Healthcare Corporation (USA). Olaparib was received as a gift sample from Dr. Reddy's Laboratory, Hyderabad, India. 2,7-dichloro-dihydro-fluorescein diacetate (DCFH-DA) procured from Sigma Aldrich, Mumbai, India. Methyl thiazolyl diphenyl-tetrazolium bromide (MTT), Trypan blue solution, and Fluoro mount-G were obtained from Himedia Labs (India). Spectra/Por dialysis membranes were purchased from Spectrum Laboratories, Inc. (USA). Dialysis membranes (1kD, 2kD, 12-14kD, 100 kD) were obtained from Spectrum Laboratories, Inc. (California, USA). Methoxy PEG (5K) amine hydrochloride (mPEG-Amine.HCl) was purchased from Jenkem Technologies (Texas, USA).1. Trypan blue and 3-(4, 5-dimethylthiazol-2-yl)-2,5-di-phenyltetrazolium bromide (MTT) were procured from Himedia Laboratories (Mumbai, India). Organic solvents and chemicals procured commercially were of analytical grade or higher.

Human TNBC cell line MDA-MB-231 was procured from National Centre for Cell Sciences (NCCS, Pune, India). Murine breast cancer cell lines 4T1 and 4T1-Luc were procured from the American Type Culture Collection (ATCC, USA). Himedia Labs (India) supplied the Penicillin Streptomycin, Dulbecco's Modified Eagle Medium (DMEM), Minimum Essential Medium Eagle (MEM), Trypsin-EDTA, 4′,6-diamidino-2-phenylindole dihydrochloride (DAPI) and fetal bovine serum (FBS). Cell lines were grown in DMEM supplemented with 10 % FBS, 100 IU/mL of penicillin, streptomycin at 37℃, and 5 % CO2.

2.2.2 Preparation of Olaparib with HSA Nanoparticles:

Different techniques available for the preparation of nanoparticles are de-solvation (Coacervation) technique, Emulsification technique, Thermal gelation, Nano-spray drying, Nano-particle albumin-bound technology, and the Self-assembly technique.

2.2.2.1 Preparation of Olaparib with Human Serum albumin (HSA) Nanoparticles using the de-solvation technique:

Olaparib with human serum albumin nanoparticles prepared using the de-solvation technique; the final optimized procedure includes the optimized procedure as dissolution of HSA (50 mg) in 2 mL of deionized (DI) water and the dissolution of OLA (2 mg) in 2 mL ethanol.

Olaparib solution was added dropwise at the rate of 1 mL/min to the Huma Serum Albumin solution under the stirring condition at 1000 rpm; after completion of the Olaparib addition, glutaraldehyde 25% w/v solution of 5 µL was added dropwise to the above olaparib-HSA solution.

After 24 h of stirring, the solution was centrifuged at 12,000 rpm, 15 min, at 4 °C. The pellet was washed twice and resuspended in DI water (2 mL). The NPs solution was lyophilized by adding mannitol (5% w/v, 1 mL) into the solution.

Mannitol was added to the NPs solution, which was kept at −80 °C for 6 h for freezing, and the frozen sample was taken for lyophilization at −99 °C until the free-flowing powder was obtained. The blank NPs were prepared following the same protocol without the drug.

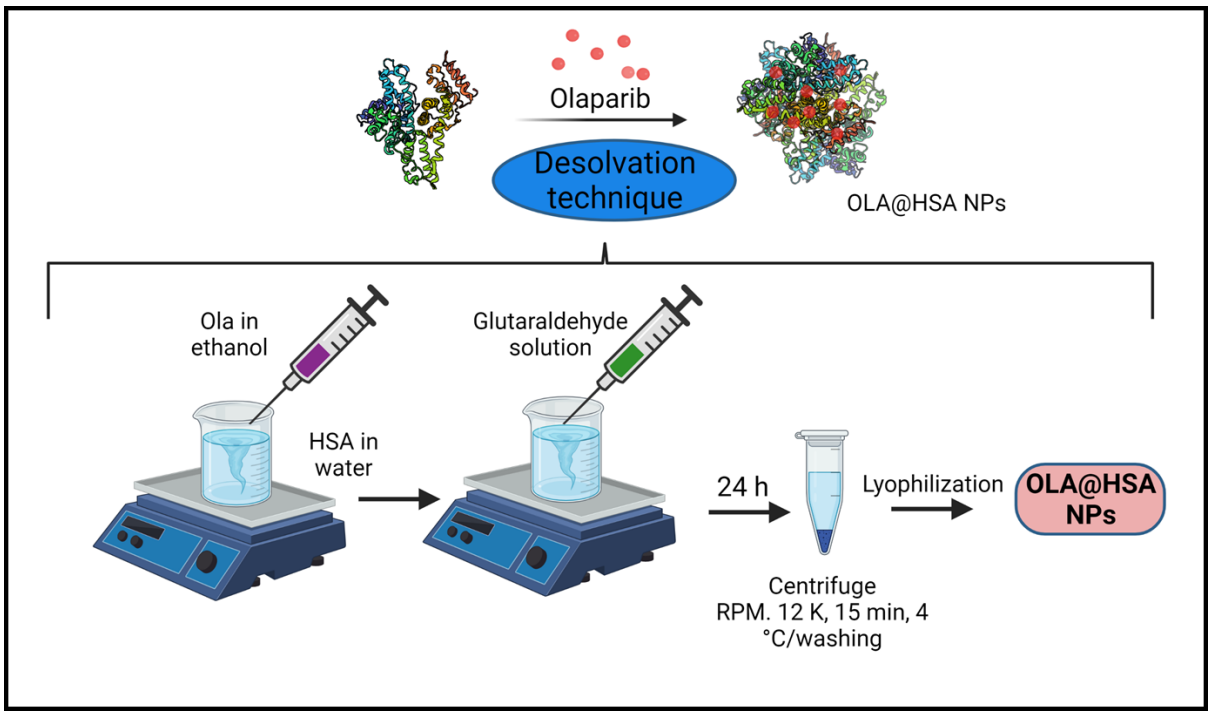

Figure-2.1: Synthesis of OLA@HSA Nanoparticles by de-solvation technique.

2.2.3.1 Optimization of Nano-particle preparation:

- Preparation of the Nano-particle by addition of Olaparib Solution to Human serum albumin solution
- Selection of the conjugating agent
- Role of the conjugating agent for the formation of nanoparticles
- DOE studies to optimize the process and establish the design space

2.2.3.3 Preparation of the Nano-particles:

Human serum albumin solution of 25mg/mL was prepared by dissolving 50 mg of human albumin in 2 mL of de-ionized (DI) water. Olaparib solution of 1mg/mL was prepared by dissolving 2 mg of Olaparib in 2 mL ethanol. Olaparib solution was added to the Human Serum albumin solution at the rate of 1mL/min and under stirring of 1000rpm.

2.2.3.4 Selection of the suitable conjugating agent for the formation of Nanoparticles:

Glutaraldehyde was selected as a cross-linking agent for the formation of the human serum albumin nanoparticles of Olaparib. The mechanism involved in the cross-linking of the human serum albumin with Glutaraldehyde is that the amino moieties in lysine residues and guanidino side chains in arginine residues of albumin will have a condensation reaction with the aldehyde group of glutaraldehyde. With this mechanism, cross-linking will happen and forms the nanoparticles.

2.2.3.5 Role of the conjugating agents:

Glutaraldehyde possesses unique characteristics that render it one of the most effective protein crosslinking reagents. Glutaraldehyde may react with proteins in multiple ways, such as aldol condensation or Michael-type addition. Conjugating agents will help in the conjugation of the human serum albumin with Olaparib.

2.2.3.6 DOE studies to optimize the process and establish the design space

The NPs were prepared following the formula derived from the Design of Experiment (Design-Expert® version 13). The central composite design (CCD) was applied to optimize the preparation procedure of OLA@HSA NPs formulation concerning suitable particle size (PS), DL, and EE. The selected independent variables, namely the polymer ratio and glutaraldehyde concentration, were considered to be the critical parameters in the preparation process that impact was assessed by studying the parameters like Particle Size (PS), Drug loading (DL), and Entrapment efficiency (EE). These two experimental factors varied in the design at 3 levels in 13 runs.

From the preliminary screening study experiments, it was identified that the amount of polymer in Human serum albumin concentration and Glutaraldehyde concentrations were identified as a critical factor, and we decided to study the impact.

A represents the amount of polymer, and B represents the glutaraldehyde concentration. The main effects of variables on the responses are presented as Particle Size (Z-avg), % Drug loading (DL), and % Entrapment Efficiency (EE).

Table-2.1: Number of runs and actual factors for Central composite design- formulation optimization

S. No	**Factors**		**Actual factors**	
	A	**B**	**Amount of polymer (mg)**	**Glutaraldehyde concentration**
1	0	0	25	5
2	-1	1	12.5	7.5
3	0	0	25	5
4	0	1.414	25	10
5	-1	-1	12.5	2.5
6	-1.414	0	1	5
7	0	-1.414	25	1
8	1	-1	37.5	2.5
9	1	1	37.5	7.5

10	0	0	25	5
11	0	0	25	5
12	0	0	25	5
13	1.414	0	50	5

2.3. Methodologies for the *In vitro* studies:

The different physicochemical parameters evaluated were as follows:

a. Size and surface charge
b. Entrapment efficiency and drug loading
c. Morphology
d. Kinetic Stability
e. X-ray diffraction analysis
f. Differential scanning calorimetry
g. FTIR analysis
h. X-ray photon electroscopy analysis
i. Protein confirmation studies- SDS-PAGE
j. Circular Dichroism spectroscopy
k. Invitro drug release study
l. Hemolysis assay

2.3.1. Size and Surface charge:

The particle size and zeta potential of the HSA NPs and OLA@HSA NPs were determined by dynamic light scattering technique using Zeta-sizer 3600 (Malvern Instruments Ltd. UK). Before the measurement; Lyophilized samples were diluted with deionized water at 25°C. All the samples were analysed to measure particle size and zeta potential.

2.3.2 Drug content estimation:

Olaparib content in the OLA@HSA NPs was checked by UV-Vis spectrophotometer (Jasco UV-670, Japan) and HPLC technique (Shimadzu, Japan). The chromatographic specifications were as follows: reverse phase C18 column of 150 mm x 4.6 mm (Phenomenex, USA), mobile phase by mixing deionized water and methanol at the ratio of 40/60 (v/v), the mobile phase flow rate of 1 mL/min, column temperature of 40 ºC, acquisition time 10 mins, and injection volume 20 µl. The detection wavelength in the photo-diode array (PDA) detector was set to 276 nm. The OLA@HSA NPs were dissolved in ethanol (HPLC grade), and the Olaparib content was measured by HPLC.

2.3.3 Encapsulation efficiency (EE) and Drug Loading (DL):

The OLA encapsulation efficiency (EE) and loading (DL) were assessed in OLA@HSA NPs as per the equation.

$$\text{EE (\%)} = \frac{\text{The weight of the drug entrapped in the nanoparticle}}{Weight\ of total\ drug\ added\ initially\ to\ prepare\ the\ nanoparticles}\ X\ 100$$

$$\text{DL (\%)} = \frac{Weight\ of\ drug\ entrapped\ in\ the\ nanoparticle}{(Weight\ of\ the\ polymer\ and\ drug)}\ X\ 100$$

2.3.4 Surface Morphology: The surface morphology of OLA@HSA NPs was determined using Field Emission Scanning Electron Microscopy (NOVA NANOSEM 450). Samples were

prepared by uniformly distributing a thin layer of nanoparticles over an adhesive carbon tape attached to aluminium stubs. The stubs were then sputter-coated with the gold of desired thicknesses and analysed at 20 kV. The morphology of the nanoparticles was visualized by Transmission Electron Microscopy (TEM, JEM-1200EX, JEOL, and Tokyo, Japan). Briefly, OLA@HSA NPs were stained with uranyl acetate (2% w/v) and later de-stained using distilled water. Further, the samples were dried for 10 min by placing them on copper grids and then visualized (103).

2.3.5. Kinetic stability: The kinetic stability of the formulation was analysed using a UV-Vis spectrophotometer (JASCO, JAPAN) for 30 days. The OLA@HSA NPs were stored at 4 ºC and room temperature for 30 days. The absorbance was recorded by dissolving OLA and OLA@HSA NPs in methanol. The drug absorbance and particle size were checked daily using a UV-Vis spectrophotometer (Jasco UV 670) at a wavelength of 207 nm and Malvern Zeta-sizer (Malvern Instruments Ltd, UK), respectively.

2.3.6. X-ray Diffraction Analysis: Olaparib (OLA) and OLA@HSA NPs were subjected to powder X-ray diffraction using an X-ray diffractometer (Rigaku, Ultima-IV). The lyophilized powder was scanned at a range from 0-100 º 2θ at a scan speed of 10 º/min using a voltage of 40 kV and an electrical current of 30 mA. The spectrum was collected and analysed using the origin software (version 9.2.0) by plotting 2θ and intensity on X and Y axis, respectively.

2.3.7. Differential Scanning Calorimetry: Thermal analysis of OLA, OLA@HSA NPs was performed using DSC (DSC 60, Shimadzu, Japan). Briefly, 5 mg of each sample was weighed and heated from 30-300 °C at a rate of 5 °C/min. The nitrogen environment was maintained by passing dry nitrogen at a 20 ml/min rate through the samples kept in the aluminium pans.

2.3.8. FTIR analysis: FTIR analysis was performed using the KBr pellet method following the previously reported protocol using an FTIR spectrometer (Jasco-4200, USA) (104). The scanning range was kept from 4000 to 400 cm-1.

2.3.9. X-ray photon electron spectroscopy (XPS) Analysis, The chemical analysis of the NPs: The chemical analysis was performed by K-Alpha X-Ray Photoelectron Spectroscopy (Thermo-Fisher, USA). The samples were analysed bypassing the x-ray source (1375 eV) at 10-6 torr vacuum pressure, and the energy of the x-ray was passed at 50 and 20 eV, respectively, for wide and narrow scanning with the electron take-off angle at 568°. The obtained data were analysed using an Advantage software package. Briefly, the survey of the XPS and the narrow spectrum was done utilizing the XPS knowledge view configuration, and a carbon correction process was performed. After the carbon correction, all the spectra were analysed.

2.3.10 Protein conformation studies using SDS-PAGE: SDS-PAGE was performed for the HSA and OLA@HSA NPs, following the previously reported procedure (92). The lyophilized NPs were resuspended in PBS, pH 7.4. Then, 15 µL of 1 mg/ml of each sample was mixed with 5 µL of loading dye. The samples were denatured by boiling at 95 °C for 5 minutes and loaded into the 10% polyacrylamide gel. The gel was run alongside the standard ladder using electrophoresis equipment (Bio-Rad, USA) at a constant voltage of 120 Volts for 3 h. After completion of the run, the gel was stained using coomassie blue for 1 h and then kept for de-staining overnight. The protein bands were observed on the gel, and the images were captured.

2.3.11 Circular dichroism (CD) Spectroscopy:

The secondary structure of HSA in OLA@HSA NPs was analysed using a CD spectrometer (JASCO-1500, USA). Briefly, protein solutions (0.1 µM HSA) were passed through a polyvinylidene difluoride (PVDF) filter. The solutions were placed in quartz cells of path length. 0.1 cm, were run for a scanning range of 190-260 nm under the nitrogen atmosphere at

a scanning speed of 100 nm/ min-1. The helical content in the free HSA and OLA@HSA NPs was analysed from the plot of mean residue ellipticity (MRE) in degcm2 dmol−1 versus wavelength (nm) in Y and X axes, respectively, according to the formula reported previously (105).

2.3.12 In vitro Drug Release Study:

The *in vitro* drug release of Olaparib from OLA@HSA NPs formulation was assessed using the dialysis method (106). In brief, OLA@HSA NPs were resuspended in PBS 7.4 (100 µg/ml OLA concentration) and placed in a dialysis bag of MWCO 12-14 kDa. The bags were placed in the dissolution media and maintained at 37 ºC under continuous stirring. Media (1 mL) was collected and refilled with fresh media at predetermined time points. The samples were analysed by UV-Vis Spectrophotometer to determine the Olaparib content.

2.3.13 Hemolysis Assay

Blood was collected retro-orbitally from the rat eye and mixed with the ethylenediamine tetra acetic acid (EDTA) solution to prevent coagulation [18]. The collected blood was centrifuged at 3000 rpm, 4 °C for 10 minutes to separate the plasma. The isolated RBCs were washed thoroughly and resuspended in PBS 7.4 to form a 5 % v/v RBC suspension. OLA@HSA NPs (12.5-250 µg/ml) were added to the RBC suspensions in tubes and incubated at 37 ºC for 1 h. Triton X-100 (1%) and PBS 7.4 were positive and negative controls, respectively. The samples were then centrifuged at 7000 rpm, 4 °C for 20 minutes. The supernatant was analyzed by measuring the absorbance at 576 nm using a spectra max Multiplate reader (Molecular Devices, USA). The % hemolysis was then calculated using the following formula:

$$\%\ hemolysis = \frac{Abs_{sample} - Abs_{-ve}}{Abs_{+ve} - Abs_{-ve}} \times 100$$

Abs sample, the absorbance of the sample

Abs-ve, the absorbance of the negative control

Abs+ve, the absorbance of the positive control.

2.4. *In vitro* cell-based assays in monolayers: Different in-vitro cell line studies were conducted and which are as follows.

- MTT Assay
- Cell-viability study
- Cellular uptake studies
- Annexin-V assay
- Cell cycle analysis study
- Nuclear staining assay
- DNA fragmentation assay
- Mitochondrial membrane potential assay.
- ROS detection assay.
- Spheroid study
- Growth inhibition/live-dead cells assay in spheroids.

2.4.1. MTT Assay:

MDA-MB-231 and 4T1 cells were seeded in 96 well plates (10000 cells/ wells) and incubated overnight. The next day, old media was replaced with fresh media containing 100 µl of Olaparib and OLA@HSA NPs (0-100 µg/mL) and incubated for 24 h. Then, 50 µl of this MTT reagent solution (5 mg/mL) was added into each well and incubated for 4 h before adding the solvent, DMSO (150 µl), to dissolve the formed purple formazan crystals. After 1 h, the absorbance was measured at 570 nm and a reference wavelength of 620 nm using the Spectramax^{TM} Multiplate Reader (Molecular Devices, USA). The equation used to calculate cell viability is given below:

$$Cell\ viability\ \% = \frac{Absorbance\ of\ sample}{Absorbance\ of\ control} \times 100$$

2.4.2. Cellular uptake studies:

Cancer cells were seeded in a 12-well tissue culture plate (50000 cells/well) and incubated overnight. Rhodamine-labeled OLA@HSA-Rh NPs were added to the cells at a 25 µg/mL OLA concentration and incubated for 1, 4, and 8 h (the procedure to prepare the rhodamine-labeled HSA has been included in the supplementary section). Next, the cells were washed thoroughly, trypsinized, and centrifuged. The cell pellets were suspended in cold PBS and analyzed using a flow cytometer (BD FACS ARIA, Germany). The Forward Scatter (FSC) and Side Scatter (SSC), which are essential for detecting the scatter path of the laser and measuring the scattering angle of 90ºC relative to the laser, were selected, and from this, the debris region was excluded, and the count vs. perCP-CY5-5a was plotted. A total of 10,000 cells were gated for the data acquisition. The data was obtained as the histogram plots in FACS Aria III, BD Biosciences, USA) Software. Similarly, for fluorescence microscopy studies, the OLA@HSA OA NPs-treated cells were washed, fixed using 4% paraformaldehyde, and stained using DAPI (5 min, 1 µg/mL). The images were captured using a fluorescent microscope (Leica, Germany).

2.4.3. Annexin-V assay:

Cancer cells were seeded at a seeding density of 0.5×106/well in 12 well plates. Following overnight incubation, the cells were treated with Olaparib and OLA@HSA NPs (OLA concentration 12.5 µg/mL, 25 µg/mL) for 24 h at 37 °C. The study was carried out as per the manufacturer's instructions. The cells with no treatment served as controls. The cell suspensions were analyzed by flow cytometry (no of gated cells. 10,000) (FACS Aria III, BD Biosciences, USA)). The Fluorescence of FITC and PI was measured at 535 nm and 550 nm, respectively. PI versus Annexin V-FITC with quadrant gating was done as dot plots. Each quadrant represents the cell populations with the following characteristics: necrotic (Q1,

Annexin V−PI+), late apoptosis (Q2, Annexin V+PI+) live cells Q3, Annexin V−PI−), early apoptosis (Q4, Annexin V+PI−).

2.4.4 Cell cycle analysis:

MDA MB231 and 4T1 cells were seeded in a 12-well plate (1 ×106 cells/well). The next day, cells were treated with Olaparib, OLA@HSA NPs (OLA concentrations. 12.5 µg/mL, 25 µg/mL) for 24 h. After the treatment, the cells were harvested and washed with 1 mL PBS (pH 7.4) and then centrifuged at 1500 rpm for 5 min. The pelleted cells were fixed in 70% ice-chilled ethyl alcohol overnight at −20 °C. Fixed cells were centrifuged at 1500 rpm for 5 min. Cell pellets were suspended in ice-chilled PBS (1 mL) followed by centrifugation at 1500 rpm for 5 min. Finally, the cells were resuspended in 0.5 ml of the staining solution (20 µg/mL propidium iodide, 200 µg/mL RNase, and 400 µl PBS 7.4). The cell cycle arrest was then analyzed using the flow cytometer.

2.4.5. Nuclear Staining Assay:

Cancer cells were seeded in a 12-well tissue culture plate (50000 cells/well). After 24 h, the cells were treated with Olaparib, OLA@HSA NPs (OLA concentration as 10 µg/mL) and incubated at 37°C, 5% CO2 for 24 h. The cells were washed using PBS 7.4, fixed using 4% paraformaldehyde, and stained using DAPI (1 µg/mL, 5 min) and acridine orange. 6 µg/mL, 20 min), and observed under a fluorescence microscope at blue (358 nm) and green (480-490 nm) channels for DAPI and acridine orange, respectively.

2.4.6. DNA fragmentation assay

MDA MB 231 and 4T1 cells were seeded in a 12-well tissue culture plate (50000 cells/well). After 24 h, the cells were treated with Olaparib and OLA@HSA NPs (Olaparib concentration. 10 µg/mL) (incubation conditions. 37°C, 5% CO2 for 24 h). After incubation, the cells were washed using PBS 7.4, trypsinized, and collected by centrifugation. Total DNA was isolated using GSure DNA genomic isolation kits. The isolated DNA was checked for absorbance at

260 nm and 280 nm, and the ratio was obtained. A ratio of 1.8 is considered to be pure DNA. The isolated DNA was run on agarose gel (1.5 %) containing 0.5 µg/ml ethidium bromide. The gel was then observed for DNA fragmentation under the microscope using the Fusion Pulse Gel Doc system (Vilber, Germany).

2.4.7 Mitochondrial membrane potential assay

The cancer cells were seeded in a 12-well tissue culture plate (50000 cells/well). After 24 h, the cells were treated with Olaparib, OLA@HSA NPs (OLA concentration. 10 µg/mL) and incubated for an additional 24 h. After incubation, the cells were washed thrice using PBS 7.4, fixed, and treated with JC-1 dye (2 µM) for 20 mins. The labeled cells were observed under the fluorescence microscope (ex./em. 504/529 nm, 20X objective). The cells were treated similarly with JC-1 dye for 30 min for flow cytometry analysis. The cells were pelleted and washed thoroughly with cold PBS, pH 7.4. The mitochondria membrane potential was analyzed for 10000 viable cells by measuring the fluorescence intensity using the flow cytometer (BD FACS ARIA, Germany). The obtained data was then processed using (FACS Aria III, BD Biosciences, USA).

2.4.8 ROS detection assay

MDA MB 231 and 4T1 cells were seeded in a 12-well tissue culture plate (50000 cells/well). After 24 h, the cells were treated with Olaparib, OLA@HSA NPs (OLA concentration as 10 µg/mL) and incubated at 37°C, 5% CO2 for 24 h. After incubation, the cells were washed using PBS 7.4, fixed using 4% paraformaldehyde, and stained with the dye, 2'-7-dichlorofluorescein diacetate (DCHF-DA) solution (5 µM) for 20 mins. The cells were visualized and photographed under the fluorescence microscope (ex/em. 504/529 nm). Likewise, the treated cells were washed, trypsinized, and collected as a cell pellet to suspend in cold PBS before analysis by flow cytometry. The obtained data was then processed using (FACS Aria III, BD Biosciences, USA).

2.4.9 Spheroid study- Penetration in spheroids

Spheroids were grown using the liquid overlay method reported previously (107). Briefly, MDA-MB-231 cells (1 x 104 Cells/well) were seeded in a 96-well plate, which is pre-coated with sterile agarose solution (1.5% w/v). Agarose was prepared by using serum-free DMEM media, and 50 µL was added to each well of a 96-well plate. The formation of dense and spherical spheroids of similar sizes was ascertained by an optical microscope. Spheroids were treated with OLA@HSA-Rh NPs (25 µg/mL OLA) for 24 h and washed with PBS. The Z-stacked images (at fixed X and Y axis) were taken at 10 µm intervals using the confocal laser scanning microscope (TCS SP8, Leica Microsystems, Germany) at 10X magnification. The images were processed using Image J software.

2.4.10 Growth Inhibition/Live-dead cells assay in spheroids

Spheroids were incubated with Olaparib and OLA@HSA NPs (Ola concentration. 6 µg/mL for 24 h). Next, the spheroids were visualized under an optical microscope (Leica Microsystems, Germany) at predetermined time points (0, 3, and 6 days). The images were captured at 10X magnification, and the diameter was measured in the images (108) For live-dead cells estimation, after 24 h of the treatment with OLA and OLA@HSA NPs (6 µg/mL), the spheroids were stained with calcein blue and PI at a concentration of 2 and 4 µM, respectively, and incubated for 30 min at 37 °C. The stained spheroids were observed under the fluorescence microscope using FITC (Ex/em. 495/519 nm) and the rhodamine (540/570 nm) filter.

2.5. *In vivo* studies of Olaparib-HSA nanoparticles:

2.5.1. Tumor inhibition study:

4T1-Luc cells (1.5 × 10 6 in 100 µL) in cold PBS were injected into the left flanks of the 6-week old female balb/c mice. Once the tumor volume reached approximately 80-100 mm3, the mice were randomly divided into three groups (control, Olaparib, and OLA@HSA NPs) (n =

5) and intravenously injected via the tail vein with Olaparib and OLA@HSA NPs (OLA dose. 50 mg/kg). The dosing was given every alternative day for ten days (treatment duration 21 days). Mice were administered with D-luciferin (150 mg/Kg, intraperitoneal) periodically at days 0, 5, 10, 15, and 21 to check the tumor progression. D-luciferin was injected into the mice, 10 min before capturing the image using the IVIS-Lumina in vivo imaging system (PerkinElmer, Inc., USA) (Ex/Em. 620/780 nm). The tumor volume was measured by the equation, length X width2/2, during the experiment every alternate day. The body weight was measured at the same time. On day 21, the tumor mass was surgically extracted from the mice anesthetized using ketamine/xylazine, and weighed. The animals revived after surgery and were monitored via bioluminescence imaging using luciferin-D on day 7, post-surgery. Following live-animal imaging, mice were sacrificed, the lung tissues were weighed and photographed, and the tumor nodules were counted.

2.5.2. Immuno histo-chemistry-TUNEL Assay/detection of Ki-67

The isolated tumor tissues were immersed in OCT medium, frozen, and cryo-sectioned at 4 µm thickness using cryotome (Leica biosystems, Germany). The TUNEL assay (R&D System TM TACS TdT In Situ Apoptosis Detection Kit, Product code- 481230K) was performed according to the manufacturers' instructions. Briefly, the tumor tissues were incubated with terminal deoxynucleotidyl transferase enzyme at 37 °C for 1 h. The TUNEL reaction mixture composed of nucleotide mix, TdT enzyme, and equilibration buffer was added to the fixed tumor tissue slides and incubated in a dark, humid atmosphere at 37 °C for 1 h. Samples were washed three times with 1× PBS to remove the unincorporated fluorescein-dUTP. Next, the tissue sections were stained with DAPI for 5 min. Slides were visualized using a fluorescence microscope (Leica, Germany). For Ki-67 analysis, the tumor sections were blocked in blocking buffer for 1 h and incubated overnight at 4 °C with Ki-67 primary antibody (Rabbit mAb #9129). Next, the tissue sections were washed thrice with PBS and incubated with a secondary antibody

(Alexa Fluor® Plus 488) for 2 h at RT in the dark. Finally, the tissues were washed with PBS and visualized under a fluorescence microscope (Leica Microsystems, Germany).

2.5.3 ROS generation in tumor tissue

The Olaparib, OLA@HSA NPs were injected intravenously into mice bearing 4T1-Luc tumors (~60 mm3) at an equivalent dose of 5 mg/kg. After 24 h of post-injection, the mice were injected intratumorally with the DCFH-DA at a concentration of 25 μM (50 μL). After 30 mins of DCFH-DA administration mice were sacrificed, and tumor tissues were collected and immersed in OCT media. The tumor tissues were cryo sectioned at 5 μm of size using a cryotome (Leica Biosystem, Germany). The frozen tissue sections were observed under a fluorescence microscope (Leica, Germany) using the FITC filter (ex/em 495/519 nm). The images were processed and the intensity of ROS was determined by Image J software. Briefly, the area of the images was selected and the intensity of the region was calculated and compared with the free drug.

2.5.4 H & E staining

Lung sections of 4 μm thickness were processed with xylene, and different concentrations of alcohol, and washed with water. Briefly, The formalin fixation step was performed after animals were sacrificed tumor tissues were dissected into multiple parts. One portion was deep in 10% formaldehyde solution for 24 hrs fixation. After 24 hrs of fixation, the tissues were processed through different concentrations of alcohols (100, 90, 70, 50, and 30%) for 1 h each and kept for dehydration, followed by xylene incubation for 4-5 mins (109). The nuclei were stained with hematoxylin (0.5%) followed by eosin (0.5 %) for staining the cytoplasm. The slides were fixed with mounting media before visualization under an optical microscope with 10 X magnification and a bright field exposure (Leica, Germany).

2.5.5 Western blot

The western blot was performed for determining the protein expression of apoptotic markers PARP1, ɣH2AX, and p53 (cell signalling technology, USA, product code PARP1- 9542, ɣH2AX – 2577 and p53- 9282) in tumor tissues. The tumor tissues were cut into small pieces and homogenized in RIPA buffer containing protease inhibitor and 200uM phenylmethylsulphonyl fluoride (PMSF) using bead homogenizer MINILYS® (Bertin Technologies, France). The protein samples were centrifuged at 16000 g for 20 min at 4 °C, and the supernatant was collected. The extracted proteins were quantified by a BCA protein assay kit (TaKaRa Bio Inc, USA). 30ug of protein were loaded on the sodium dodecyl sulfate-polyacrylamide gels (SDS-PAGE) for separation. The separated proteins were then transferred onto PVDF membranes (Bio-Rad, USA) using the wet transfer method. Then membranes were blocked with 5% (W/V) non-fat milk powder prepared in Tris-buffered saline containing 0.1% (v/v) Tween-20 (TBST) for one hour. The membranes were incubated with primary antibodies for proteins, ɣH2AX and P53(CST, dilution 1:7000 each) overnight at 4 °C. On the next day, the membranes were washed thrice with TBST for 30 min each washing and incubated with secondary antibodies (Anti-rabbit, CST, and 1:7000) for 2 h at room temperature. After completion of the incubation period, the membranes were thoroughly washed. The blots were developed using enhanced chemiluminescence (ECL; Bio-Rad, USA) solution. The blots were detected using ChemiDoc TM Gel Imaging System (Eppendorf fusion plus,). The protein bands were further quantified using Image J software (Version 6.0). β-actin was used as a housekeeping gene for normalization with other proteins.

2.6 Results and Discussion:

2.6.1 Physicochemical characterization of the OLA@HSA NPs

Particle size, DL, and EE were optimized through the response surface method. In the CCD-RSM, 13 experiments were conducted for two factors at three levels. From the experimental results of the CCD, a quadratic polynomial equation was obtained (Z-avg, % DL and % EE) of 13 experiments with the change of the polymer amount and the glutaraldehyde, and the details are as below:

Table 2.2: Data from the DOE design of the formulation experiment by CCD

S. No	Factors		Actual factors		Responses		
	A	B	Amount of polymer (mg)	Glutaraldehyde concentration	Particle size (nm)	Drug loading (%)	Entrapment Efficiency %
1	0	0	25	5	143	7.2	74.12
2	-1	1	12.5	7.5	503.8	4.8	41.6
3	0	0	25	5	143	7.2	74.12
4	0	1.414	25	10	271	6.08	66.8

5	-1	-1	12.5	2.5	161	0.8	6.78
6	-1.414	0	1	5	293	8.51	51.5
7	0	-1.414	25	1	134	1.3	14.7
8	1	-1	37.5	2.5	208.6	1.03	14
9	1	1	37.5	7.5	333	3.9	67.4
10	0	0	25	5	143	7.2	74.12
11	0	0	25	5	143	7.2	74.12
12	0	0	25	5	143	7.2	74.12
13	1.414	0	50	5	261	5.21	83.5

Particle size= 143.00 -21.06 A+ 82.51 B -54.60 AB+ 82.42 A^2+45.32 B^2

A represents the amount of polymer, and **B** represents the glutaraldehyde concentration.

The predicted Z-avg for the experiment with a polymer concentration of (25 mg) and glutaraldehyde volume of (5 μL) is 143 nm, the observed experimental value of Z-avg was 142.3 nm. The particle size of the HSA NPs and OLA@HSA NPs were 127.8 ± 0.32 and 143.5 ± 0.43 nm, respectively, as measured by the dynamic light scattering technique (Figure 1A).

Table 2.3: Particle size data of the optimized formulation using the CCD -DOE design.

Response	Predicted Mean	Observed Value	n value
Particle size	143	142.3	3

2.6.2. Particle-Size:

Dynamic light scattering technique was used to determine particle size, polydispersity index, and surface charge by Zetasizer (Nano ZS90, Malvern Instruments Ltd., U.K.). The hydrodynamic radius was obtained by measuring the nanoparticle size at 25ºC. All samples were analyzed in triplicates **(Figure 2.2).**

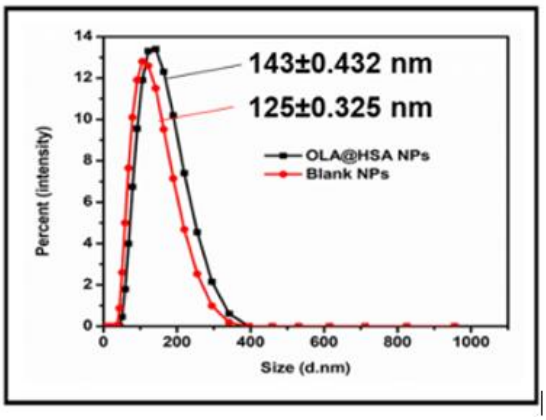

Figure-2.2: Particle Size Histogram of the optimized formulation of OLA@HSA NPs and Blank NPs.

Disussion: The increased size of OLA@HSA NPs compared to HSA NPs was due to the Olaparib entrapment in the NPs. An increase in the polymer concentration leads to higher particle size being observed compared to the lower amount of the polymer; this was due to the cross-linking of the nanoparticles.

2.6.3 Zeta Potential: Zeta potential of the nanoparticles was measured using the Zeta Sizer ZS-90. Samples were diluted with water for injection and evaluated for particle size. The zeta potential was −8.27 ± 1.23 for blank and −11.27 ± 3.25 mV for OLA@HSA NPs **(Figure 2.3)**

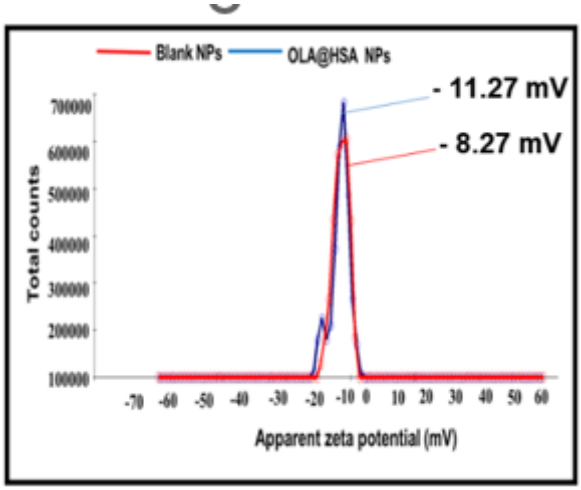

Figure-2.3: Zeta Potential Histogram of the optimized formulation of OLA@HSA NPs and Blank NPs.

Discussion: The slight decrease in the zeta potential in OLA@HSA NPs was observed compared to the plain HSA nanoparticles; this could be due to the anionic nature of the drug-Olaparib.

2.6.4. Drug loading and entrapment efficiency:

% DL and % EE using the polymer amount (25 mg) and glutaraldehyde volume (5 µL) for the predicted values were 7.2% and 74.12%, respectively. The observed experimental values of DL% and EE% were 7.3% and 74.35%, respectively.

Drug loading= 7.20- 0.67 A+1.70 B- 0.28 AB -0.83 A^2-2.42 B^2 and

Entrapment efficiency = 74.12 +9.78 A+20.24B+ 4.65AB -8.73A^2-22.10B^2.

Table 2.4: Drug loading and entrapment efficiency of the optimized formulation using the CCD -DOE design

Response	Predicted Mean	Observed Value	Standard deviation	n value
Drug loading (%)	7.2	7.3	1.51	3
Entrapment efficiency	74.12	74.35	11.85	3

2.6.5.Transmission electron microscopy:

The TEM analysis of the sample proved the nano-size of both blank and drug-loaded NPs. The morphology of the prepared NPs was determined using Transmission electron microscopy and proved to be in the nanosized for the test sample and blank formulation **(Figure 2.4).**

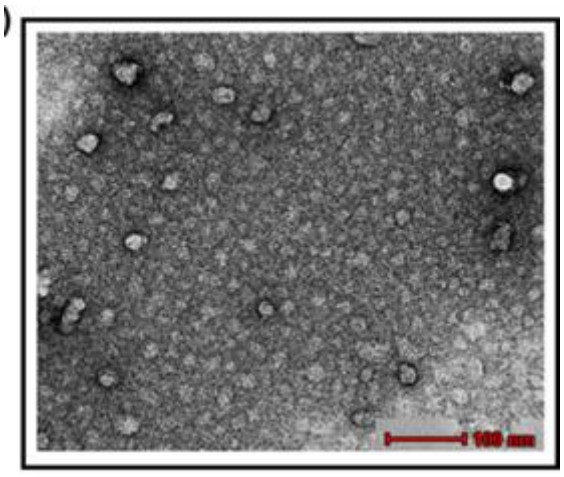

Figure-2.4: TEM analysis of Olaparib- Human Serum albumin nanoparticle

2.6.6. Scanning electron microscopy:

The morphology of the prepared NPs was determined using scanning electron microscopy and found to be spherical **(Figure 2.5).**

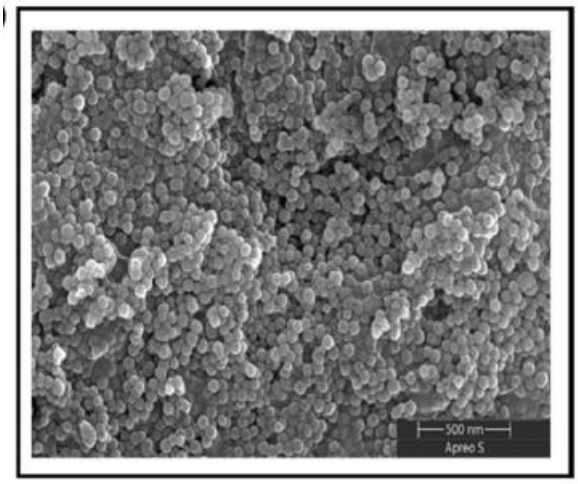

Figure-2.5:SEM analysis of Olaparib- Human Serum albumin nanoparticle.

2.6.7. Kinetic Stability Studies-Particle Size:

The stability of OLA@HSA NPs on storage at 4 °C and the room temperature was determined by analyzing the particle size and % drug loading (DL). The particle size and DL were 212.32 ± 2.61, 7.12 ± 1.21%, respectively, for OLA@HSA NPs after 30 days of storage at 4 °C, compared to 655.40 ± 2.1, 0.56 ± 0.05% at room temperature.

Table 2.5: Kinetic stability study data of the formulation stored at 4℃ and 25℃ for 30 days.

Storage Condition	No of days stored	Particle Size	% Drug Loading	Remarks
Refrigerated condition (4℃)	30	212.32 ± 2.61	7.12 ± 1.21%,	n=3
Room Temperature (25℃)	30	655.40 ± 2.1	0.56 ± 0.05%	n=3

Disucssion: The storge stability data indicated that the NPs could be considered stable for 5-10 days following reconstitution, after which the NP's size increased the size with a decrease in %DL. The stability of NPs at 4°C was not compromised to the extent as NPs at 25°C

2.6.8.XRD Analysis:

The XRD analysis of the OLA@HSA NPs revealed the amorphous nature of olaparib in the NPs with no characteristic peaks of OLA **(Figure 2.6).**

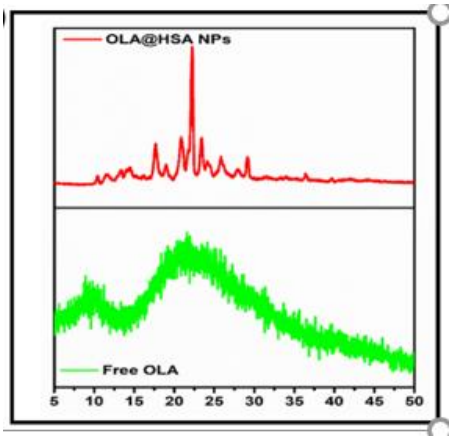

Figure-2.6: XRD spectrum of Free Olaparib and OLA@HSA Nano-particle formulation

Discussion: The disappearance of 2θ peaks of Olaparib in the X-ray powder diffractogram spectrum of OLA@HSA NPs is indicative of its entrapment of Olaparib into the NPs.

2.6.9. DSC Thermal Analysis:

The DSC analysis showed an endothermic peak of Olaparib at The DSC analysis showed an endothermic peak of olaparib at 236 °C, which disappeared in the thermograms of OLA@HSA NPs **(Figure 2.7).**

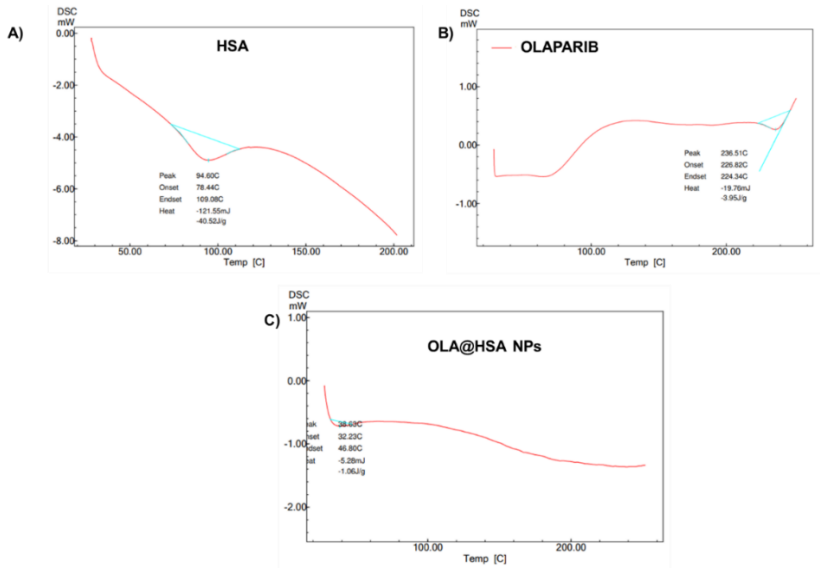

Figure-2.7: DSC thermogram of HSA (A), Olaparib (B)and OLA@HSA (C) Nano-particle formulation

Discussion: From the DSC studies the disappearance of the melting point of OLA in the DSC thermogram of OLA@HSA NPs indicated successful encapsulation. Them endothermic peak at 94° is characteristic of HSA (111). Therefore, the DSC thermograms supported the reliability of the NPs – preparation procedure. (Figure 2.7).

2.6.10. FTIR Analysis:

FTIR spectra of HSA, OLA, and OLA@HSA NPs. Characteristic transmittance peaks of OLA were found at 1440.2, 1653.1, and 3215.9 cm−1 wavenumbers corresponding to the C-F bond, carbonyl group, and secondary amide stretching vibrations, respectively. The FTIR spectra of HSA showed characteristic peaks at 1648.3 cm−1 (N-H bending), 1722.8 (C = O stretching), and 3432.7 cm−1 (OH group H-bonded). OLA@HSA NPs showed peaks at 1236.1, 1560.3, 1724.2, and 3462.7 cm−1 wave numbers representing amine group, C-F bond, amine group, and OH group stretching vibrations, respectively (Figure 2.8). FTIR analysis was performed using an FTIR (Jasco-4200, USA) by using the KBr pellet method (15). FTIR spectra were recorded by scanning pellets over a range of 4000 to 400 cm^{-1}.

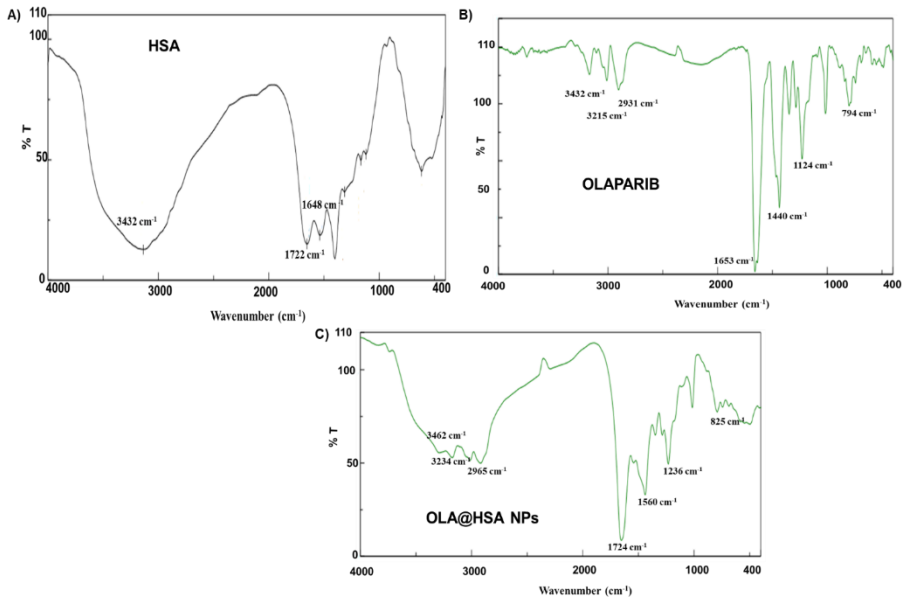

Figure-2.8: FTIR analysis of HSA(A), Olaparib(B), and OLA@HSA(C) Nano-particle formulation

Discussion: The characteristic peaks of both OLA and HAS were observed in the FTIR spectra of OLA@HSA NPs. Hence, the analysis confirmed the chemical structure of the NPs.

2.6.11. Circular Dichroism (CD) spectroscopy:

The CD spectra of HSA and OLA@HSA NPs showed two negative bands, at 208 and 222 nm, characteristic of α-helix. The mean residue ellipticity values at 208 and 222 nm decreased in OLA@ HSA NPs compared to native HSA. The α-helix and β-sheet values were calculated to be 63.65 ± 0.88 and 7.52%, respectively, for HSA and 50.22 ± 0.32 and 14.22% for OLA@HSA NPs **(Figure 2.9).**

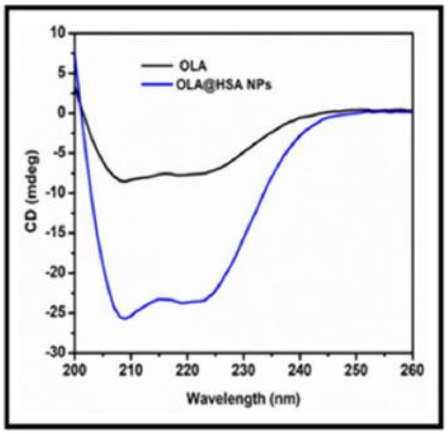

Figure 2.9: CD spectra Analysis of HSA, OLA@HSA NPs

Discussion: The CD spectroscopic data determines the ligand binding with the protein, influencing the protein's secondary structure (112). The decrease in the MRE values at 208 and 222 nm in OLA@HSA NPs indicated the decrease in α-helical content (113). The decrease of α-helical contents by approximately 13.4% indicated the influence of glutaraldehyde conjugation or interaction with Olaparib with HSA in OLA@HSA NPs. The slight conformational changes induced by the protein binding were observed. However, the secondary protein structure remained predominantly α-helical in OLA@HSA NPs.

2.6.12. SDS PAGE Analysis:

The SDS PAGE bands for HSA and OLA@HSA NPs matched the protein marker at 66 KDa. The bands were of equal thicknesses **(Figure 2.10).**

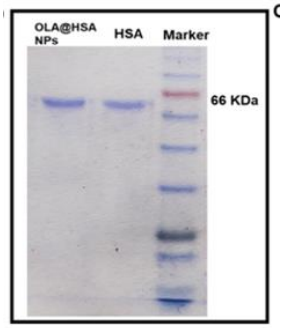

Figure2.10: SDS PAGE of HSA, OLA@HSA NPs

Discussion: The SDS-PAGE analysis revealed the presence of HSA in OLA@ HSA NPs. The molecular weight of HSA did not increase, which indicated that there was no aggregation, and the NPs formation did not change the overall protein charge.

2.6.13. Hemolysis study:

A hemolysis study was performed to determine the maximum cytocompatibility of the nano-particles concentration. The assay result indicated that the percent hemolysis increased with increasing NPs concentration in the plasma. The highest tested concentration of OLA@ HSA NPs (250 µg/mL) was observed to be as high as 5.1% hemolytic, considering the positive control to be 100% hemolytic **(Figure 2.11).**

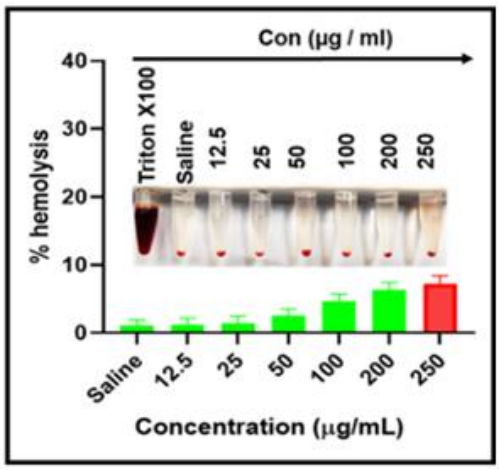

Figure 2.11: percent hemolysis of OLA@HSA NPs at different concentrations

Discussion: Haemolysis is the damage to the red blood cells resulting in the release of hemoglobin in the plasma (114). As the clinical use of NPs is increasing, a thorough understanding of the safety of the circulating NPs in the bloodstream is much needed. Hemolysis occurs if the red blood cell membranes are damaged by the NPs, which causes the release of haemoglobin into the bloodstream. The haemoglobin release could lead to severe side effects, including renal toxicity, hypertension, and anaemia (115). In our study, the haemolytic % of 5.1, as displayed by the maximum tested concentration of 250 µg/mL is considered to be slightly haemolytic.

2.6.14. Invitro-release study:

The cumulative Olaparib release from OLA@HSA NPs under three different pH conditions, pH 7.4, 6.5, and 5.5, at different time points up to 48 h, is represented in Figure 2.12. The drug release was highest at pH 5.5 (83.3%) and the least at pH 7.4 (39.2%) after 48 h. The UV absorption spectrum indicated increased absorbance of OLA@HSA NPs at pH 5.5 than at pH 6.5 and 7.4 **(Figure 2.12).**

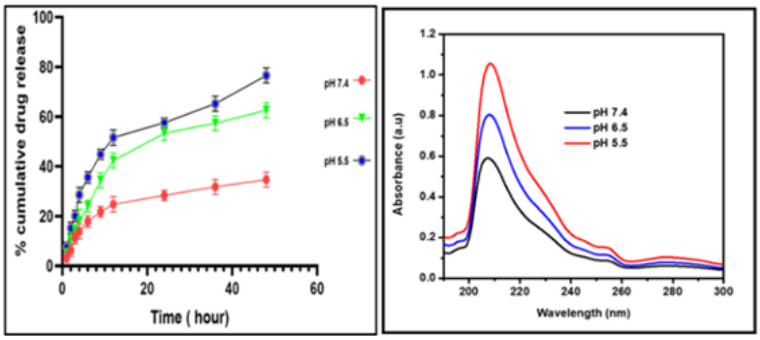

Figure 2.12: UV−vis absorbance spectra of OLA@HSA NPs at different pH

Discussion: OLA release from OLA@HSA NPs might involve two different mechanisms. The initial burst release within 10 h might be attributed to the diffusion/pH-dependent drug dissolution. Further, a sustained release might be related to polymer hydrolysis and erosion, as indicated previously (116).

2.6.15. In-Vitro cell-based assay in monolayers- Cell Viability:

A time and concentration-dependent decrease in cell viability was observed following the treatment of both the cancer cells with Olaparib and OLA@HSA NPs in the MTT assay **(Figure 2.13).** In general, the cytotoxicity produced by OLA@HSA NPs was higher compared to the free Olaparib treatment. OLA@HSA NPs demonstrated cell viability of 32.21±2.60% (24 h), 21.21±3.85% (48 h), OLA 43.66±2.43% (24 h), 30.25±3.42 (48 h) in 4T1 cells. Similarly, in MDA MB 231 cells, OLA@HSA NPs demonstrated cell viability of 25.36±1.25 (24 h), 12.36±2.65 (48 h) compared to 39.36±2.34 (24 h), 25.32±1.35 (48 h) after free Olaparib treatment at the highest drug concentration (100 µg/ml). The IC50 values of OLA@HSA NPs towards 4T1 were calculated as 10.52 and 6.54 µM following 24 h and 48 h of treatment compared to 15.41 and 11.47 µM after free Olaparib treatment, respectively. The IC50 values of OLA and OLA@HSA NPs towards MDA MB 231 were 7.22 and 3.12 µM at 24 h, and 12.32, and 9.72 µM for 48 h, respectively.

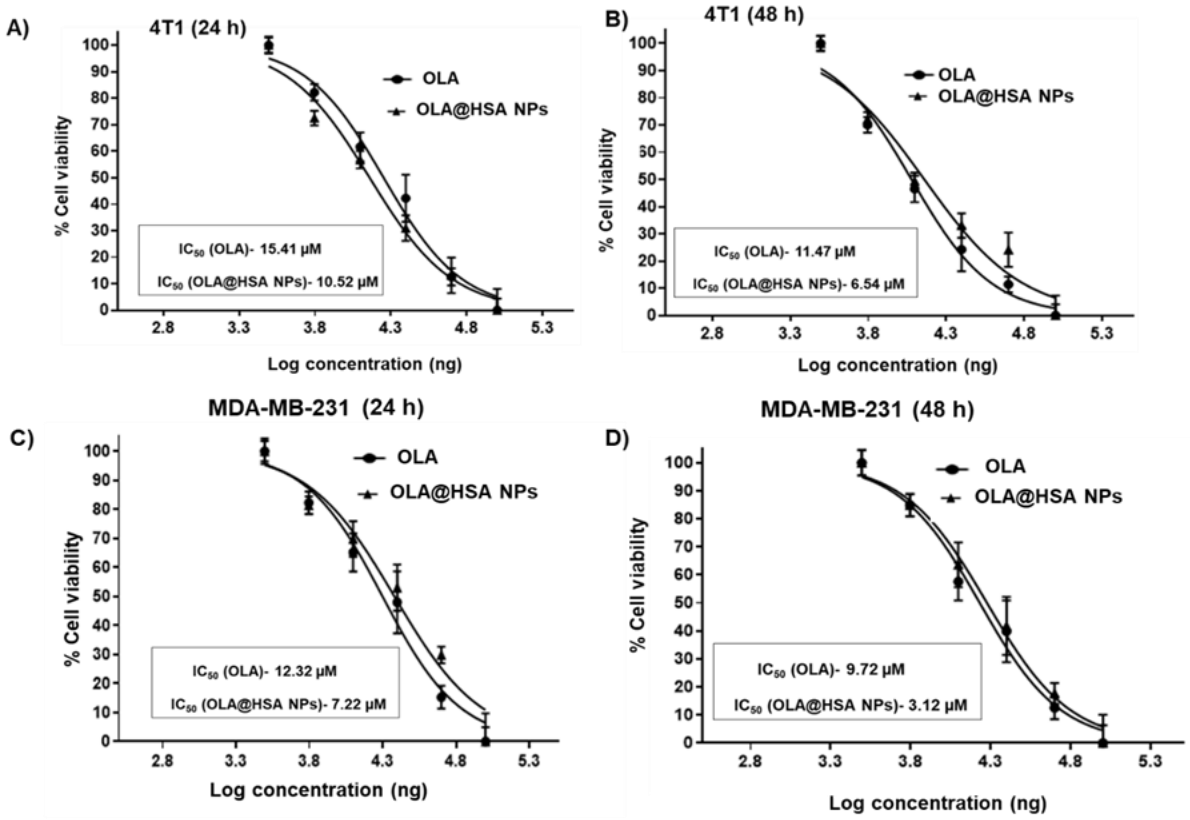

Figure 2.13: *In vitro* evaluation of the anticancer activity of OLA, OLA@HSA NPs. The dose-response curve for the determination of IC_{50} values of free OLA, OLA@HSA NPs (24 and 48 h) in cultured 4T1 (A, B) and MDA-MB-231 cancer cells (C, D).

Discussion:

According to the cell viability assay data, the OLA@HSA NPs showed superior cytotoxicity than OLA at all concentrations due to their ability to penetrate efficiently into the cells compared to free Olaparib (117). The formulations induced a higher level of apoptosis, which could be due to the enhanced cellular uptake of Olaparib via the nanocarrier systems.

2.6.16 Cellular uptake assay

An increase in the fluorescence intensity of cells when observed under 530 nm of emission wavelength was indicative of the cellular association of OLA@HSA-Rh NPs. A time-dependent increase in the cellular internalization of NPs was observed in both cell lines, as

visualized under a fluorescence microscope and quantitatively measured using flow cytometry **(Figure 2.14).** The bright red fluorescence of OLA@HSA-Rh NPs was increased in a time-dependent manner in both the tested cell lines. The geometric mean fluorescence intensities of OLA@HSA-Rh NPs-treated 4T1 cells at 1, 4, and 8 h were 832.21 ± 20.32, 2122.56 ± 32.45, 3054.74 ± 52.32, respectively. Likewise, MDA-MB-231 cells improved NPs cellular association observed in the incremental geomean values of 982.36 ± 24.59, 2381.74 ± 48.53, and 3456. 65 ± 51.32, at 1, 4, and 8 h, respectively.

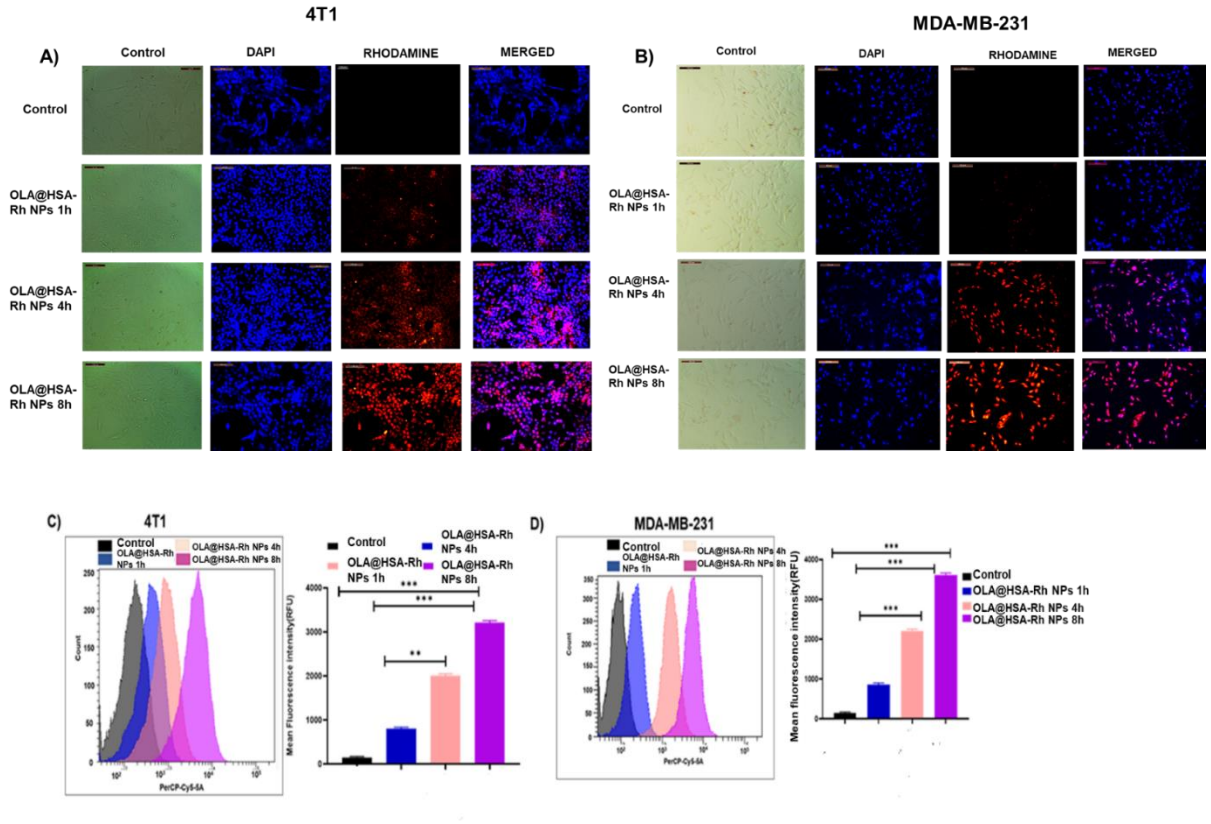

Figure 2.14: Cellular uptake of rhodamine-labeled, OLA@HSA-Rh NPs in 4T1 cell, MDA-MB-231 cell lines (Olaparib concentration. 25 µg/mL) (A and B). Red and Blue signals present cells stained by rhodamine and DAPI, respectively; assessment of the geometric mean of fluorescence of the 4T1 (C), MDA-MB-231 cells (D) at 1, 4, 8 h incubation by histogram plots and bar graphs. The data in the bar graphs represent mean ± standard deviation, calculated from three sets of experiments.

Discussion:

A cellular uptake study revealed that the HSA NPs were taken up by the cancer cells effectively in a time-dependent manner (118). More DNA damage was indicated by increased cell cycle arrest in G2/M by OLA@HSA NPs than free Olaparib treatment. The increase in G2/M arrest by OLA@HSA NPs suggests the ability of the formulation to inhibit the cellular division at the mitotic phase and thus control the doubling time and proliferation rate (119).

2.6.17. Annexin-V assay:

Annexin V assay measured the extent of cellular apoptosis following treatment with Olaparib and OLA@HSA NPs **(Figure 2.15).** The concentration-dependent increase in apoptosis and necrosis was observed for OLA@HSA NPs. The total apoptotic/necrotic 4T1 cells populations in Q2 and Q4 quadrants were 12.32 ± 1.24%, 29.41 ± 0.85 %, and 43.02 ± 0.25, for Olaparib (conc25 µg), OLA@HSA NPs (12.5 µg) and OLA@HSA NPs (25 µg), respectively. Likewise, the percentage apoptotic/necrotic MDA-MB-231 cells populations for Olaparib, OLA@HSA NPs (12.5 µg), OLA@HSA NPs (25 µg) were 15.02 ± 1.15%, 36.02 ± 0.32 % and 45.02 ± 0.25, respectively.

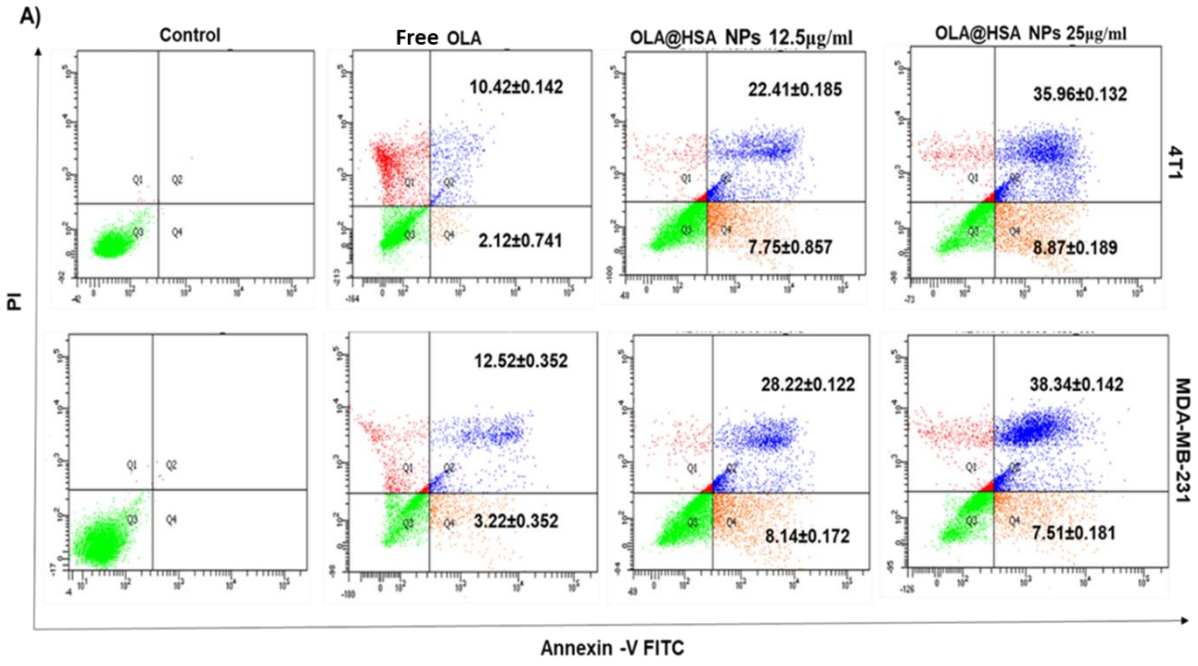

Figure 2.15: Annexin V assay (A). The extent of apoptosis was evaluated by analysing 4T1, MDA-MB-231 cells treated with free drug (OLA), OLA@HSA NPs at Olaparib concentration of 25 µg/mL (incubation time. 24 h) by using flow cytometry. The Q3 and Q4 quadrants represent early and late apoptosis, respectively (gated cell number. 10,000); cell cycle arrest by OLA, OLA @HSA NPs.

Discussion:

The increase in G2/M arrest by OLA@HSA NPs suggests the ability of the formulation to inhibit the cellular division at the mitotic phase and thus control the doubling time and proliferation rate (119). The OLA-loaded HSA NPs caused significantly higher DNA fragmentation and cytoplasmic shrinkage in cells than free Olaparib treatment. The formation of apoptotic bodies and chromatin condensation were more noticeable in OLA@HSA NPs. The DNA damage was more prominent in gel electrophoresis [109].

2.6.18. Cell cycle analysis

The cell cycle analysis plot is represented in Figure 2.16. The maximum arrest of cells in the G2-M phase by OLA@HSA NPs treatment was observed compared to Olaparib treatment, with 8.42 % for control cells, 16.23, 21.23, and 34.36 % for 4T1 cells, and 15.32, 22.32, and 35.32 % for MDA-MB-231 cells for free Olaparib, OLA@HSA NPs at concentrations, 12.5 and 25 µg/mL, respectively. Migration of the cell population from the G1 phase to the G2/M phase predominantly was observed with the OLA@HSA NPs treatment at both the tested concentrations **(Figure 2.16).**

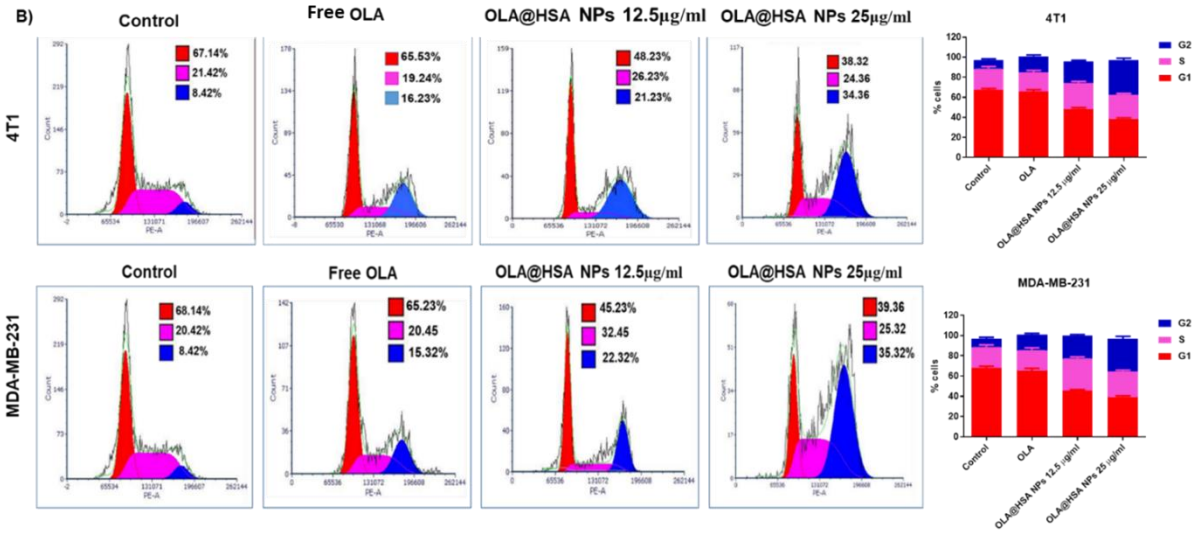

Figure 2.16: Cell cycle Analysis (B) as analyzed by flow cytometry. The histogram plots (left) and the representative bar graph show cell populations in various stages of cell cycles.

Discussion:

The formulations induced a higher level of apoptosis, which could be due to the enhanced cellular uptake of Olaparib via the nanocarrier systems. A cellular uptake study revealed that the HSA NPs were taken up by the cancer cells effectively in a time-dependent manner (118). More DNA damage was indicated by increased cell cycle arrest in G2/M by OLA@HSA NPs than free Olaparib treatment. The increase in G2/M arrest by OLA@HSA NPs suggests the

ability of the formulation to inhibit the cellular division at the mitotic phase and thus control the doubling time and proliferation rate (119).

2.6.19. DNA fragmentation/nuclear staining assay

The appearance of fragmented DNA bands with a ladder-like pattern was more prominent in OLA@HSA NPs-treated cells' total DNA than in free Olaparib-treated DNA extract (Figure 2.17). OLA@HSA NPs treated cells exhibited more nuclear fragmentation (NF) and cytoplasmic shrinkage (CS) than Olaparib treatment. Blebbing in the cell membranes indicative of late apoptosis was observed in OLA@HSA NPs-treated cells **(Figure 2.17).**

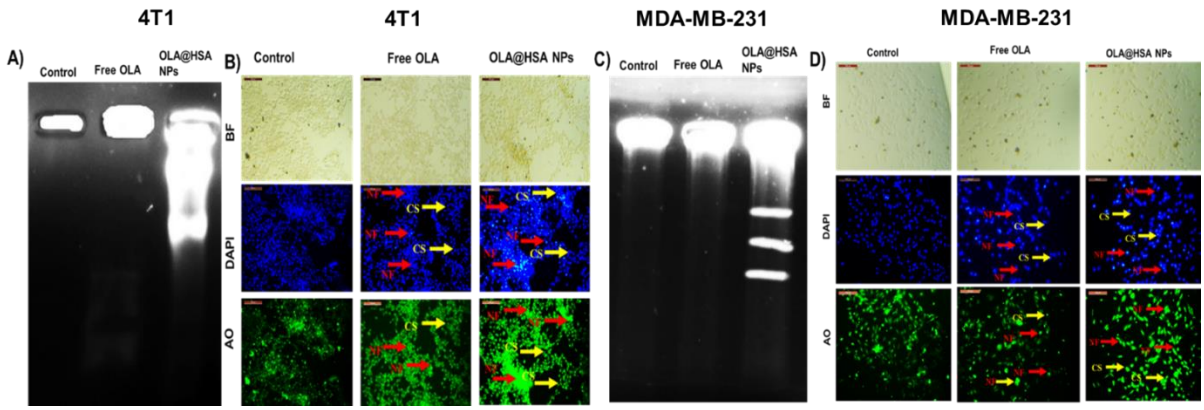

Figure 2.17: Analysis of DNA fragmentation. DNA extracted from 4T1 cells and MDA-MB-231 cells was viewed on ethidium bromide-stained gel. DNA from untreated cells (Control), free Olaparib, OLA@HSA NPs-treated cells (A and C). Nuclear staining of 4T1 cells, MDA MB231 cells with acridine orange (AO) (stained in green color) and DAPI (stained in blue color). Arrows indicate cytoplasmic shrinkage (CS) and nuclear fragmentation (NF) (B and D).

Discussion:

The OLA-loaded HSA NPs caused significantly higher DNA fragmentation and cytoplasmic shrinkage in cells than free Olaparib treatment. The formation of apoptotic bodies and chromatin condensation were more noticeable in OLA@HSA NPs. The DNA damage was more prominent in gel electrophoresis (120).

2.6.20. Mitochondrial membrane potential assay.

The fluorescence micrograph of control cells treated with JC-1 exhibited strong red fluorescence, which merged with the green fluorescence of the cells with Olaparib treatment giving rise to orange and yellow signals in Olaparib-treated 4T1 and MDA-MB-231 cells, respectively (Figure 2.18A and B). The OLA@HSA NPs-treated cells showed a bright green signal under the fluorescence microscope, indicating the presence of depolarized mitochondria. The flow cytometry data supported the fluorescence spectroscopic observation **(Figure 2.18C).** The fluorescence emission shift from red to green was observed with the highest shift of cell population from Q2-1 to Q4-1 in OLA@HSA NPs-treated cells than free Olaparib-treated cells. The JC-1 monomer/ aggregate ratio (green/red cell populations) was 35% in Olaparib-treated cells and 75 % in the OLA@HSA NPs-treated group. 4T1 and MDA MB 231 cells treated with OLA@HSA NPs showed mitochondrial membrane disruption, a major apoptosis hallmark.

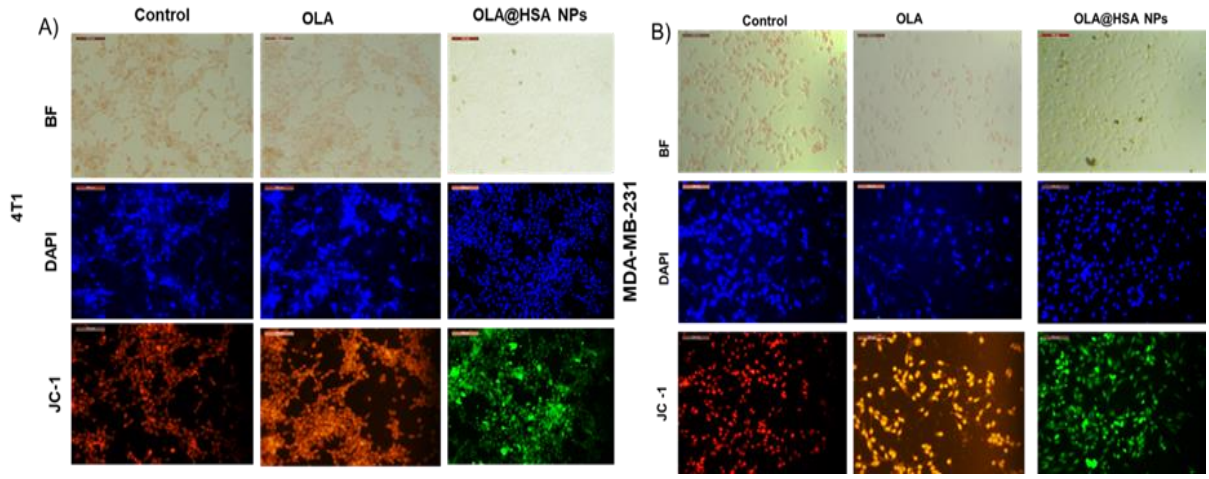

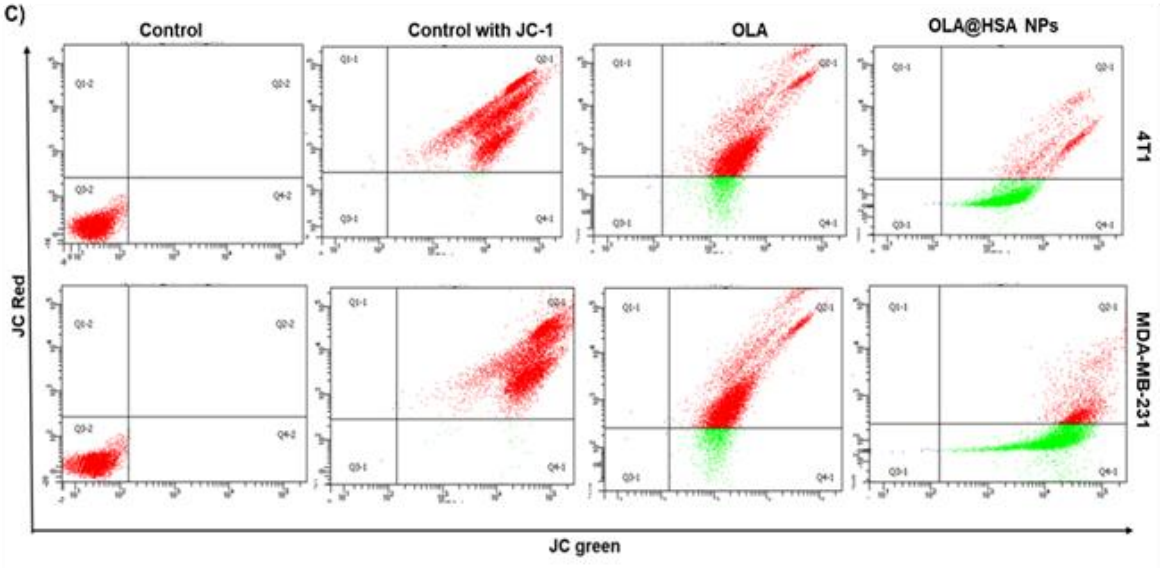

Figure 2.18: Detection of mitochondrial membrane potential by JC-1 staining in OLA, OLA@HSA NPs treated cells, 4T1 and MDA-MB-231 by fluorescence microscopy (A and B), and flow cytometry (C). Nuclei stained with DAPI were visualized under laser, ex/em. 358/461. The JC-1 fluorescence was visualized under a laser, ex/em. 488/530 nm in both fluorescence microscopy and flow cytometry. Gated cell population. 10,000 for the flow cytometry analysis.

Discussion:

A remarkably higher level of mitochondrial damage was observed in OLA@HSA NPs groups than the free drug, as indicated by the strong green signal of monomeric JC-1.

2.6.21. ROS generation

The generation of reactive oxygen species following treatment was indicated by the strong green fluorescence of 2'-7' dichlorofluorescein. OLA@HSA NPs-treated cells displayed more intense green fluorescence than the free Olaparib-treated cells **(Figure 2.19A).** The quantitative estimation of fluorescence was performed by flow cytometry **(Figure 2.19B).** The result indicated that the 4T1 cells treated with OLA@HSA NPs showed a geometric mean of fluorescence, 2800± 18.65, compared to 1425 ± 17.63 after Olaparib treatment. Similarly, a significant increase in ROS generation was observed in MDA-MB-231 cells treated with

OLA@HSA NPs (than free Olaparib, with the geomean of fluorescence of 3452 ± 30.41 and 1635. ± 18.71 for OLA@HSA NPs and free Olaparib, respectively.

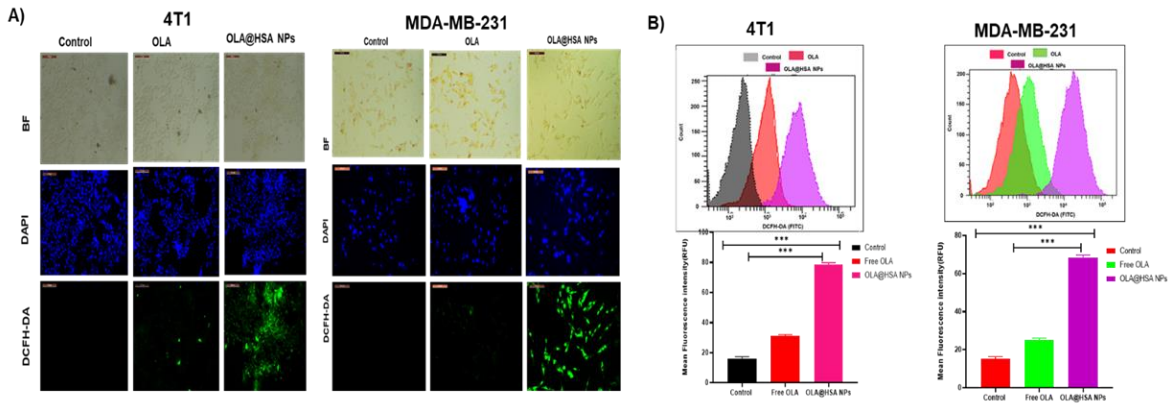

Figure 2.19: Intracellular ROS generation in 4T1 and MDA-MB-231 cells treated with OLA, OLA@HSA NPs by fluorescence microscopy (A) and Flow cytometry (B). The ROS level was detected by tracking the fluorescence of DCFHDA dye (ex/em. 488/525 nm).

Discussion:

Cytotoxic intracellular ROS could cause damage to mitochondria in cells, resulting in cell death (121). High levels of ROS could disrupt the mitochondrial permeability transition pore and destroy the integrity of the mitochondrial membrane, resulting in immediate dissipation of mitochondrial Transmembrane potential and osmotic swelling of the mitochondrial matrix (122).

2.6.22. Spheroids study

As shown in Figure 2.20A, the growth of the OLA@HSA NPs treated spheroids was significantly reduced than the free Olaparib group. Over time, an increment in the diameter of untreated spheroids (size reached up to about 925 µm) was observed, which was significantly bigger in volume than the spheroids treated with OLA@HSA NPs and free Olaparib. The average diameter was found to be 925.23 ± 22.61, 514.15 ± 23.52, and 352.20 ± 10.61 µm in

control, free Olaparib, and OLA@HSA NPs treated spheroids, respectively, on day 4 **(Figure 2.20A)**. A live/dead cell assay was performed to estimate the treatment-induced cytotoxicity. The spheroids treated with OLA@HSA NPs showed intense red fluorescence compared to the spheroids with free Olaparib treatment, suggesting the presence of a higher number of dead cells population (**Figure 2.20B**). The Z-stacked images of spheroids treated with OLA@HSA-Rh NPs showed red fluorescence in the canter slices (50-70 µm) after 4 h, indicating time-dependent spheroid uptake **(Figure 2.20C).**

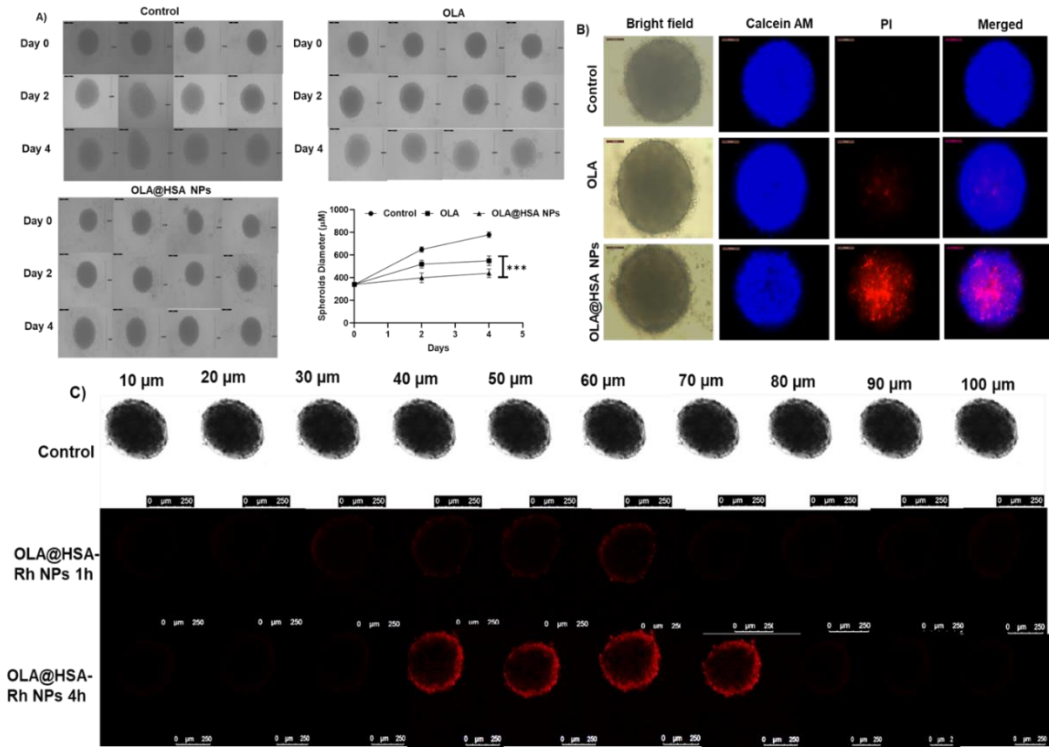

Figure 2.20: Growth inhibition study in spheroids. Bright-field images of MDA-MB-231 spheroids following treatment with OLA, OLA@HSA NPs at continuous OLA concentration of 6 µg/mL, captured at day 0, 2, and 4 days at 10×magnification. A graph representing the change in spheroidal diameter over time (mean of diameter in µm with standard deviation; n = 3). The significance of difference was assessed by one-way ANOVA, and **p < 0.01, ***p < 0.001 (A); Live-dead cells assay in spheroids treated with OLA, OLA@HSA NPs at OLA

concentration of 6 μg/mL for 24 h (B); uptake of rhodamine-labeled OLA@HSA-Rh NPs by MDA-MB-231 spheroids. Confocal microscopic Z-stacked images of MDA-MB-231 spheroids treated with OLA@HSA NPs at an OLA concentration of 25 μg/mL for 1 h (up) and 4 h (down) (C).

Discussion:

Multicellular spheroids mimic the three-dimensional tumor growth pattern, unlike cells grown in monolayers (123). Deeper tissue penetration of NPs was observed in a time-dependent manner. The NPs treatment showed improved tumor tissue damage/necrosis, as indicated by the strong red PI fluorescence. The cell death resulted in spheroid shrinkage significantly to both free drug/drug-loaded NPs-treatments compared to the untreated spheroids (124).

2.6.23 *In vivo* study:

In the tumor inhibition study, both the treatments, OLA@HSA NPs, and free olaparib, suppressed the growth of the tumor to a significantly greater extent than the control (no treatment). OLA@HSA NPs treatment showed higher tumor volume reduction than free Olaparib treatment. The tumor volumes on day 21 were 1205.32 ± 6.35, 639.22 ± 5.2, and 205.32 ± 2.5 mm3 for saline, free Olaparib, and OLA@HSA NPs treated animals' groups **(Figure 2.21A).** The mouse body weight increased slightly during the treatment **(Figure 2.21B)**. The average weight of the tumors for control, free Olaparib, and OLA@HSA NPs groups were 3.85 ± 0.12, 1.66 ± 0.32, and 0.56 ± 0.22 g, respectively **(Figure 2.21C and D).** The luciferin D-mediated bioluminescence in 4T1-Luc tumors was captured in IVIS-Lumina live animal imaging facility, and the images have been displayed in a series (n=3) in Figure 10E. The spike in the signal in the region of interest in control groups indicated the highest tumor growth rate, followed by free Olaparib groups and OLA@HSA NPs **(Figure 2.21E).**

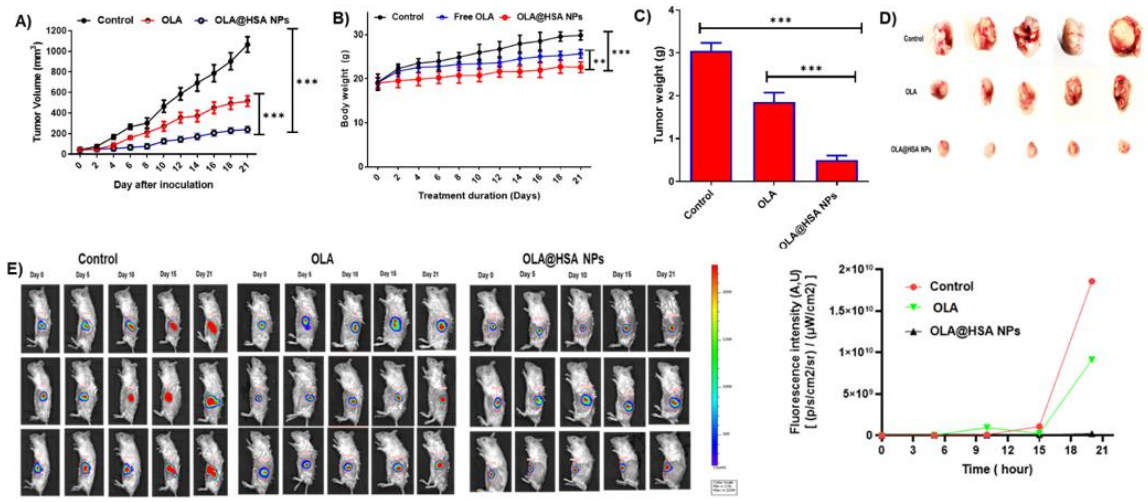

Figure 2.21: Assessment of therapeutic Efficacy of OLA, OLA@HSA NPs in 4T1-Luc-tumor-bearing BALB/C mice. Graphical representation of tumor volume vs. days during treatment (A); measurement of body weight during the treatment (B); the average weight of tumors isolated from various treatment groups (C); and representative tumors isolated from mice post-treatment. Data represent mean ± SEM, n =4. **p < 0.01, and ***p < 0.001 (D); Tumor growth was assessed at the indicated time points by whole animal bioluminescence imaging as shown in a representative mouse and bioluminescence expressed as photon flux/second (ph/s) (E);

Discussion:

The *in vivo* experiment strongly proved that the OLA@HSA NPs treatment was superior in producing a therapeutic effect than the free drug treatment. The solid tumor represents acidic conditions (low PH), hypoxia, and nutrient-deprived microenvironments, creating favorable conditions for drug release due to the pH-dependent activity of formulation. The leaky tumor vasculature and the EPR effect, on the other hand, create a space for formulation to enter inside the tumor vascular space. Represent, among many obstacles, an opportunity for the facilitated delivery of macromolecular drugs into the extravascular space (125). There was a significant reduction in the tumor volume in the OLA@HSA NPs-treatment group to control and free Olaparib treatments. The non-reducing body weights indicated the safe use of the NPs. The

live animal imaging sheds light on the tumor growth pattern over 21 days. The reduction in bioluminescence intensity in the OLA@HSA NPs treatment groups due to cell death indicated successful treatment outcomes.

2.6.24. Immunohistochemistry

The TUNEL-positive cells, as indicated by the green fluorescence, were abundant in cryo-sectioned tumor tissues from the mice which received the OLA@HSA NPs treatment (**Figure 2.22F)**. The treatment with free Olaparib caused a relatively greater extent of DNA fragmentation than saline treatment. The nuclear protein Ki-67 was reduced in OLA@HSA NPs-treated tumors **(Figure 2.22G).** The intense green fluorescence signal in control tumors indicated the presence of the proliferative marker, Ki-67, which was drastically reduced in the nanoparticles-treated tumor. The reduction in the rate of cell proliferation could be due to the induction of apoptosis to a greater extent in OLA@HSA NPs treatment groups, as evident further in the ROS production to a greater extent than in free Olaparib-treated groups (**Figure 2.22H).**

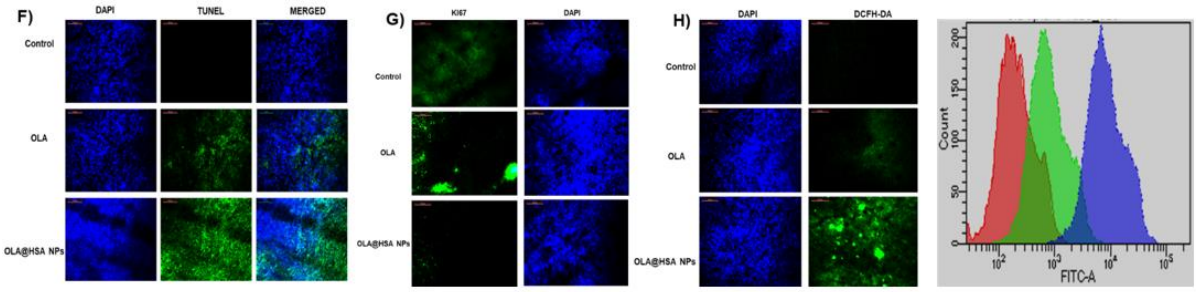

Figure 2.22: representative images of tumor sections after TUNEL staining (F); fluorescent images of tumor tissue sections for immune-histochemical analysis of Ki-67 (G); detection of ROS level in tumor tissues by fluorescence microscopy and flow cytometry analysis (H).

Discussion:

The immunohistochemistry of the tissue sections indicated a higher number of apoptotic nuclei in OLA@HSA NPs-tumor groups than untreated control and Olaparib groups in the TUNEL assay, where the free 3'-hydroxyl termini of DNAs are labeled. The higher labeling is indicative of the presence of more fragmented DNA by double strands break, leading to apoptosis. The decreased presence of proliferative marker, ki-67, and increased presence of ROS was also observed in the tumor tissue section of the OLA@HSA NPs treatment group, revealing the promising treatment outcome.

2.6.25. Lung metastasis

The breast cancer metastasis in the lungs was visualized by imaging the live animals using the *in vivo* imaging system (IVIS). The highest bioluminescence signal was evident in control, reduced in free Olaparib-treated groups, and practically invisible in the OLA@HSA NPs group **(Figure 2.23A).** The bar graph representation in Figure 2.23A compared the photon flux in the lung tissues of mice in three treatment groups. The bioluminescence was significantly lower following NPs-treatment than the free drug. The ex vivo images of lung samples dissected from the tumor-bearing mice supported the live animal imaging data **(Figure 2.23B).** The growth of cancer cells in the lungs in colonies indicated by white nodules was visible in the control group, which decreased significantly in the treatment groups, including free Olaparib and OLA@HSA NPs **(Figure 2.23D).** The histology of the lung of a normal mouse has been represented in Figure 2.23C as a control. The loss of alveoli and airway was distinct in the infected lung, whereas the shrinkage in the airways and denser cell growth as nodules were evident in the free Olaparib-treated groups. The microscopic view of the lungs from the OLA@HSA NPs-treated groups showed no sign of hyperplasia or cancer metastasis. Colonizing cancer cells in the lungs increased their size and weight proportionally. The weight of the lungs in the OLA@HSA NPs-

treated group (0.213 g) was significantly lower than free Olaparib (0.412 g) and saline-treated groups (0.652 g), respectively (Figure 2.23E).

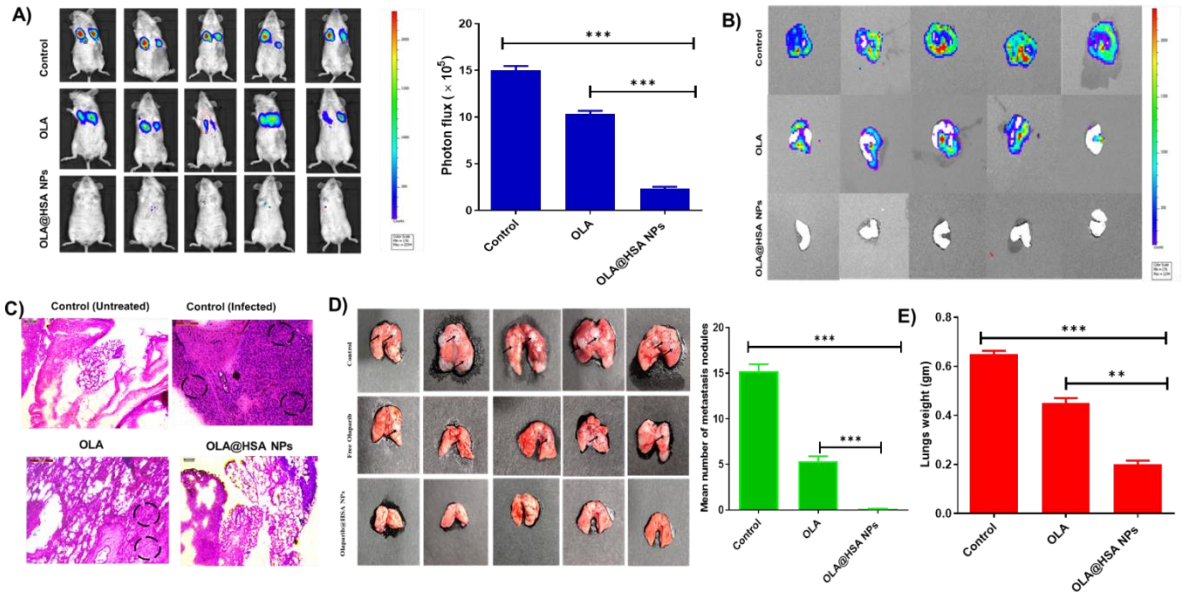

Figure 2.23: Suppression of metastasis of 4T1-Luc cells in lungs by OLA@HSA NPs treatment. Imaging of live mice to assess metastasis on day 7 following surgery (n = 5) and the bar graph representation of bioluminescence (A); ex-vivo bioluminescence intensities in lungs tissues of free Olaparib, OLA@HSA NPs-treated mice (B); tumor metastasis in lung sections detected using hematoxylin and eosin staining (marked with circles). Scale bar.100 μm (C); visualization of lungs of free Olaparib and OLA@HSA NPs-mice groups to check the development of metastatic nodules of 4T1 cells, and bar graph representation of the number of nodules/ lungs in the free Olaparib and OLA@HSA NPs-treatment groups (D); bar graph representation of lung weight (E). The significance of the difference was analyzed by paired t-test, **p < .01 and ***p < .001.

Discussion:

Spontaneous metastasis is the hallmark of the delayed and advanced stage of cancer progression (126). Lung tissue is the primary site of metastasis for 4T1 breast cancer cells miming human breast cancer. In the lung metastasis experiment, the PBS group mice revealed

tumor lesions and protruding nodules compared to the free Olaparib group. Metastatic nodules were hardly visible in OLA@HSA NPs-treated animals, as visualized by the naked eye and under the IVIS system via bioluminescence following luciferin treatment. The presence of nodules increased lung weight, which was highest in the tumor-bearing untreated control group and lowest in the OLA@HSA NPs group. A similar observation was also reported elsewhere (127). The histopathological observation revealed that the lung in the tumor-bearing untreated mice had a dense tissue population indicative of metastatic loci. However, lung histology of the OLA@HSA NPs-treated group was similar to the normal, non-tumor implanted mice.

2.6.26. Western blotting

The expressions of PARP1, γH2AX, and p53 proteins were analyzed by the western blot technique. Treatment with OLA@HSA NPs significantly downregulated PARP1 expression levels compared to free OLA. The γH2AX and p53 protein expressions were increased in the tumor tissues after treatment with free Olaparib and OLA@HSA NPs, as evident from our immunoblotting experiment. The representative bar graph of protein expressions, as quantified by Image J software, is shown in (**Figure 2.24).** A significant upregulation of γH2AX and p53 protein expressions ($p<0.001$) in OLA@HSA NPs-treatment groups indicated the superiority of the nano-formulation over the free drug in developing apoptosis.

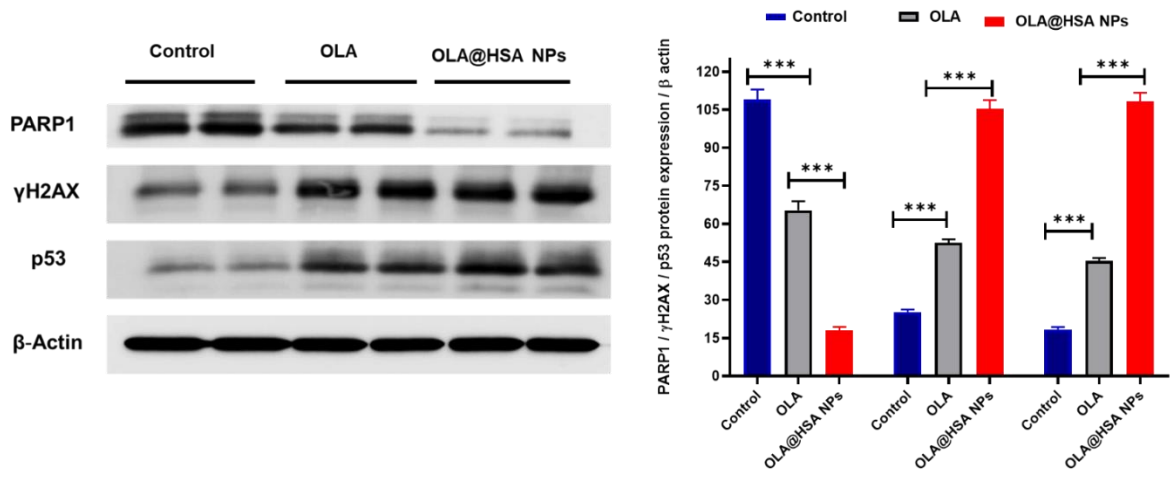

Figure 2.24: Western blot analysis of tumor tissues of mice from the treatment groups of salines, OLA@HSA NPs, and free Olaparib. The protein band's grey values for PARP1, P53, and γH2AX are represented on the left using β-actin as the internal standard. Bar graphs represent grey values of the protein bands (right). The significance of the difference was analyzed by paired t-test ***p < 0.001.

Discussion:

Western blot analysis revealed the expression of several apoptosis-inducing cancer biomarkers. As indicated earlier, the PARP1 protein mediates post-DNA damage repair and assists cells in passing through the G2/M phase. Downregulation of the PARP1 in the tumor tissues was significantly higher in OLA@HSA NP-treated mice compared to the control and free Olaparib group. The suppression of the G2/M phase in the cell cycle could be due to PARP inhibition, which resulted in robust apoptosis in the NPs-treatment group (128). The enhanced accumulation of Olaparib in tumors of the OLA@HSA NPs-treatment group is due to the combination of active and passive targeting phenomena. The NPs accumulated in the tumor environment via the Enhanced Permeability and Retention (EPR) effect due to the nanosize (129). Simultaneously, HSA has strong interaction with endothelial cells and tumor-microenvironment-associated SPARC protein and gp-60 receptors, resulting in an active

nanocarrier targeting the tumors (130). The cleavage of the double standard DNA is initiated by the phosphorylation of Ser-139 residue over histone H2AX, forming γH2AX. Increased expression of γH2AX is indicative of DNA damage. A significantly higher expression of γH2AX in tumor tissues was observed. Similarly, the tumor suppressor protein, p53 expression, was drastically increased in the OLA@HSA NPs-treatment group, indicating the triggering of apoptosis. Overall, the expressions of cancer-related biomarkers indicated the shifting of cancer cells' equilibrium towards apoptosis from replicative immortality.

2.7. Conclusion:

Here, the PARP inhibitor, Olaparib-loaded, stable human serum albumin nanoparticles system, was prepared by de-solvation technique. The nanosized particles, OLA@HSA NPs, were characterized to determine various physicochemical parameters. The particles exhibited low polydispersity, optimal drug loading, entrapment, and sustained release at blood pH with accelerated release at tumor pH. The OLA@HSA NPs were stable at 4 °C, non-hemolytic, and demonstrated lower half-maximal inhibitory concentrations than free Olaparib in mouse and human triple-negative breast cancer cell lines. The cellular uptake study revealed that the NPs were internalized time-dependently. A concentration-dependent increased expression level of the apoptotic marker phosphatidylserine was noted in OLA@HSA NPs-treated cells than free Olaparib and untreated cells in both the cell lines. The OLA@HSA NPs caused the highest cell cycle arrest in the G2/M phase, DNA fragmentation, mitochondrial membrane depolarization, and ROS generation. The *in vivo* study demonstrated that the OLA@HSA NPs suppressed the tumor volume significantly compared to control and free Olaparib-treated tumors. The isolated OLA@HSA NPs-treated tumors had increased expressions of fragmented DNAs, proliferative marker, Ki-67, p53, γH2AX, and ROS and reduced expressions of PARP-1. The lung metastasis study revealed that the OLA@HSA NPs-treatment slowed the cancer cells' migration to distal organs. Overall, the OLA@HSA NPs induced a strong apoptotic response

in vitro and *in vivo*, demanding further exploration and revealing their potential for successful utilization as chemotherapy in triple-negative breast cancer.

Chapter 3

Preparation, In vitro Characterization, In vitro studies, and in vivo studies of the Olaparib, Oxaliplatin-Human Serum Albumin Nano-particles

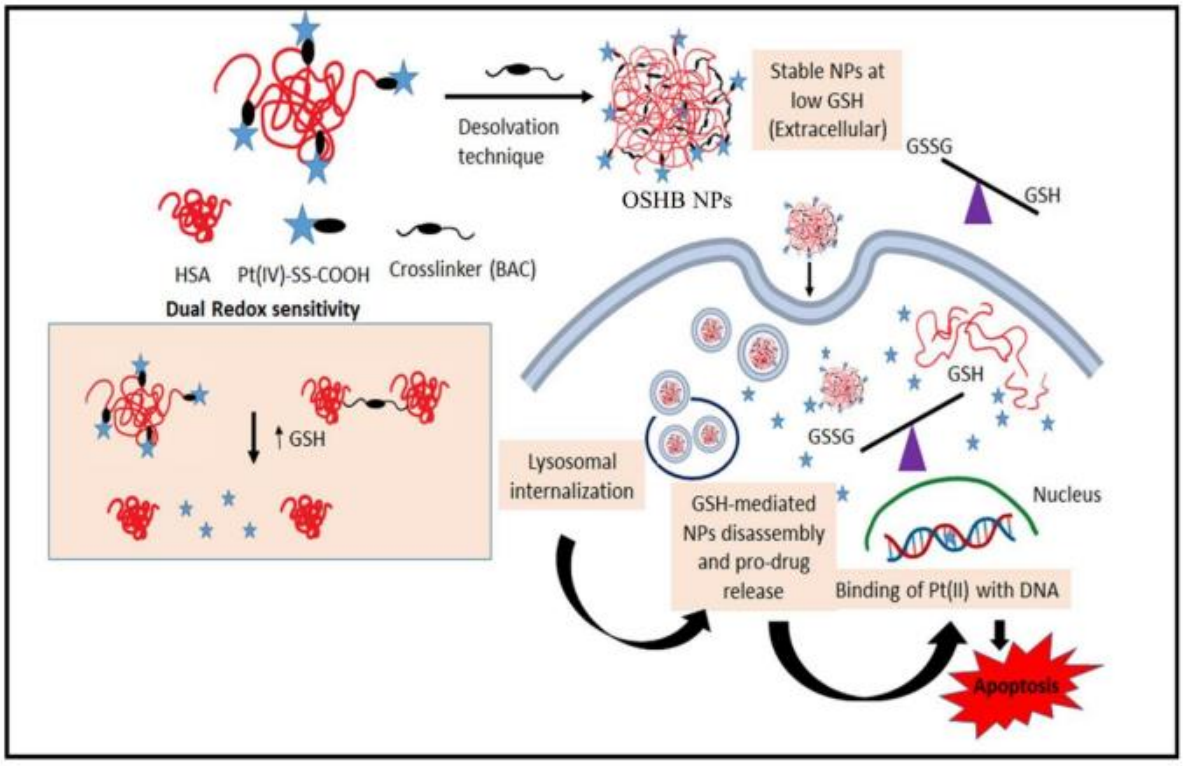

3.1 Introduction

One of the most common types of cancer affecting the women population forms breast cancer. According to recent reports, 20% of the cases reported under breast cancer fall under the category of HER2-positive breast cancer. Surgery, radiation, and chemotherapy are the treatment strategies for TNBC. Chemotherapy responds well in TNBC compared to other breast cancers (130). The DNA-repair complexes, including platinum compounds, anthracyclines, microtubule-stabilizing agents, and taxanes, are commonly used as chemotherapeutic agents (131). Adjuvant therapy using novel chemotherapeutic agents with existing chemotherapeutic agents has proven effective. Platinum drugs are effective chemotherapy in TNBC. It has been found that TNBC with BRCA mutation is sensitive to DNA-crosslinking agents, such as cisplatin and mitomycin C. The success of cisplatin in the clinical setup has led to a significant leap in the development of Pt anticancer compounds. Due to the multiple adverse reactions of Pt-based compounds, a safer and more potent compound development has been the focus in the past decades. Nevertheless, only a few Pt-based compounds have reached clinical trials, while two of them, carboplatin and Oxaliplatin (OXA), have been approved by the FDA as chemotherapeutic drugs for the treatment of malignant tumors (132). Platinum-based drugs are considered an effective treatment option as neoadjuvant therapy for TNBC (133).

The FDA has approved three PARP inhibitors (PARPi), Olaparib, Rucaparib, and Niraparib, for treating recurrent breast cancers. Approximately 50% of epithelial breast cancers exhibit defective DNA repair via homologous recombination (HR) (134). PARP inhibitors exploit the fundamental vulnerability of breast cancer with homologous recombination repair deficiency and have shown promising anti-tumor effects on breast cancers with deleterious BRCA1/2 mutations or BRCAness. Increasing evidence also indicates the efficacy of PARP inhibitors in breast cancers in the absence of BRCA1/2 mutations, presumably resulting from other

molecular deficiencies in the HR repair (134). Indeed, emerging novel combination therapeutic strategies designed to disrupt HR repair in cancer cells and render vulnerabilities to PARP inhibitors have been evaluated preclinically and in early clinical trials of various cancer types, including breast cancer.

Targeted treatment employing nanocarriers such as nanoparticles, liposomes, micelles, and dendrimers is a potential and actively investigated approach to address the non-specificity difficulties of chemotherapeutic drugs. Due to the increased permeability caused by the abundant supply of nutrients and oxygen needed for their fast multiplication, their nanosize makes it simple for them to pass through the vascular endothelial cells surrounding the tumor (135). The enhanced permeability and drug retention caused by the leaky vasculature and inadequate lymphatic drainage is known as the EPR effect. Nanoparticles' use of passive targeting, which makes it easier for them to permeate the interstitium layer, is another crucial characteristic. Due to its biocompatibility, flexibility, and clinical safety, albumin has traditionally attracted special interest as a material for nanoparticle production. Additionally, the abundance of albumin receptors (GP60) greatly enhances the internalization of albumin-bound nanoparticles, increasing their potency and targeting potential for the treatment of cancer. The vital glycoprotein SPARC, which also transports albumin and functions as a nutrition transporter for the tumor cells, is overexpressed in tumor tissues (136). As a result, effective targeted distribution of albumin-bound nanoparticles into the tumor tissues is made possible by SPARC. Recent studies have shown that the amphiphilicity and self-assembly properties of HSA are enhanced by conjugation with a variety of different ligands.

In this project, we develop an effective therapy against insensitive breast cancer with a combination of therapeutic agents utilizing two drugs with non-overlapping mechanisms which induce cell death. Combining therapeutic agents with different mechanisms of action could produce additive or synergistic therapeutic responses, which is more beneficial than

monotherapy. In this project, to develop an effective therapy against insensitive breast cancer, OLA was encapsulated in the HSA(OXA) complex using chemical conjugation and physical entrapment techniques. HSA was conjugated with oxaliplatin and allowed to self-assemble. The drug was added using the de-solvation technique with and without glutaraldehyde. Multiple drug-to-polymer ratios were considered, and the efficiency of both methods was evaluated by performing particle size analysis. The optimal formulation was considered for further physicochemical characterization and *in vitro* efficacy using breast cancer cell lines.

3.2 Materials and Methods

3.2.1 Materials

Human Serum Albumin was procured from the market which was manufactured by Baxter Healthcare Corporation's (USA), Dr. Reddy's Laboratory, Bachupally, Hyderabad, India, gifted the Olaparib, Oxaliplatin was received as a gift sample from Neon Pharmaceuticals Ltd, Mumbai, India. Sigma Aldrich, Mumbai, India, supplied the chemicals of 2,7-dichloro-dihydro-fluorescein diacetate (DCFH-DA). Himedia Labs (India) supplied Trypan blue solution, Fluoromount-G and Methyl thiazolyl diphenyl-tetrazolium bromide (MTT). Dialysis membranes required for the dissolution studies were acquired from Spectrum Laboratories, Inc (USA).

3.2.2. Cell Lines:

NCCS, National Center for Cell Sciences Laboratories Pune, India, provided the Human triple-negative breast cancer cell line MDA-MB-231. American Type Culture Collection (ATCC, USA) supplied the cell lines of 4T1 and 4T1-Luc. Himedia Labs (India) supplied the materials fetal bovine serum (FBS), 4′,6-diamidino-2-phenylindole dihydrochloride (DAPI), Trypsin-EDTA, Dulbecco's Modified Eagle *Medium (DMEM),* Penicillin Streptomycin, Minimum Essential Medium Eagle (MEM) Murine breast cancer cell lines.

3.2.3. Animals:

The Institutional Animal Ethics Committee of BITS-Pilani, Hyderabad campus approved all the pharmacological studies. 18−20 g weight Female Blab/C mice of 5-7-week-old age were obtained for the anti-tumor activity studies from Hyderabad's National Centre for Laboratory Animal Sciences. The animals were kept in the conditions at controlled room temperature (RT) of 25ºC ± 2ºC with relative humidity (50-70 %) with a standard chow diet and water. The hemolysis study requires female Wister rats, which were received from Sainath Agency, Hyderabad, India.

3.2.4. Methods

3.2.4.1. Preparation of HSA(OXA) Nanoparticles:

3.2.4.1.1. Synthesis of OXA(IV)(OH)2

Oxaliplatin (0.25 g, 0.063 mmol) was dissolved in 4 ml of 30 % H2O2. The reaction was maintained for 24 hours at room temperature. The solution was condensed using a rotary evaporator. To acquire OXA(IV)(OH)2 as a white powder, the resulting product was re-dissolved in cold methanol, precipitated in cold diethyl ether, thrice washed with ether and dried under vacuum. (Yield 78%).

3.2.4.1.2. Synthesis OXA(IV)-Succinic acid:

OXA(IV)(OH)2 (100 mg, 0.2345 mmol) and Succinic acid (42.74 mg, 0.2345 mmol) were dissolved in 3 ml of DMF in the presence of dimethyl aminopyridine (DMAP) (57.29 mg, 0.469 mmol) and N, N dicyclohexylcarbodimide (DCC) (96.76 mg, 0.469 mmol). The reaction continued in the dark at room temperature for 24 hours. Then the solution was evaporated and precipitated in cold diethyl ether (Yield. 75%).

3.2.4.1.3. Synthesis of OXA-HSA conjugate:

Into the solution of OXA(IV)(OH)2-succnic acid (2.61 mg, 4 mmol), N-(3-Dimethylaminopropyl)-N -ethyl carbodiimide hydrochloride (EDC) (3.45 mg, 0.021 mmol) and N-hydroxysuccinimide (NHS) (5.75 mg, 0.021 mmol) in DMSO, human serum albumin (70 mg) was added dropwise. The reaction mixture was stirred for 24 h. The DMSO was evaporated, and the crude product was dialyzed against water using a cellulose ester membrane (molecular weight cut off 2 KDa). The dialysate was lyophilized to obtain the white product (Yield. 80%).

3.2.4.1.4. Olaparib+Oxaliplatin-Human Serum Albumin Nanoparticles OLA@HSA(OXA) - NPs Preparation:

The NPs loaded with both drugs, oxaliplatin, and Olaparib. Briefly, oxaliplatin conjugated with human serum albumin (HSA) by initially reacting oxaliplatin with hydrogen peroxide to introduce hydroxyl groups, which further react to HSA to form a Pt (IV)-Oxaliplatin-HSA. The HSA(OXA) NPs were prepared by using the de-solvation technique. The HSA(OXA) dissolved in water, into which an ethanolic solution of Olaparib was added dropwise under stirring. The protein forms loose aggregates and incorporates Olaparib. The solution was supplemented with the crosslinking agent BAC that is N, N-bis acryloyl cystamine, and the reaction mixture was stirred overnight at a controlled room temperature of 20-25°C. The obtained OLA@HSA(OXA) NPs separated by centrifugation, lyophilized using mannitol as a cryoprotectant.

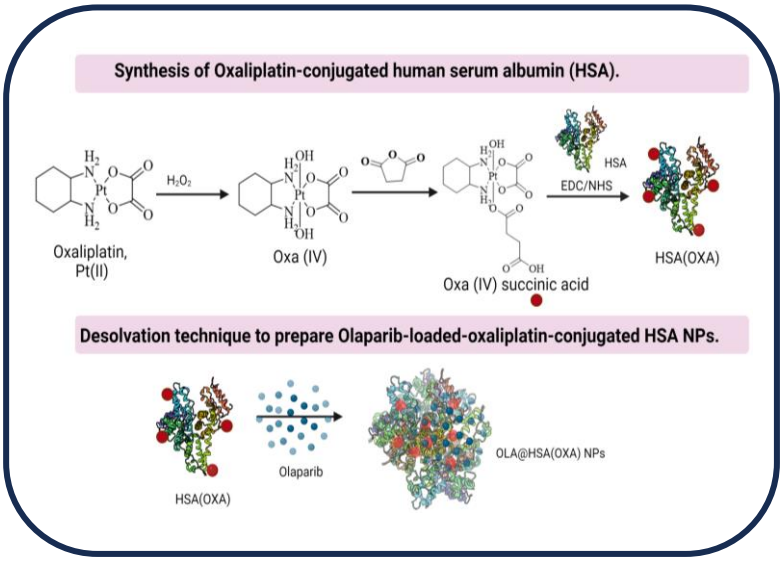

3.2.5. Characterization Nanoparticles: Morphology, Particle Size, Surface charge by Zeta potential, Drug loading (DL) efficiency, Drug entrapment efficiency (EE):

3.2.5.1. Morphology by SEM:

NOVA NANOSEM 450 Scanning Electron Microscopy was used to identify the surface morphology of OLA@HSA NPs, HSA(OXA) NPs, and OLA@HSA(OXA) NPs. For SEM analysis sample was prepared as a thin layer of the nanoparticle sample on the adhesive carbon tape which was further attached to aluminium stubs. Further, onto this, gold sputter-coating was applied to the desired thicknesses, which were analyzed at an applied charge of 20 kV analyzed for SEM analysis.

3.2.5.2. Particle Size by using Zeta Sizer:

The hydrodynamic diameter (Particle Size) of the nanoparticles was measured by using the Dynamic light scattering technique, and the instrument for determination was Zetasizer 3600 from Malvern Instruments Ltd. The same instrument was used to determine the zeta potential. Lyophilized samples for the blank nanoparticles that are OLA@HSA NPs, HAS(OXA) NPs, and OLA@HSA(OXA) NPs were reconstituted to the required concentration with water for Injection, and the reconstituted samples were used for the determination of the Zeta potential, Particle Size, and PDI.

3.2.5.3. Estimation of Drug Content, Entrapment Efficiency, and Drug Loading Efficiency:

Dug content in the prepared nanoparticles OLA@HSA NPs, HSA(OXA) NPs, and OLA@HSA(OXA) NPs were estimated by using the HPLC technique. HPLC is from Shimadzu, Japan, which was equipped with a UV detector. The chromatography details are with a 40;60 ratio of deionized water: methanol as a mobile phase, 1 mL/min flow rate, 40ºC

column temperature, and by using 150 mm x 4.6 mm C18 reverse phase column of a column from Phenomenex, USA, 20 µl injection volume, 10 mins run time, detector wavelength of 276 nm for the estimation of Olaparib. The NPs solution was prepared in HPLC grade ethanol, and by using the HPLC technique, Olaparib was measured.

Oxaliplatin was also estimated using the HPLC technique. Oxaliplatin content from HSA(OXA) NPs, and OLA@HSA(OXA) NPs was estimated using the chromatographic method by Shimadzu, HPLC. Nanoparticles were reconstituted with ethanol (HPLC grade) to interrupt the Oxaliplatin association with Human Serum Albumin and to dissolve the Oxaliplatin. Reverse phase chromatography involves the usage of 5 µm particles of Phenomenex, a column of 150 mm x 4.6mm, C18 column; chromatographic conditions are a flow rate of 1 mL/min 95:5 v/v ratio 0.01M phosphoric acid: acetonitrile as mobile phase, 20 µl injection volume, column temperature of 40°C also the PDA detector was used at the wavelength of 261 nm. The nanoparticle samples were diluted using HPLC-grade ethanol to disrupt the nanoparticle assembly.

OLA@HSA NPs, HSA(OXA) NPs, and OLA@HSA(OXA) NPs % entrapment efficiency (% EE) and % drug loading efficiency (% DL) were assessed using the below equation.

Encapsulation efficiency of Olaparib and Oxaliplatin in the NPs estimated as given by the below equation:

$$\text{EE (\%)} = \frac{\text{The weight of the drug embedded in the nanoparticle}}{Weight\ of total\ drug\ added\ initially\ to\ prepare\ the\ nanoparticles}\ X\ 100$$

The drug Loading efficiency of OLA and OXA in NPs estimated as per the equation:

$$\text{DL (\%)} = \frac{\text{The } Weight\ of\ drug\ embedded\ in\ the\ nanoparticle}{(Weight\ of\ the\ polymer\ and\ drug)}\ X\ 100$$

3.2.5.4. Protein conformation studies: SDS-PAGE

Protein confirmation studies were performed by using the gel-electrophoresis technique (SDS-PAGE) for the OLA@HSA(OXA)NPs, HSA(OXA)NPs, OLA@HSA NPs, and HSA. Reconstitute the lyophilized NPs with a pH 7.4 Phosphate buffer system. From the reconstituted nanoparticle preparation, concentrations were adjusted to 1 mg/ml for all the nanoparticles, from which 15 µL was collected, and to this, 5 µL of loading dye was added. These sample mixtures were exposed for 5 minutes with a boiling temperature of 95 °C to denature the protein, followed by all the samples loading was done into the 10% polyacrylamide gel. These nanoparticle samples were transferred to the gel wells along with the control sample (HSA) and ran for 3 hours at 120 volts by using the Bio-Rad, gel-electrophoresis equipment. After the 3 hours of gel-electrophoresis, all the nanoparticle samples, along with the control, were stained for 1 hour using Coomassie brilliant blue, followed by overnight de-staining. After completion of the study, protein bands were assessed, and further images were taken.

3.2.5.5. Circular dichroism (CD) Spectroscopy

The circular Dichroism spectroscopy technique was used to determine drug interaction with human serum albumin, and the modification in the secondary structure was analyzed and compared with control samples of Human Serum Albumin. The study was performed by using a JASCO-1500 CD spectrometer (USA). Nanoparticle samples were prepared in the phosphate buffer with a protein quantity of 0.1 µM Human Serum Albumin and filtered with a PVDF filter. Quartz cells of 0.1 cm path length were used for the study and scanned at a range of 190-260 nm for each sample at a 100 nm/ min scanning speed. An inert nitrogen atmosphere was maintained for all the samples. Mean residue ellipticity (MRE) was plotted and drawn for all the samples (HSA, OLA@HSA NPs, HSA(OXA) NPs and OLA@HSA(OXA) NPs and to

determine the helical content degcm^2 dmol^{-1} on the Y axis and wavelength (nm) X axis by using the, previously recorded formula.

3.2.5.6. *In vitro* Drug Release Study

Olaparib and Oxaliplatin *in vitro* release was estimated by doing the dialysis technique from the OLA@HSA(OXA)NPs and OLA@HSA NPs formulations. Samples were prepared in pH 7.4 Phosphate with an OLA concentration of 100 µg/ml and OXA concentration of 100 µg/ml, and then the samples were loaded into the 12-14 kDa molecular weight cut-off dialysis bag. Samples containing dialysis bags were suspended into the dissolution media and maintained at a temperature of 37 ºC at 100 rpm of continuous stirring. At every pre-defined time interval, a 1 mL sample was taken and replenished with 1 mL fresh media. Samples were collected and analyzed for the estimation of Olaparib or Oxaliplatin by using the UV-Vis Spectrophotometer.

3.2.5.7. Haemolytic Assay

For the Haemolytic Assay study, fresh blood was collected rat-eye retro-orbitally and transferred to the container containing ethylenediamine tetraacetic acid (EDTA) and which will avoid the coagulation of the blood. Centrifugation of the blood was done at 3000 rpm for 10 minutes at 4 °C, and then plasma separated, followed by RBCs, were collected thoroughly washed and immersed in 7.4 phosphate buffer saline at 5 % v/v concentration. Different concentration ranges (12.5-250 µg/ml of drug concentration) of Nanoparticles of OLA@HSA(OXA) NPs were suspended along with the suspended RBC cells containing tubes, incubated at 37 ºC for 50min along with this controls samples also incubated in Triton X-100 (1%) as positive control PBS 7.4 was as a negative control. After the defined incubation, all the samples were centrifuged at 7000 rpm for 30 minutes at 4 °C. Carefully, the supernatant was collected and analyzed at 576nm by using UV- Spectramax Multiplate reader, and the %

absorbance was recorded. Percentage hemolysis has been determined by using the following formula:

$$\%\ hemolysis = \frac{Abs_{sample} - Abs_{-ve}}{Abs_{(+)} - Abs_{(-)}} \times 100$$

From the above Abs_{sample}, sample absorbance,

Abs_{-ve}, negative control absorbance (0.9% Sodium chloride)

Abs_{+ve}, positive control absorbance (Triton X-100)

3.2.6. *In vitro* cell-based assays in monolayers-

3.2.6.1. Cell viability assay (MTT) and IC50:

Cell viability study was performed for the free drugs OLA, free drug OXA, OLA@HSA NPs, HSA(OXA) NPs, and OLA@HSA(OXA) NPs in 96 well plates of MDA-MB-231 and 4T1 cell lines, and in each well $1X10^6$ cells were seeded and kept for overnight incubation humidified atmosphere (at +37 °C, 5-6.5% CO_2). Further, after 24 hours, the old media was replenished with new media. After these cells were exposed to 0-100 µg/mL concentrations of free Olaparib, free Oxaliplatin, OLA@HSA NPs, HSA(OXA) NPS, OLA@HSA(OXA) NPS, blank control sample for 24 hours in a humidified atmosphere (at +37 °C, 5-6.5% CO_2). To this 5 mg/mL concentrated solution of MTT solution of 50 µl was added to each well and then incubated for 4 hours in a humidified atmosphere (at +37 °C, 5-6.5% CO_2). Further to this, 150 µl DMSO solvent was added to dissolve the formazan crystals and to obtain the purple color. Further, After 1 h of holding, the absorbance was recorded by using the Spectramax™ Multiplate Reader (Molecular Devices, USA at 570 nm and the reference wave length of 630 nm.) Further cell viability has been calculated by using the following equation:

$$Cell\ viability\ \% = \frac{Absorbance\ of\ sample}{Absorbance\ of\ control} \times 100$$

3.2.6.2. Cellular uptake studies (*In vitro* cellular internalization studies by confocal microscope and flowcytometry):

4T1 Cancer cells with $5*10^{6,}$ that is 50,000 cells per well, were seeded in the 12-well plate and incubated overnight. For the study using fluorescence, nanoparticle samples were prepared by tagging with Rhodamine. Rhodamine-labeled free drugs that are Rhodamine-Olaparib, Rhodamine-Oxaliplatin, Rhodamine-labelled NPs are OLA@HSA-Rh NPs, - HSA(OXA)-Rh NPs, OLA@HSA(OXA)-Rh NPs, were treated with the cells at the concentration of 0 to 25 µg/mL of drug concentration, incubated and the fluorescence was recorded at 1, 4 and 8 hours. Each time after the incubations, cells were isolated, thoroughly washed with PBS, trypsinized, and then centrifuged. The obtained cell pellets were immersed in the cold PBS buffer solution, and cell counting was performed using a flow cytometer from BD FACS ARIA for quantification, and visualization was performed through fluorescence microscopy. For the flow cytometry studies, 10,000 cells were gated for the acquisition of the data to understand the cellular uptake. Histogram plots were done using the software obtained from BD Biosciences, USA, and this is FACS Aria III. Apart from this, fluorescence microscopy studies were performed for the control, free drug, and NPs-treated cells were thoroughly washed, followed by fixation with 4% paraformaldehyde solution, further stained for 5 minutes using 1 µg/mL DAPI solution. After completion of the staining, images were taken using the Leica (Germany) Confocal fluorescent microscope.

3.2.6.3. Annexin-V assay:

MDA MB231 and 4T1 cancer cell lines were seeded in a 12-well plate with 0.5×10^{6} Cells/well and further incubated overnight. After the cell wall growth, the cells were treated at a concentration of 12.5 µg/mL, 25 µg/mL of free Olaparib, free Oxaliplatin, OLA@HSA NPs, OXA@HSA NPs, OLA@HSA(OXA) NPs and were incubated for 24 hours at 37 °C. The study was carried out as per the manufacturer's instructions. Controls were also included in the study without any treatment. Further to this, Annexin-V FITC and PI were added and incubated. After the incubation, cells were isolated and counted using flow cytometry gated at 10,000

cells, and cell cycle data was assessed using the software of BD Biosciences, FACS Aria III, USA). Also, further to this, fluorescence microscopy studies were performed by measuring the fluorescence at 535 nm and 550 nm for Annexin-V FITC and PI, respectively. Dot plots were drawn for the PI versus Annexin V-FITC and further divided as quadrants to understand the apoptosis. Quadrant 1 represents the necrotic, Quadrant 2 represents late apoptosis, Quadrant 3 represents early apoptosis, and Quadrant 4 represents live cells.

3.2.6.4. Cell cycle analysis:

In a 12-well plate, cancer cell lines of MDA MB231 and 4T1 were seeded with a population of 60,000 cells/well, followed by incubation. On the next day, drug samples were added to the cells at the concentration of 12.5 µg/mL to 25 µg/mL concentrations of free Olaparib, free Oxaliplatin, OLA@HSA NPs, HAS(OXA) NPs, and OLA@HSA(OXA) NPs for 24 hours. Further cells were harvested and washed with pH 7.4 PBS solution, then centrifuged at 20,000 rpm for 5 min. The obtained pellet cells were fixed with ice-chilled ethyl alcohol (70%) at −20 °C overnight and then, after the fixation, centrifuged at 1500 rpm for 5 min. Ice-chilled cells were suspended in 1 mL of pH 7.4 PBS buffer solution and further centrifuged at 1500 rpm for 5 min. A staining solution was prepared with 200 µg/mL RNase, 20 µg/mL propidium iodide, and 400 µl PBS 7.4. Cells were suspended in the staining solution, and then cell cycle analysis was performed using a flow cytometer.

3.2.6.5. ROS detection assay

12 well tissue culture plate was used to culture the cancer cells of MDA-MB 231 and 4T1 at $5*10^6$ cells/well. After 24 hours of incubation time, cells were treated with the free drug Olaparib, free drug Oxaliplatin, HSA(OXA) NPs, OLA@HSA NPs, and OLA@HSA(OXA) NPs at a concentration of 10 µg/mL and then incubated for 24 hours at 37°C, 5% CO_2. Further cells were washed using PBS 7.4 buffer fixing with 4% paraformaldehyde and then stained with 2'-7-dichlorofluorescein diacetate (DCHF-DA) dye solution of 5 µM concentration for 20

mins. Further cells were observed using the fluorescence microscope (ex/em. 504/529 nm), and the photographs were recorded. Apart from this, treated cells were washed, trypsinized, and obtained as a cell pellet suspended in PBS buffer and used for flowcytometry analysis, and then the obtained data were processed by using the FACS Aria III, BD Biosciences, USA software.

3.2.6.6. Mitochondrial membrane potential assay

12 well tissue culture plate was used to culture the cancer cells of MDA-MB 231 and 4T1 at $5*10^6$ cells/well. After 24 hours of incubation time, cells were treated with the free drug Olaparib, free drug Oxaliplatin, HSA(OXA) NPs, OLA@HSA NPs, and OLA@HSA(OXA) NPs at a concentration of 10 µg/mL and then incubated for 24 hours at 37°C, 5% CO_2. Next, cells were washed in 7.4 PBS buffer thrice, and then the treatment was given with 2 µM concentration JC-1 dye for 20 mins and imagined using the fluorescence microscope (Leica Microsystems, Germany). For the FACS analysis, Cells were treated, further pelleted, and washed in pH 7.4 cold PBS buffered and used for the flow cytometry analysis, and the data was processed using the FACS Aria III, BD Biosciences, USA software.

3.2.6.7. Live-dead cell assay using Propidium iodide:

In a 12-well plate of 4T1 and MDA-MB-231, cells were seeded at a concentration of 1 × 105 cells/well and incubated for 24 hours. On the next day, the culture medium was replaced by a fresh medium containing drug concentrations of 10 µM of Olaparib, Oxaliplatin, OLA@HSA NPs, HAS(OXA) NPs, OLA@HSA(OXA) NPs and saline control. Further, the cells were washed with PBS pH 7.4 buffer, and incubated for another 48 hours in the dark. Cells were isolated and stained with PI (8 µM) and calcein-AM (3 µM) and further visualized using the fluorescence microscope.

3.2.6.8. Acridine Orange Assay:

For the RNA and DNA can be stained with the Acridine orange which can become fluorescent at 650 and 526 nm, respectively. In a 12-well plate of 4T1 and MDA-MB-231, cells were seeded at a concentration of 1 × 105 cells/well and incubated for 24 hours. On the next day, the culture medium was replaced by a fresh medium containing drug concentrations of 10 μM of Olaparib, Oxaliplatin, OLA@HSA NPs, HAS(OXA) NPs, OLA@HSA(OXA) NPs and saline control. Cells were isolated and stained with Acridine orange and Eosin Blue and visualized using the fluorescence microscope.

3.2.7. *In vivo Anti-tumor efficacy* Study

3.2.7.1. Tumor inhibition study

4T1-Luc cells were prepared with a concentration of 90,000 cells in 100 μL in a cold phosphate buffer solution. This 100 μL solution containing cells was injected into the 6-week-old female balb/c mice into the left flanks and further monitored for the tumor volume. Mice were randomly divided into three groups after achieving a tumor volume of 80 to 100 mm^3; the mice were randomly segregated into five groups, with each group of 5 mice. This 1^{st} group was given with the control sample, the second group for Olaparib, a third group for Oxaliplatin, a fourth group for OLA@HSA NPs, and a fifth group for OLA@HSA(OXA) NPs. Animal in each group was administered with a dose of 50mg/kg intravenously through the tail vein. This dosing was given every alternative day and was done for 10 days, and the monitoring duration was for 21 days. D-luciferin was administered at 150 mg/Kg dose intraperitoneally to the mice, and the tumor progression was observed periodically for 21 days at an interval of 0, 5, 10, 15, and 21, and the tumor progression was monitored. This process of D-luciferin administration was done before 10 min of image capturing using the PerkinElmer IVIS-Lumina *in vivo* imaging system (Ex/Em. 620/780 nm). The tumor volume (length X $width^2/2$) and body weight was measured

every alternate day for the entire duration of 21 days. On the 21st day, mice were anesthetized using ketamine/xylazine, and surgically extracted the tumor mass, and the weight was recorded. After surgery, the animals were revived; on the 7th day of the post-surgery, bioluminescence imaging was performed using luciferin-D. After the live-animal imaging, mice were sacrificed, then the lung tissues were photographed and weighed, and counting of tumor nodules was done.

3.2.7.2. Immunohistochemistry- TUNEL Assay/detection of Ki-67

The TUNEL assay was done to the isolated tumor tissues using the TM TACS TdT In Situ Apoptosis Detection Kit, Product code- 481230K. After the isolation, the tumors were immersed in OCT medium and frozen, and further tumors were cryo-sectioned using Leica biosystems cryotome to a 4 µm thickness. The obtained tumor tissues were incubated at 37 °C for 1 h with terminal deoxynucleotidyl transferase enzyme. Tumor tissues were fixed to the slides, and this TUNEL reaction mixture was added, which contains the equilibration buffer, TdT enzyme, and nucleotide mix, and then further incubated in a dark, humid atmosphere for 1 hour at 37 °C. Further tissue samples were washed with PBS buffer solution three times to remove the excess unincorporated fluorescein-d UTP. Further staining was done with DAPI to the tissues containing slides for 5 min, and then the images were captured by using a Leica fluorescence microscope (Germany). For Ki-67 analysis, the tumor sections from the above four groups were blocked for 1 hour in a blocking buffer and incubated with Ki-67 primary antibody (Rabbit mAb #9129) overnight at 4 °C; Further, the tissue sections were washed thrice in pH 7.4 PBS buffer solution and then incubated for 2 hours with secondary antibody (Alexa Fluor® Plus 488) in RT in the dark condition. Finally, PBS buffer washing was given to the tissues, and then the images were captured by using the fluorescence microscope (Leica Microsystems, Germany).

3.2.7.3. Reactive Oxygen species (ROS) generation in tumor tissue:

Tumor-bearing mice 4T1-Luc tumors (~60 mm3) were taken for this study of ROS generation and given with a dose of 5mg/kg of Olaparib, Oxaliplatin, OLA@HSA NPs, and OLA@ HSA(OXA) nanoparticles with respect to each group. After 24 hours of the dosing, 50 µL DCFH-DA (25 µM) was injected into the mice intratumorally. Mice were sacrificed after 30 mins of DCFH-DA administration, and tumor tissues were isolated and then immersed into the OCT media. Further tumor tissues were cryo-sectioned using Leica Biosystem cryotome (Germany) to a 5 µm of the size range. The frozen tissue sections were observed at (ex/em 495/519 nm) using the Leica fluorescence microscope with a FITC filter. *Image J* software was used to determine the images and to determine the intensity of ROS. The intensity of the region with nanoparticle formulations was compared against the free drug in the images.

3.3. Results and Discussion:

3.3.1 Physicochemical characterization of the OLA@HSA NPs:

The OLA@HSA NPs, HSA(OXA) NPs, and OLA@HSA(OXA) NPs were prepared by the de-solvation technique. The NPs were physiochemically characterized using zeta potential measurements, particle size analysis, X-ray diffraction spectroscopy (XRD), drug loading, and encapsulation efficiency.

The particle size of OLA@HSA NPs, HSA(OXA) NPs, and OLA@HSA(OXA) NPs 115 ± 2.3 nm, 125 ± 2.3 nm, and 138.32± 6.3 nm **(Figure 3.1A)** with a very narrow polydispersity index (PDI) (0.178, 0.124, 0.181).

Optimized formulations of OLA@HSA NPs, HSA(OXA) NPs, and OLA@HSA(OXA) NPs showed a negative ζ-potential of −12.1 ± 3.2 mV, - 10.1 ± 3.2 mV, -17.2± 3.2 mV, which may facilitate the elongation of *in vivo* blood circulation time **(Figure 3.1B).**

The SEM analysis of OLA@HSA NPs, HSA(OXA) NPs, and OLA@HSA(OXA) NPs indicated uniform spherical particles with particle sizes 120.32±2.5 nm, 125.32±2.5 nm, and 140.47±3.4 nm respectively which supported the data obtained through the DLS study **(Figure 3.1D).**

The DL% of OLA@HSA NPs, HSA(OXA) NPs, and OLA@HSA(OXA) NPs was 10.5%, 11.2 % and 12.3 and the EE% of OLA@HSA NPs, HSA(OXA) NPs, and OLA@HSA(OXA) NPs was 80.3%, 78% and 84% respectively.

The UV spectrum indicated Olaparib having the maximum absorbance at 207nm and Oxaliplatin having the maximum absorbance at 261nm. OLA@HSA NPs, HSA(OXA) NPs, and OLA@HSA(OXA) NPs formulations, when dissolved in ethanol, showed maximum absorbance at the same wavelength. This confirmed that OLA and OXA were encapsulated into the NPs while the addition of ethanol disrupted the NPs leading to drug release.

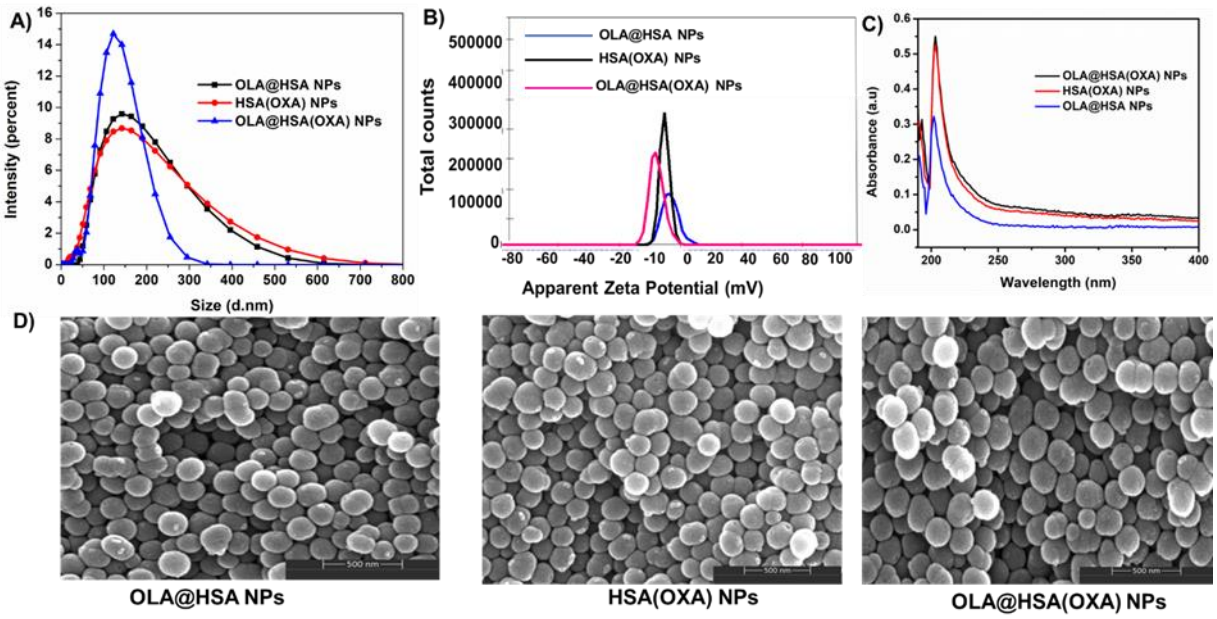

Figure 3.1: Physicochemical characterization of NPs. Particle size and zeta potential of OLA@HSA NPs, HSA(OXA) NPs and OLA@HSA(OXA) NPs by DLS measurement (A) & (B); UV−vis spectra of OLA@HSA NPs, HSA(OXA) NPs and OLA@HSA(OXA) NPs (C);

scanning electron microscopy image of OLA@HSA NPs, HSA(OXA) NPs and OLA@HSA(OXA) NPs (D);

3.3.2. Protein Confirmation Studies by SDS-PAGE:

The SDS PAGE image indicated uniformly thick bands around 66500 Da for HSA, OLA@HSA NPs, HSA(OXA) NPs, and OLA@HSA(OXA) NPs, as seen in **Figure 3.2**. This confirmed the presence of HSA in the NPs.

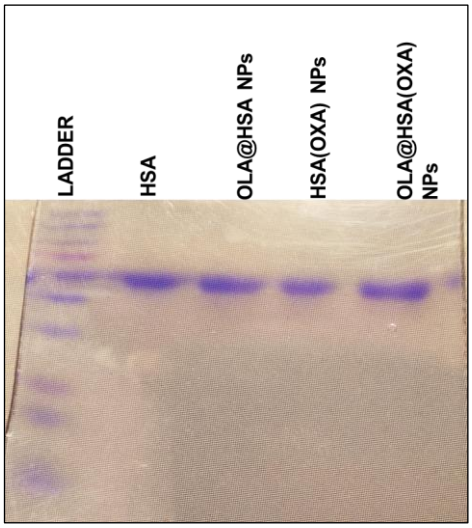

Figure 3.2: Photograph of the gel after SDS-PAGE (Left to right, lane 1: ladder, lane 2: HSA, lane 3: OLA@HSA NPs, lane 4: HSA(OXA) NPs and OLA@HSA(OXA) NPs.

Disucssion: From the SDS-PAGE study it was indicating the presence of both the drugs Olaparib and Oxaliplatin in the Human serum Albumin nanoparticles.

3.3.3. Circular Dichroism (CD) Spectroscopy:

The protein structure of the nanoparticles was further confirmed by the CD spectroscopy data. The negative trough showed at 208 nm and 222 nm for all three nanoparticle formulations, which was a characteristic feature of HSA. These bands were also present in all the formulations of

OLA@HSA NPs, HSA(OXA) NPs, and OLA@HSA(OXA) NPs but with reduced CD values (**Figure 3.3**).

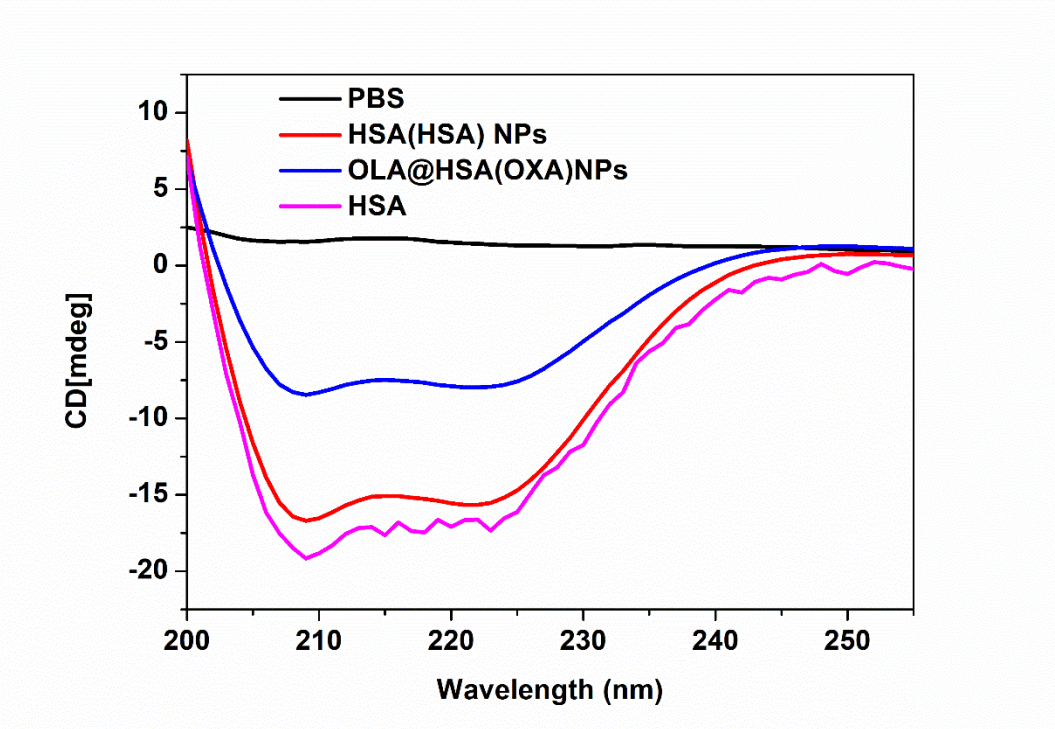

Figure 3.3: Circular dichroism spectroscopy of HSA, OLA@HSA NPs, HSA(OXA) NPs and OLA@HSA(OXA) NPs

Discussion: The α-helix and β-sheet values for standard HSA were observed as 60.71±0.79 % and 8.21 %, respectively, representing α-helix to be the dominant secondary structure. A decrease of α-helix and an increase of β-sheet were observed for all the Nanoparticle formulations. The OLA@HSA NPs, HSA(OXA) NPs, and OLA@HSA(OXA) NPs had α-helix and β-sheet values as 55.33±0.22 %, 12.75 % and 57.33±0.35 %, 11.97 % respectively.

3.3.4. *In vitro* Drug release study:

The cumulative drug release of OLA@HSA(OXA) NPs was evaluated by mimicking three different pH conditions, pH 7.4, 6.5, and 5.5 (**Figure 3.4, 3.5**). The highest release was observed at a pH of 5.5 when compared to a pH of 7.4.

The OLA@HSA NPs showed a maximum release of 72.41±2.89 % within 24 h at pH 5.5, while the NPs showed sustained release up to 79.74±3.43 % for 48 hours at the same pH.

The HAS(OXA) NPs showed a maximum release of 75.41±1.89 % within 24 h at pH 5.5, while the NPs showed sustained release upto 79.74±3.43 % for 48 hours at the same pH.

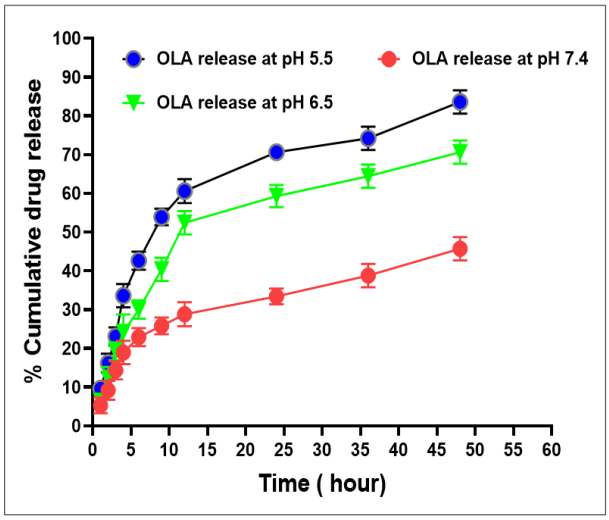

Figure 3.4: *In vitro* drug release of Olaparib from OLA@HSA(OXA) NPs in pH 5.5, pH 6.5 and pH 7.4

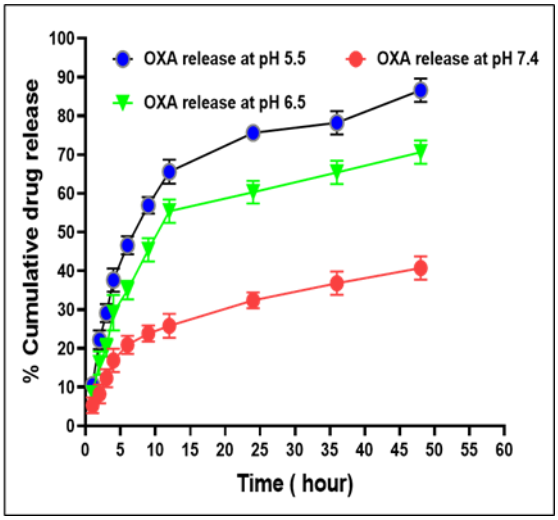

Figure 3.5: *In vitro* drug release of Oxaliplatin from OLA@HSA(OXA) NPs in pH 5.5, pH 6.5 and pH 7.4

Discussion: The highest drug release was observed at pH 5.5 which is a lysosomal pH for the tumor cells and could be an efficient treatment option with the least off-target toxicity for both Olaparib and Oxaliplatin from the nanoparticles.

3.3.5. Haemolytic Assay;

The hemolytic assay was performed using both qualitative and quantitative methods (**Figure 3.6**). The SEM images indicated hemolytic RBCs in the positive control, while no significant hemolysis was observed in 500 µg/mL of OLA@HSA(OXA) NPs. The quantitative analysis supported the qualitative result. It was observed that OLA@HSA(OXA) NPs indicated the highest haemolysis of 3.45±0.22 % at a concentration of 500 µg/mL. These percentages were well under the approved limits of 5 %, and hence the prepared NPs were safe for *in vivo* administration.

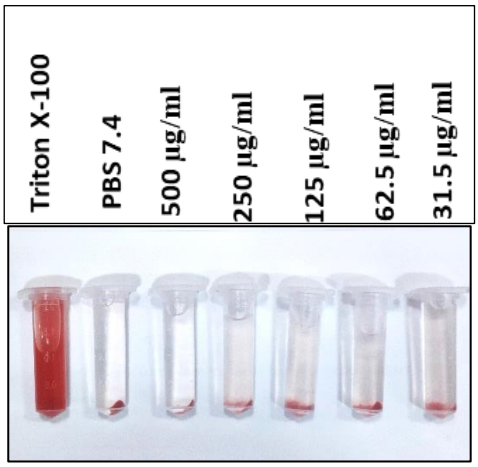

Figure 3.6: haemolytic study Photograph and SEM image of OLA@HSA(OXA) NPs

3.4.0. Invitro Cell Studies

3.4.1. Cell viability and IC50 (Half maximal inhibitory concentration):

The MTT assay performed indicated a decrease in the cell viability in 4T1 and MDA MB 231 cell lines in both time and concentration-based manner, as indicated in **figure 3.7**. It was observed that the cytotoxicity for OLA@HSA(OXA) NPs was higher compared to OLA@HSA

NPs, HSA(OXA) NPs, free OXA and free OLA NPs in both the cell lines of 4T1 and MDA MB 231. OLA@HSA(OXA) NPs showed an IC50 of 7.38 µg/mL, HSA(OXA) NPs (7.44 µg/mL) for 24 h on MDA MB 231 cell lines as compared to free OXA which had an IC50 of 10.73 µg/mL. Similarly, treatment for 48 h on MDA MB 231 cell lines of OLA@HSA(OXA) NPs had an IC50 of 4.70 µg/mL, HSA(OXA) NPs (4.58 µg/mL) while free OXA had an IC50 of 6.36 µg/mL.

Combination indices (CI) provide insight into the synergistic, additive, or antagonistic response of the combination therapy. A CI value less than 1 indicates synergism, 1 represents an additive effect, while a value above 1 is projected as an antagonistic therapeutic response. It was observed that only optimal OLA@HSA(OXA) NPs formulation with a loaded drug ratio of 50:50 (OLA: OXA) showed synergism with all Fa (fraction affected) values below 1 in MDA-MB-231 cells for both 24 h and 48 h **(Figure 3.7).** Also, a significant synergistic effect was observed in 4T1 cells showing all the combination indices values significantly below 1 **(Figure 3.7).**

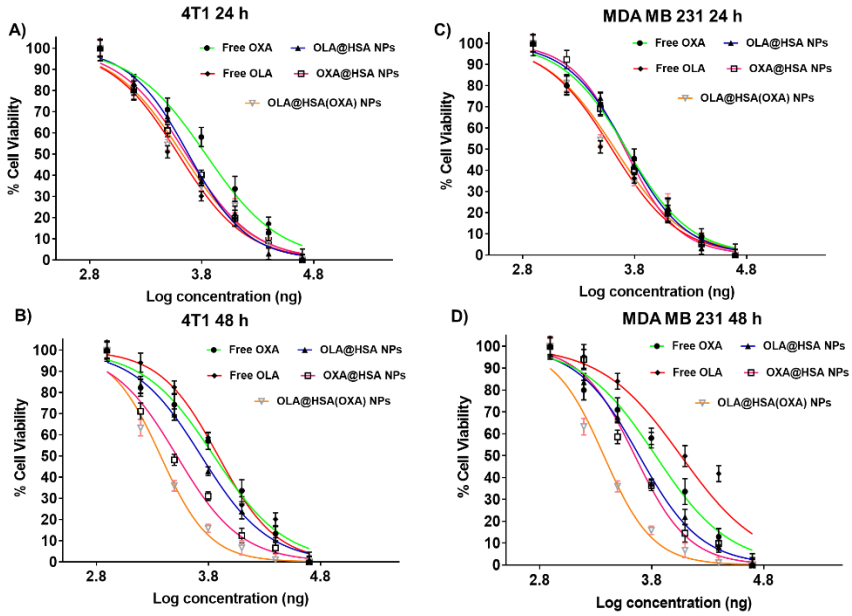

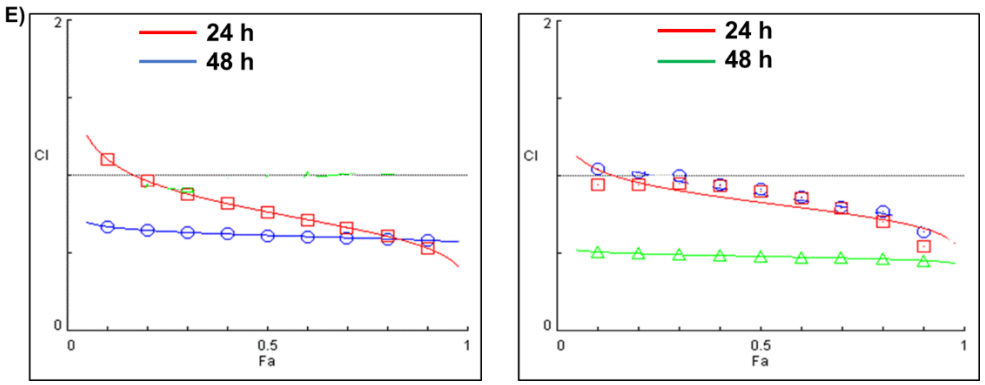

Figure 3.7: *In vitro* evaluation of the anticancer activity of free OLA, free OXA, OLA@HSA NPs, HSA(OXA) NPs, and OLA@HSA(OXA) NPs. Thedose–response curve for the determination of IC_{50} values of free OLA, free OXA, OLA@HSA NPs, HSA(OXA) NPs, and OLA@HSA(OXA) NPs (24 and 48 h) in cultured 4T1 (A, B) and MDA-MB-231 cancer cells (C, D); Combination index of both cell lines (E).

3.4.2. Cellular Uptake (In vitro cellular internalization by confocal microscope and flow cytometry):

Cellular uptake of rhodamine-labeled OLA@ HSA(OXA) NPs showed a significantly increased NPs uptake with time in 8 hours of treatment in 4T1 and MDA MB-231 cells compared to the OLA@HSA NPs and HSA(OXA) NPs **(Figure 3.8A&B).** Fluorescence intensity increased with the treatment incubation period. The flow cytometry graphs confirmed this. The peak shift in both cell lines showed time-dependent fluorescence enhancement. Fluorescence intensity which is illustrated in (**Figures 3.8 C&D)** for MDA MB231 and 4T1 cells treated with OLA@HSA(OXA) NPs were 922.85 ± 08.18, 2201 ± 10.18, and 3452.98 ± 14.82 (MDA MB 231) and 720.85 ± 08.18, 2101 ± 13.18, and 3302.98 ± 14.82, 42138.43 ± 1184.12 (4T1) for 1 h, 4 h, and 8 h respectively.

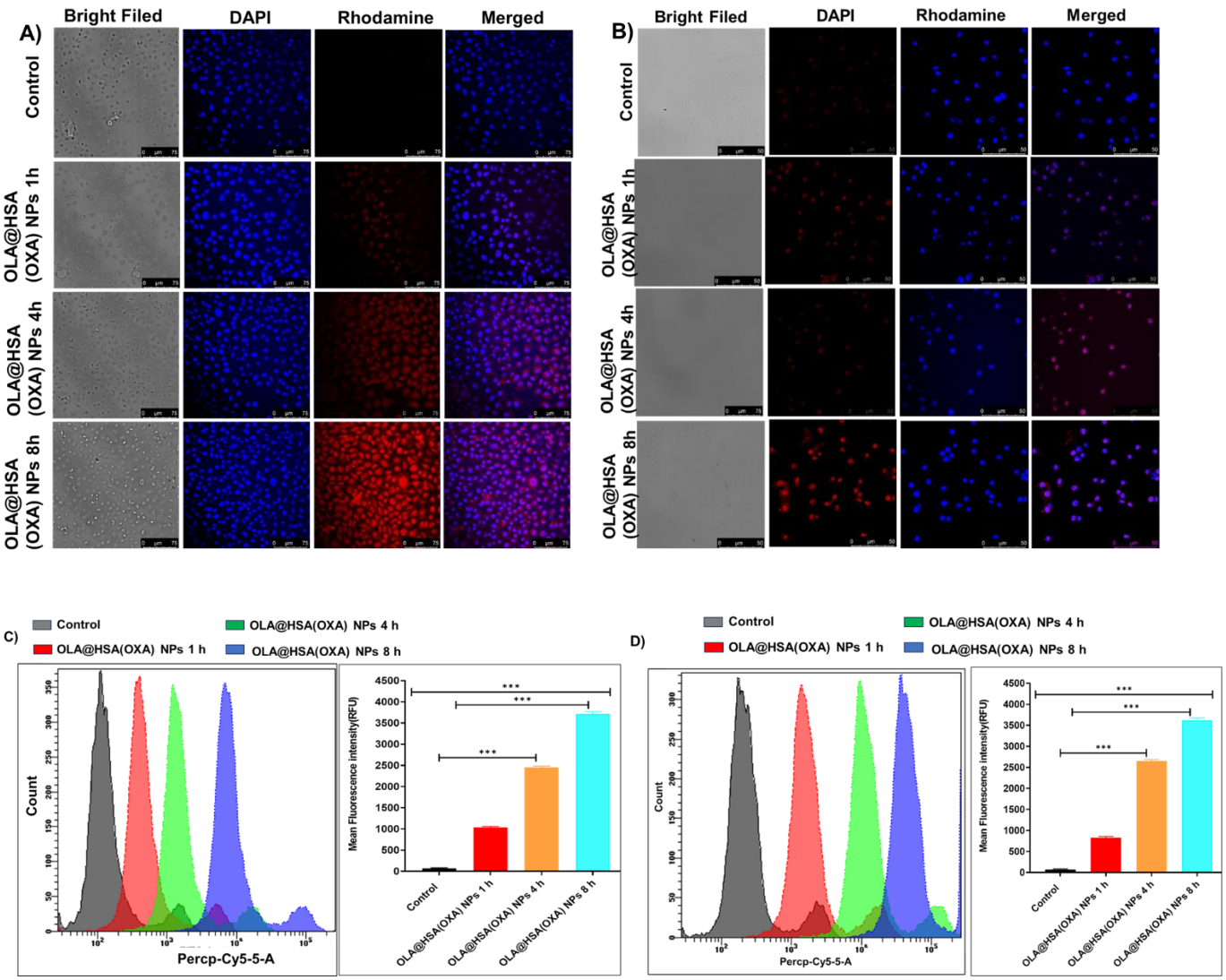

Figure 3.8: *In vitro* cellular association OLA@HSA(OXA) NPs by tracking the fluorescence of rhodamine-labeled HSA. Qualitative analysis by visualizing monolayer cells by fluorescence microscopy, MDA MB 231 cells and 4T1 cells (A & B); quantitative analysis by flow cytometry MB 231 cells data and 4T1 cells data the bar graph of fluorescence intensity of both cell lines (C and D).

3.4.3. Annexin-V Assay:

Annexin-V assay measured the extent of cellular apoptosis following treatment with Olaparib, Oxaliplatin, OLA@HSA NPs, HSA(OXA) NPs, and OLA@HSA(OXA)NPs (**Figure 3.9 A**). It can be observed that for MDA-MB-231 cell lines, while free OXA showed an apoptosis % of 20.38 %, HSA(OXA) NPs showed apoptosis of 65.63 %, OLA@HSA NPs showed apoptosis of 60.21 %, and

OLA@HSA(OXA)NPs showed apoptosis of 82 .83 % for OXA concentration of 10 μM respectively. Similarly, in 4T1 cell lines **(Figure 3.9 B**)., free OXA showed an apoptosis % of 18.38 %, HSA(OXA) NPs showed apoptosis of 70.63 %, OLA@HSA NPs showed apoptosis of 65.21 %, and OLA@HSA(OXA)NPs showed apoptosis of 85 .83 % respectively. Annexin-V assay was studied at 10 μm concentration of the drugs for both OLA and OXA, and the cellular apoptosis was observed in the increasing order for free OLA> free OXA> OLA@HSA NPs> OXA@HSA NPs >OLA@HSA(OXA) NPs. Thus, it was affirmed that HSA led to increased cellular uptake of the drug into the cells leading to increased apoptosis, while a combination of OXA with OLA increased the apoptosis efficiency of the NPs showing a synergistic effect in both MDA-MB-231 and 4T1 cell-lines.

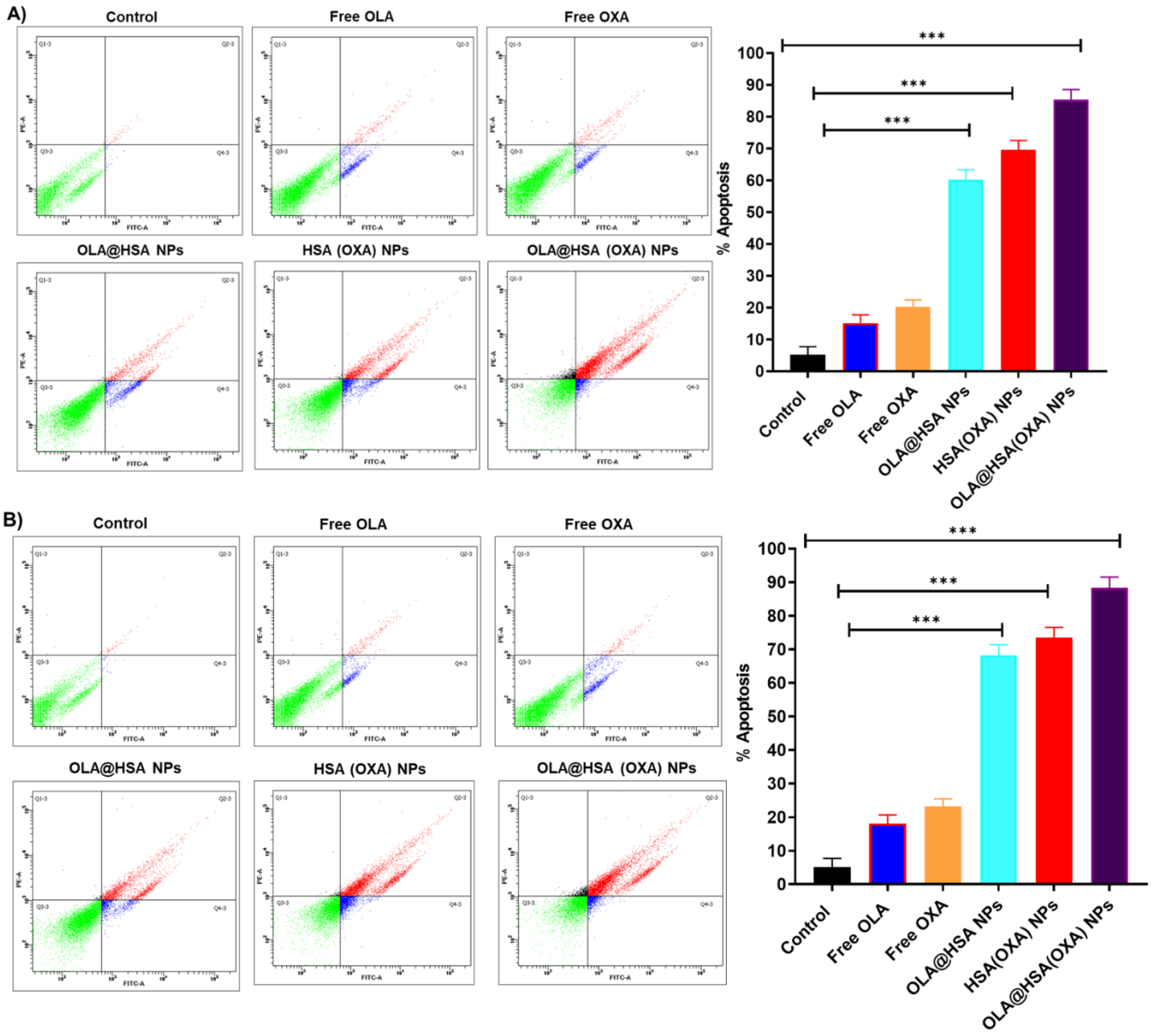

Figure 3.9: Annexin V assay. The extent of apoptosis was evaluated by 4T1 cells (A) and MDA MB 231(B) cells treated with free OLA, free OXA, OLA@HSA NPs, HSA(OXA) NPs, and OLA@HSA(OXA) NPs at an Oxa and Ola concentration of 10 µM (incubation time 24 h) by using flow cytometry. The Q3 and Q4 quadrants represent early and late apoptosis, respectively. 10,000 gated cells were analyzed to obtain the percent cell population in apoptotic stages. The cells were labeled with FITC-labelled annexin V, which tagged the over-expressed early apoptotic marker phosphatidylserines on the cell surface.

Discussion: The highest increase in G2/M arrest by OLA@HSA(OXA) NPs compared to the free drug as well as the individual nanoparticles with human serum albumin which suggests that the ability of the combination shows the highest level of inhibition at the cellular division at the mitotic phase and thus control the doubling time and proliferation rate. The combination drug formulation OLA@HAS(OXA)-NPs showed significantly higher DNA fragmentation and cytoplasmic shrinkage in cells than free drugs or individual nanoparticle formulations.

3.4.4. Cell-cycle Analysis:

The cell cycle analysis plot is represented in **(Figure 3.10A and Figure 3.10B).** The maximum arrest of cells in the G2-M phase was observed with OLA@HSA(OXA) NPs treatment was observed compared to free drug and nanoparticles prepared with individual drug NPs OLA@HSA NPs and HAS(OXA)-NPs. All the formulations and free drugs were evaluated at 10 µm drug concentration, with 8.42 % for control cells, 18.23, 25.23, and 42.36 % for 4T1 cells, and 17.32, 24.32, and 45.32 % for MDA-MB-231 cells for free Olaparib, free Oxaliplatin, HSA(OXA) NPs, OLA@HSA NPs at concentrations, 10 µM/mL, respectively. Migration of cell population from the G1 phase to the G2/M phase predominantly was observed with the OLA@HSA(OXA) NPs treatment compared to free drug and nanoparticles prepared with individual drugs.

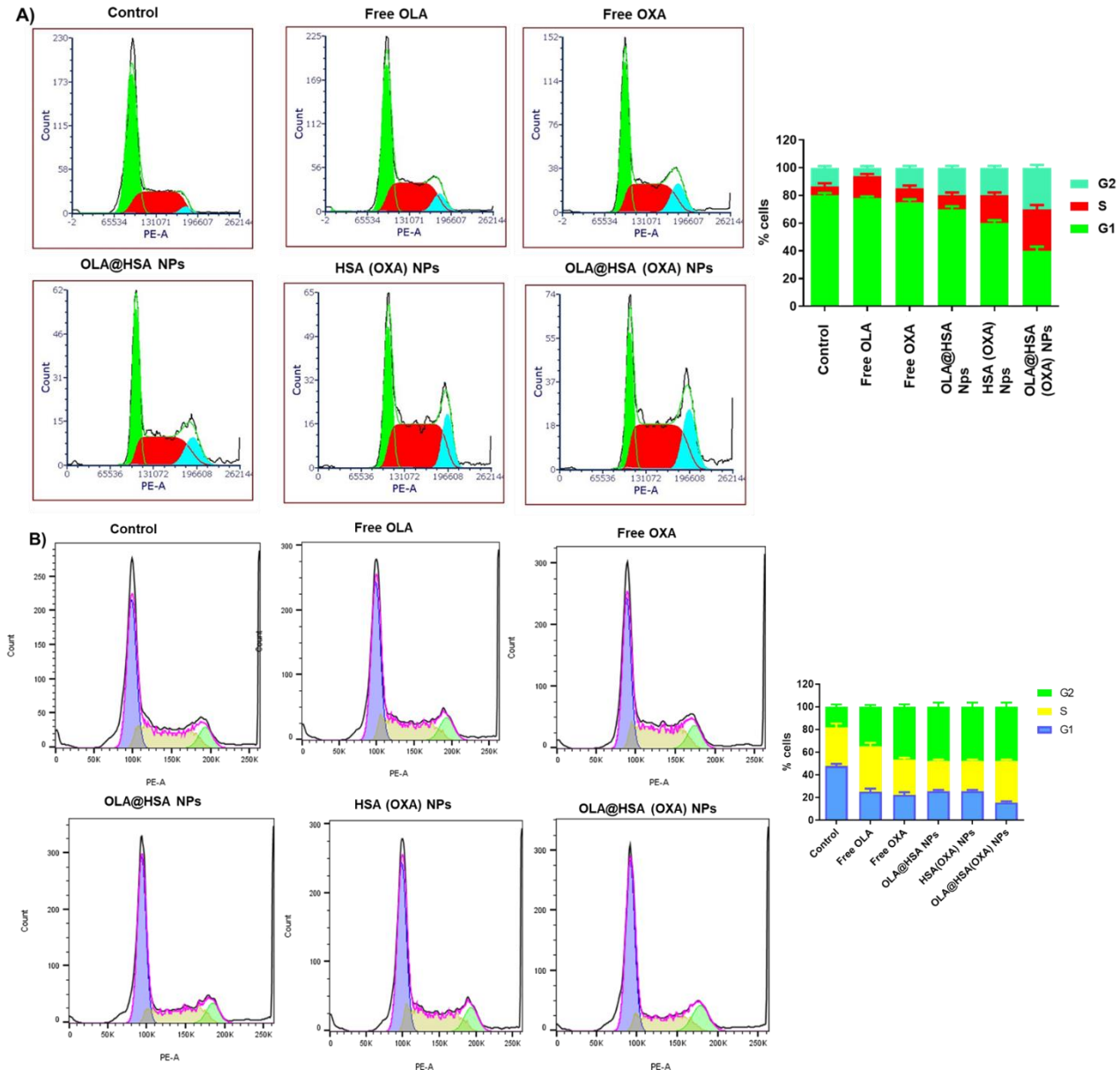

Figure 3.10: Cell-cycle analysis of 4T1 (A) and MDA MB 231 (B) cell lines after 24 h of treatment with free OLA, free OXA, OLA@HSA NPs, HSA(OXA) NPs and OLA@HSA(OXA) NPs. The NPs treatment caused a transition S-phase delay with the cell-cycle arrest at the G2 phase.

Discussion: The combination formulation of OLA@HSA(OXA) NPs induced the highest level of apoptosis, which could be due to the enhanced cellular uptake of Olaparib and Oxaliplatin via the nanocarrier systems. A cellular uptake study revealed that the HSA NPs prepared with both the drugs (OLA and OXA) were more effective on the cancer cells in a time-dependent manner

compared to the free drug and NPs formulations prepared with individual drugs. More DNA damage was indicated by increased cell cycle arrest in G2/M by OLA@HSA(OXA) NPs than free drug treatment and individual NPs formulations. The increase in G2/M arrest by OLA@HSA(OXA) NPs suggests the ability of the formulation to inhibit the cellular division at the mitotic phase and thus control the doubling time and proliferation rate.

3.4.5. Reactive Oxygen species (ROS) generation:

The generation of reactive oxygen species following treatment was indicated by the strong green fluorescence of 2'-7' dichlorofluorescein. OLA@HSA(OXA) NPs-treated cells displayed more intense green fluorescence than the free drug treatment with free Olaparib or free Oxaliplatin treated cells or Nanoparticles prepared with Olaparib or Oxaliplatin individually (**Figure 3.11A).** The quantitative estimation of fluorescence was performed by flow cytometry (**Figure 3.11B).** The result indicated that the 4T1 cells treated with OLA@HSA(OXA) NPs showed a geometric mean of fluorescence, 3800± 18.65, compared to the nanoparticles of Olaparib or Oxaliplatin 2225 ± 17.63, 1805 ± 12.63, treatment respectively. Similarly, a significant increase in the ROS generation was observed in MDA-MB-231 cells treated with OLA@HSA(OXA) NPs (than free Olaparib, free Oxaliplatin, OLA@HSA NPs, OXA@HSA NPs) with the geomean of fluorescence of 3952, 2225 ± 17.63, and 1635. ± 18.71 for OXA(HAS)-NPs, and OLA@HSA NPs respectively.

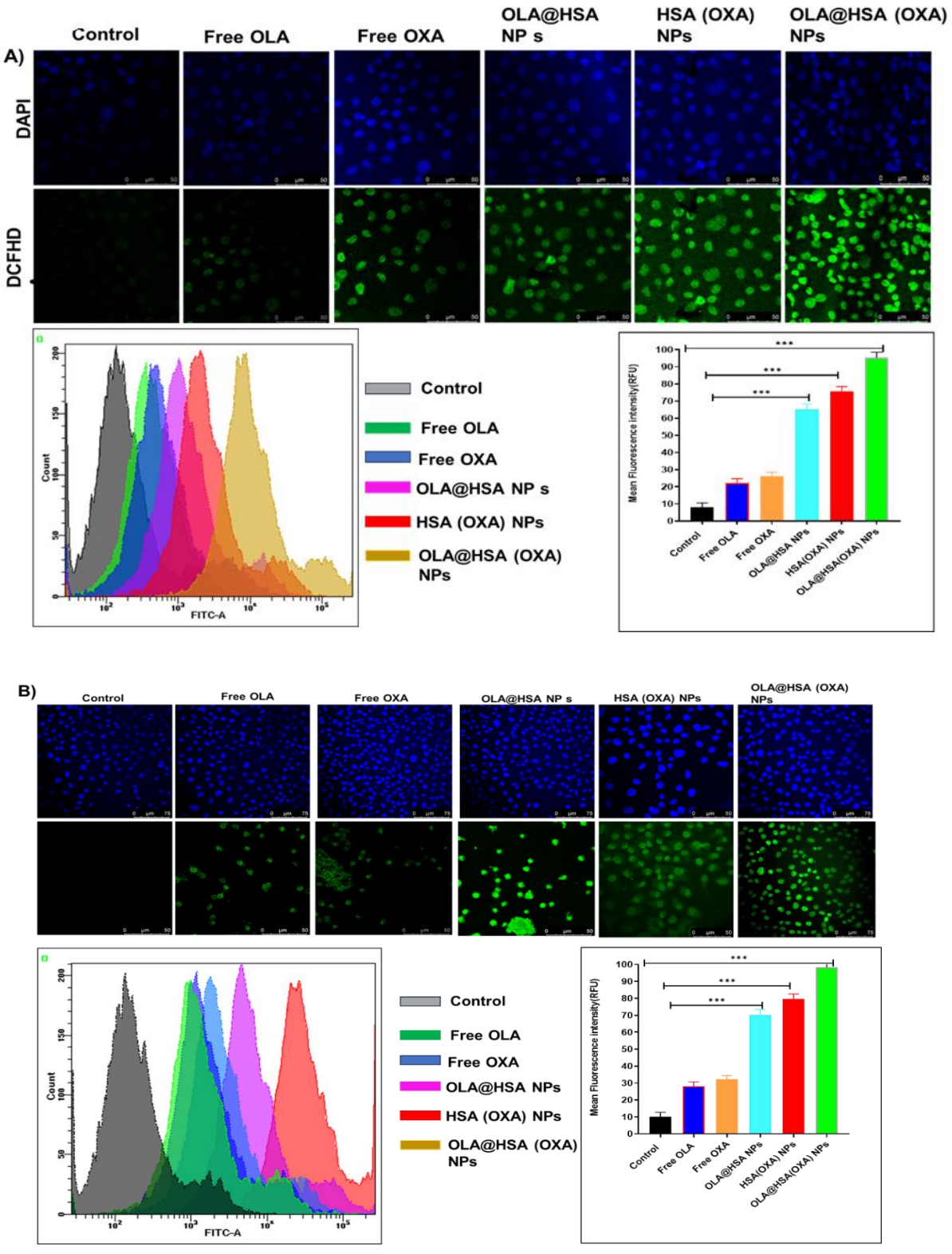

Figure 3.11: Intracellular ROS generation of 4T1 cell (B) and MDA MB 231 cell (A) treated with free OLA, free OXA, OLA@HSA NPs, HSA(OXA) NPs and OLA@HSA(OXA) NPs

followed by incubation of cells with DCFHDA using fluorescence microscopy(A); and the bar graph of average fluorescence intensities of both cell lines (B).

Discussion:

Cytotoxic intracellular ROS could cause damage to mitochondria in cells, resulting in cell death. High levels of ROS could disrupt the mitochondrial permeability transition pore and destroy the integrity of the mitochondrial membrane, resulting in immediate dissipation of mitochondrial transmembrane potential and osmotic swelling of the mitochondrial matrix.

3.4.6. Mitochondrial Membrane Potential Assay:

The fluorescence micrograph of control cells treated with JC-1 exhibited strong red fluorescence, which merged with the green fluorescence of the cells with Olaparib and Oxaliplatin treatment giving rise to orange and yellow signals in Olaparib and Oxaliplatin treated 4T1 and MDA-MB-231 cells, respectively **(Figure 3.12A and B).** The light green signal was observed with the OLA@HSA formulation, OXA@HSA formulation. Combination formulations of OLA@HSA(OXA) NPs-treated cells showed a bright green signal under the fluorescence microscope, indicating the presence of depolarized mitochondria. The flow cytometry data supported the fluorescence spectroscopic observation. The fluorescence emission shift from red to green was observed with the highest shift of cell population from Q2-1 to Q4-1 in OLA@HSA(OXA) NPs-treated cells than free Olaparib, free Oxaliplatin, OLA@HSA NPs, OXA@HSA NPs treated cells.

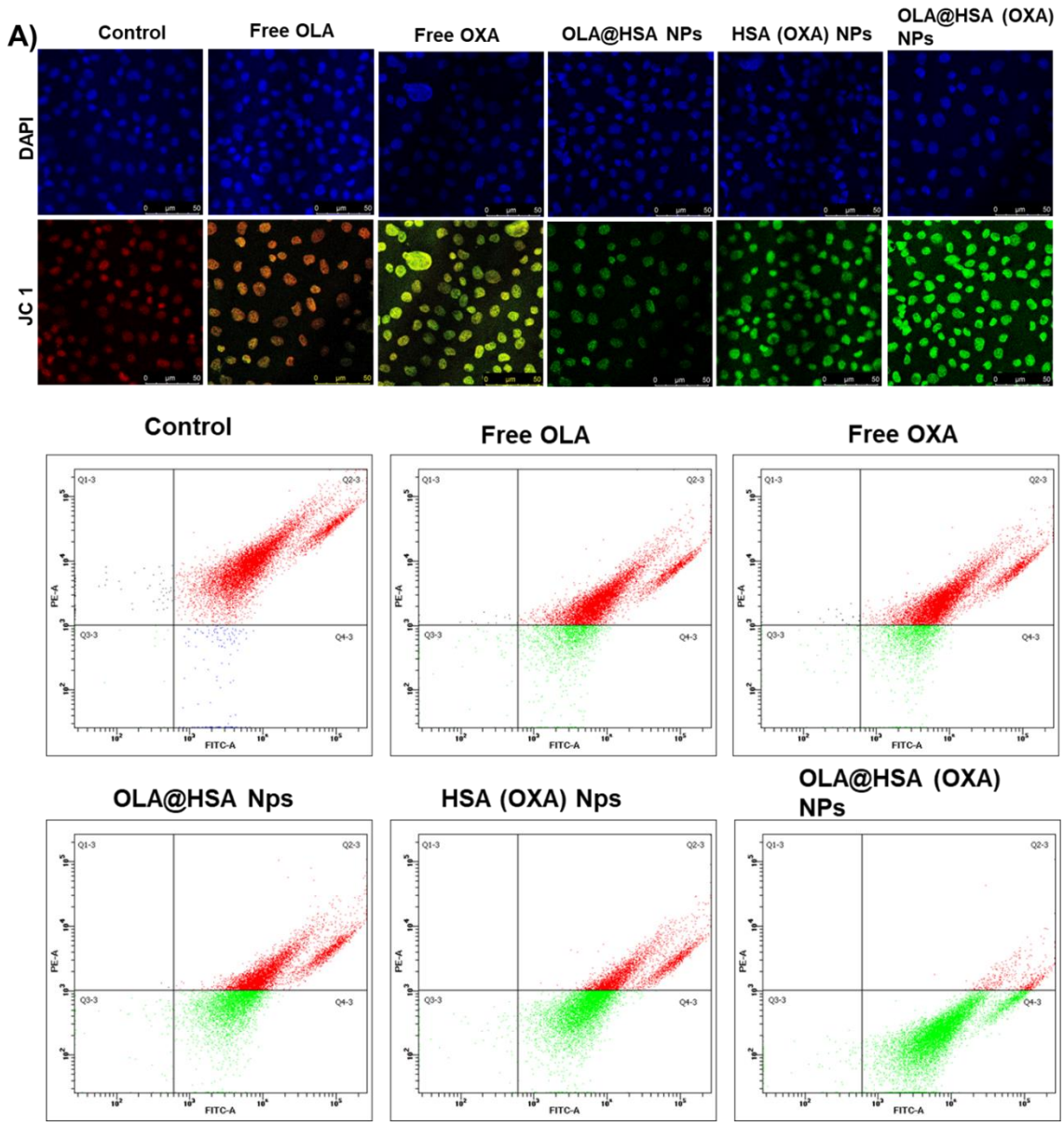
A)
Control
Free OLA
Free OXA
OLA@HSA NPs
HSA (OXA) NPs
OLA@HSA (OXA) NPs
DAPI
JC 1
Control
Free OLA
Free OXA
OLA@HSA Nps
HSA (OXA) Nps
OLA@HSA (OXA) NPs
PE-A
FITC-A
Q1-3
Q2-3
Q3-3
Q4-3

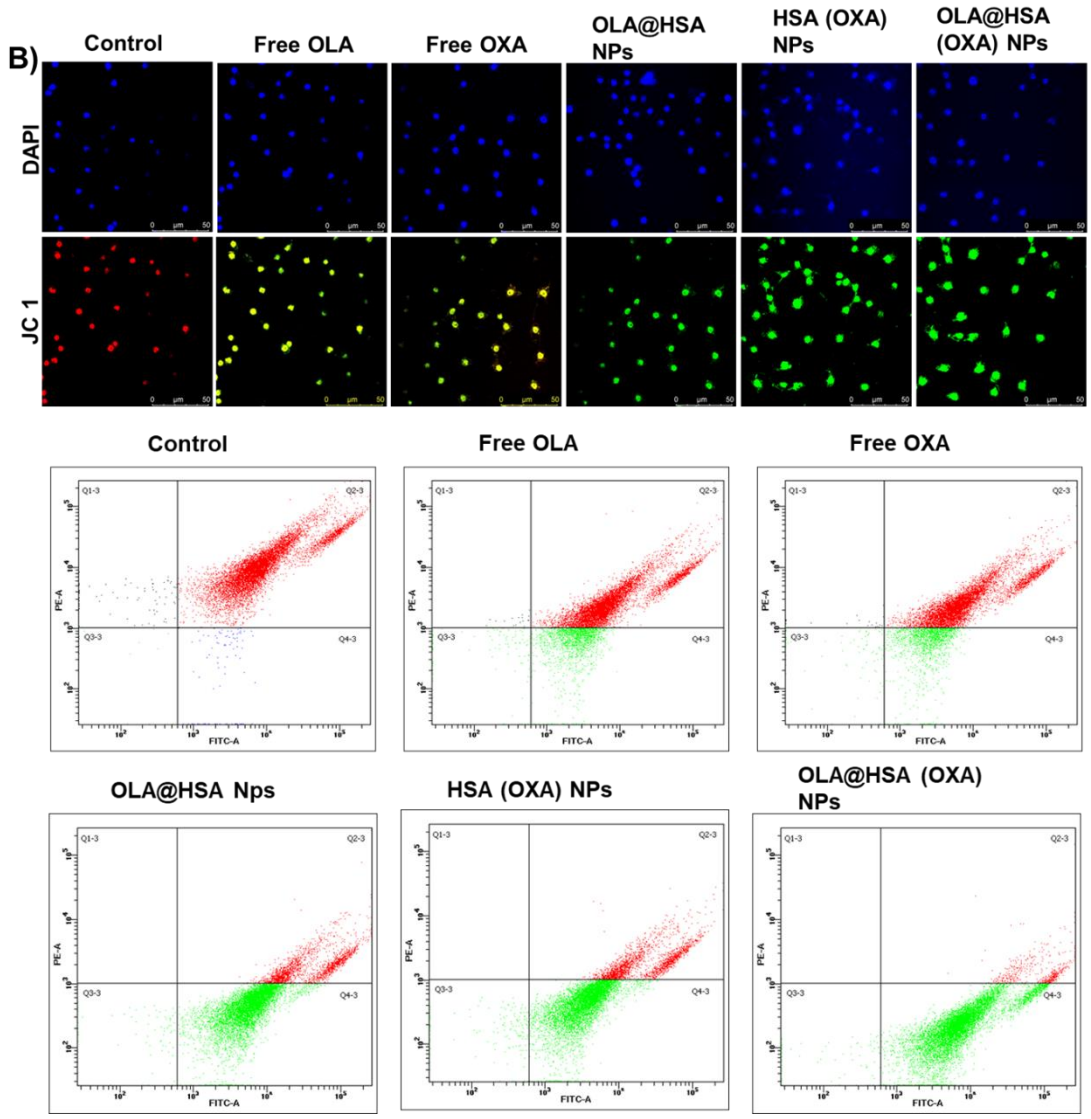

Figure 3.12: Mitochondrial membrane potential assay by JC-1 staining method. Fluorescence microscopic images of 4T1 cell, MDA MB 231 lines cells labeled with DAPI (nuclear staining) and JC-1 (mitochondrial staining), treated with free OLA, free OXA, OLA@HSA NPs, HSA(OXA) NPs and OLA@HSA(OXA) NPs for 24 h, untreated cells as control (A); corresponding flow cytometry analysis of the 4T1, MDA MB 231 (B). JC-1 (red) and JC1 (green) indicate aggregated and monomeric forms of the dye. Scale bars: 100 µm.

3.4.7. Live and Dead Cell Assay

LIVE/DEAD cell assay was conducted at a concentration of 10µm for the free Olaparib, free Oxaliplatin, OLA@HSA NPS, OXA@HSA NPS, and the combination nanoparticle formulation OLA@HSA(OXA) NPs by measuring the two-color fluorescence and, to evaluate cell viability after treatment with free drug and NPs prepared individually and the combination nanoparticle formulation of Olaparib and Oxaliplatin. The highest level of red fluorescence was observed with the combination formulation OLA@HSA(OXA) NPS, indicating increased cell death after treatment with combination drug formulation of OLA@HSA(OXA) NPs derivatives was observed in line cell MDA-MB 231 when compared to control, free Olaparib, free Oxaliplatin, OLA@HSA NPs, and OXA@HSA NPs **(Figure 3.13).**

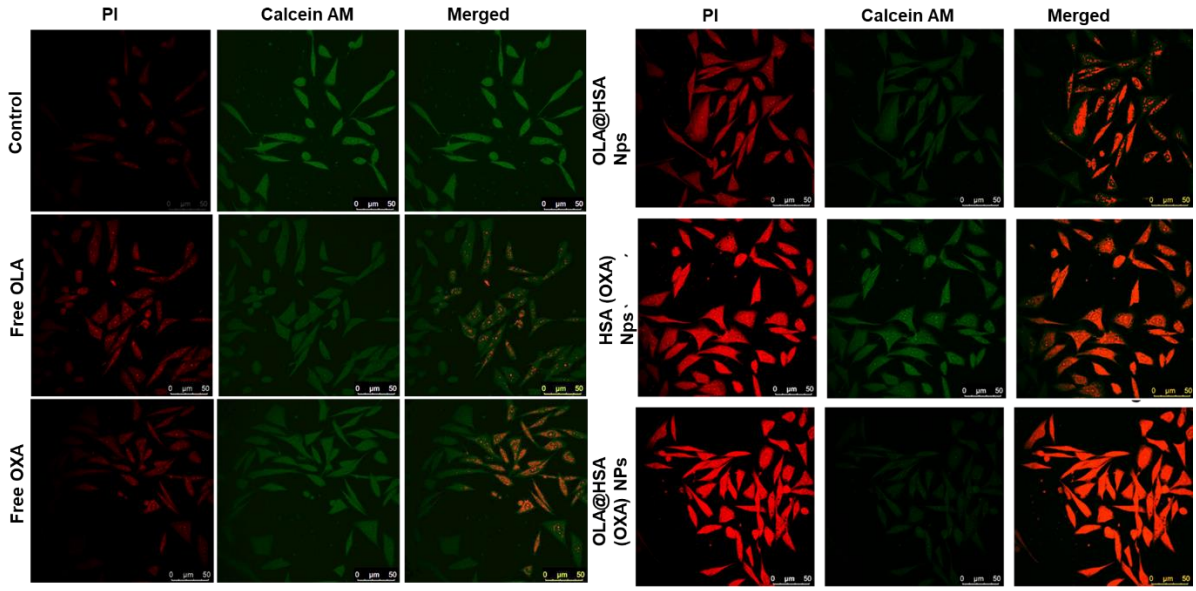

Figure 3.13: Live and dead cell assay of MDA MB 231 cell lines using free OLA, free OXA, OLA@HSA NPs, HSA(OXA) NPs, and OLA@HSA(OXA) NPs treatment.

Discussion: The reduction in cell number can be observed in the tumor cell line MDA-MB 231, with a cell death rate

3.4.8. Acridine orange Assay:

Acridine orange and propidium iodide staining was performed to visualize and understand the apoptotic and necrotic changes of the cells treated with free Olaparib, free Oxaliplatin, OLA@HSA NPs, OXA@HSA NPS at 10µm concentration and combination drug formulation of OLA@HSA(OXA) NPs in this drug concentration (5 µM concentration for each drug) was treated in MDA MB 231 cell lines. Green fluorescence was clearly visible in the control as well as the treatment with free Olaparib, free Oxaliplatin and decreased in the cells treated with OLA@HSA NPs, OXA@HSA NPs and significantly decreased for the combination formulation OLA@HSA(OXA) NPs formulation. It was observed that the cells treated with OLA@HSA(OXA) NPs formulation showed the strongest red fluorescence highlighting the synergistic effect of OXA and OLA. As HSA improved the internalization of the NPs into the cells, the NPs exhibited significantly higher apoptotic activity compared to the free drug treatment (indicated early apoptosis stage)**.**

Discussion: Normal green nuclei were observed for the viable cells observed for the control sample, free Olaparib and free Oxaliplatin indicated uniform with an organized structure, and minimal cell death was observed compared to nanoparticles formulation of Olaparib and Oxaliplatin and combination drug formulation of Olaparib and Oxaliplatin.

3.5.0. *In vivo* antitumor efficacy studies-

3.5.1. Tumor Inhibition study:

To understand the inhibition efficacy of the various groups considered, 4T1-Luc cells were orthotopically injected into female Balb/C mice, and after tumor development up to 60 mm3, the mice were divided into different groups and treated intravenously with free OLA, free OXA, OLA@HSA NPs HSA (OXA) NPs and OLA@HSA(OXA) NPs at a concentration of 50mg/kg. The tumor inhibition was compared with the control. The body weight of the mice

throughout the treatment period for all the groups did not change significantly, though precisely, there was a faster increase in weight in control groups compared to the treatment groups. Free OLA, free OXA, OLA@HSA NPs, HSA (OXA) NPs, and OLA@HSA(OXA) NPs showed less increase in body weight in order **(Figure 3.15B).** The tumor volume, measured at the end of 21 days, for free OLA, free OXA, OLA@HSA NPs, HSA (OXA) NPs, and OLA@HSA(OXA) NPs were 502 ± 30.23, 405.24 ± 21.32, 350 ± 24.32, 205.54 ± 15.63 and 102.54 ± 15.63 mm3 respectively which compared to the control group, 1083 ± 20.35 mm^3 showed a reduction of 9 folds (for OLA@HSA(OXA) NPs) **(Figure 3.15A).** The elevated decrease of tumor volume of OLA@HSA(OXA) NPs compared to free OXA could be attributed to the presence of HSA as the shell of the nanoparticles, which increases its internalization to the tumor environment specifically, through GP60 and SPARC mechanism, thus increasing the site specificity which is not observed in the case of free drug treatment.

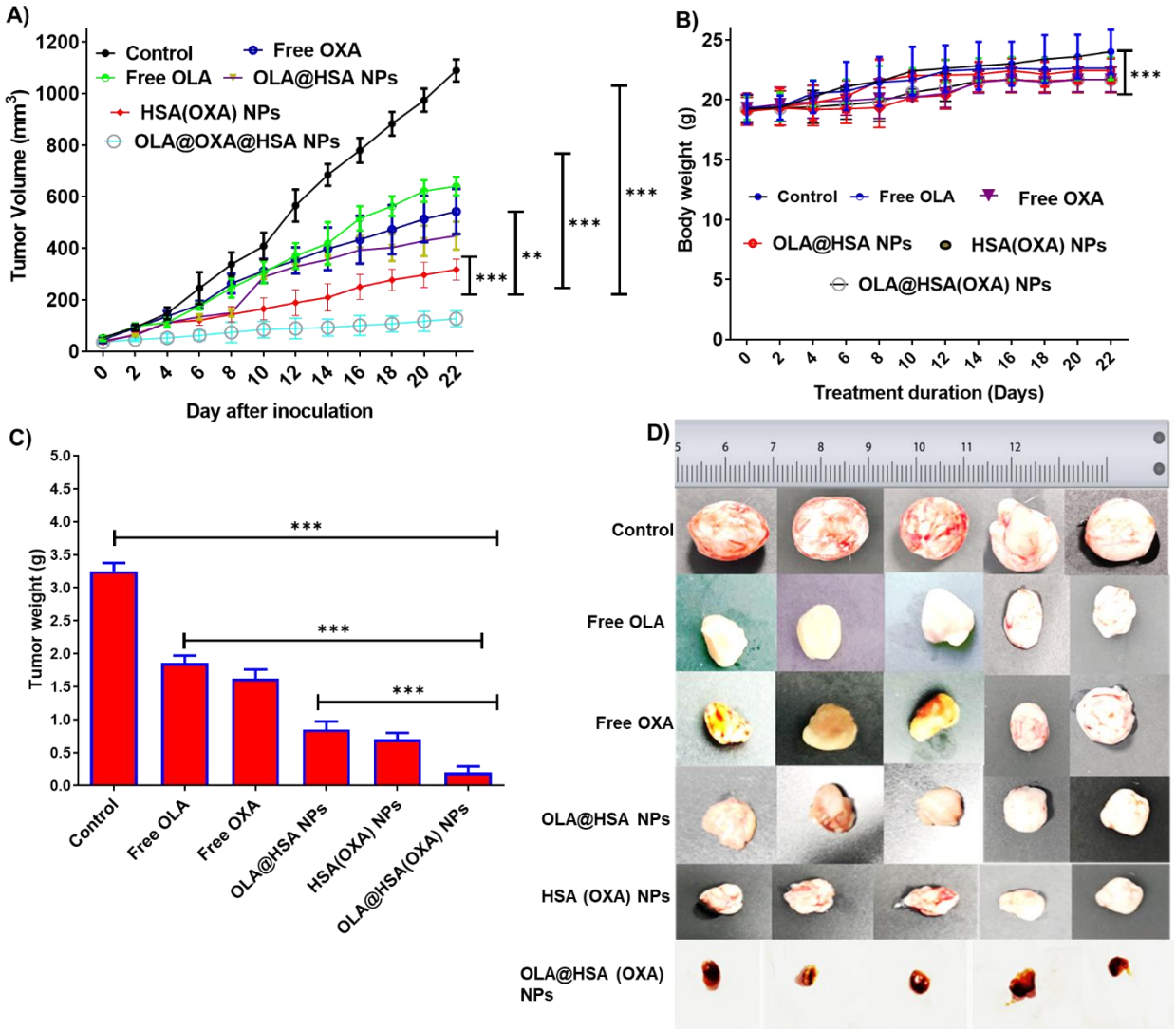

Figure 3.15: *In vivo* antitumor efficacy. Macro views of excised tumors of 4T1 tumor-bearing BALB/c mice after different treatments (A); tumor volume (B); body weight changes (C); and excised tumor weight (D); data represent mean ± SD. Arrows represent the administration. n = 5; **, $p < 0.05$; ***, $p < 0.001$.

The mice were injected with D-luciferin and observed for fluorescence intensity and tumor progression, as depicted in Figure 3.16. The tumors extracted from all the mice of the different groups on day 21 were weighed and imaged, as represented in Figure 3.15D, respectively. It was observed that free OLA and free OXA showed slight growth inhibition, followed by OLA@HSA NPs, OXA(HAS) NPs, and maximum inhibition by OLA@HSA(OXA)NPs.

Comparing this, the OLA@HSA(OXA)NPs showed maximum inhibition of tumor progression, indicating the synergistic effect of OXA and OLA and validating the results obtained in the *in vitro* assays.

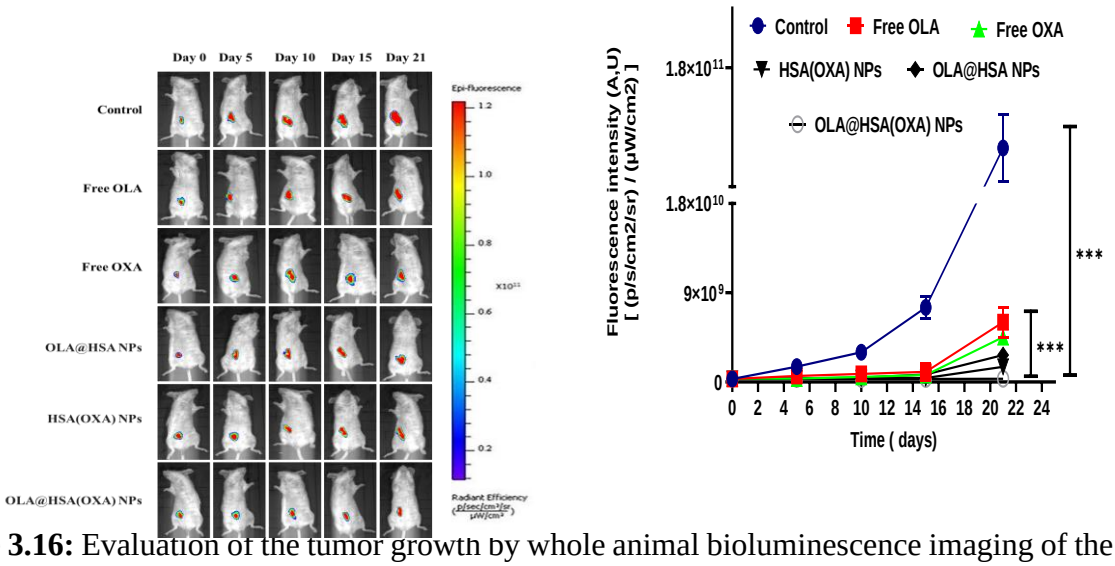

Figure 3.16: Evaluation of the tumor growth by whole animal bioluminescence imaging of the 4T1-Luc tumors from Control, free Olaparib, free Oxaliplatin, OLA@HSA NPs, HSA(OXA) NPs, OLA@HSA(OXA)NPs

3.5.2. Immunohistochemistry by tunnel assay in tumors:

The immunohistochemistry of the tissue sections indicated a higher number of apoptotic nuclei in OLA@HSA(OXA) NPs-tumor groups than untreated control and Olaparib groups in the TUNEL assay, where the free 3'-hydroxyl termini of DNAs are labelled. The higher labelling is indicative of the presence of more fragmented DNA by double strands break, leading to apoptosis **(Figure 3.17).**

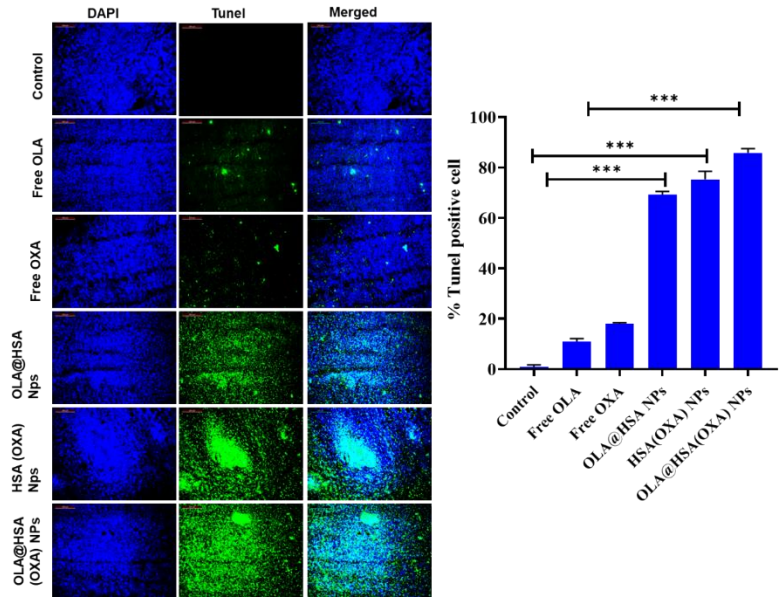

Figure 3.17: Tunel assay of Control, free OLA, free OXA, OLA@HSA NPs, HSA(OXA) NPs, and OLA@HSA(OXA) NPs treatment.

The TUNEL-positive cells as indicated by green fluorescence where abundant in cryo-sectioned tumour tissues from the mice, which received the OLA@HSA(OXA)- NPs treatment compared to other formulations made with the individual drug and free drugs.

3.5.3.ROS generation in tumor tissue:

ROS generation is considered an essential feature of apoptosis in the tumor microenvironment. This was studied by injecting DCHFDA into the mice of all groups. Post 30 min, the mice were sacrificed, and tumors were isolated and sectioned to be observed under fluorescence microscopy. The images, as represented in **(Figure 3.18)**, indicated that the green fluorescence observed was significantly high in the case of OLA@HSA(OXA) NPs as compared to OLA@HSA NPs, HSA(OXA) NPs and least in the case of free OXA. The control group showed almost negligible fluorescence. The strong fluorescence could be attributed to the combined effect of OXA and OLA with high internalization to the tumor region, leading to increased generation of ROS species. DCHFDA gets cleaved due to the presence of cellular esterases

present, producing 2'-7'-dichlorofluorescein, which is easily oxidized, producing strong green fluorescence.

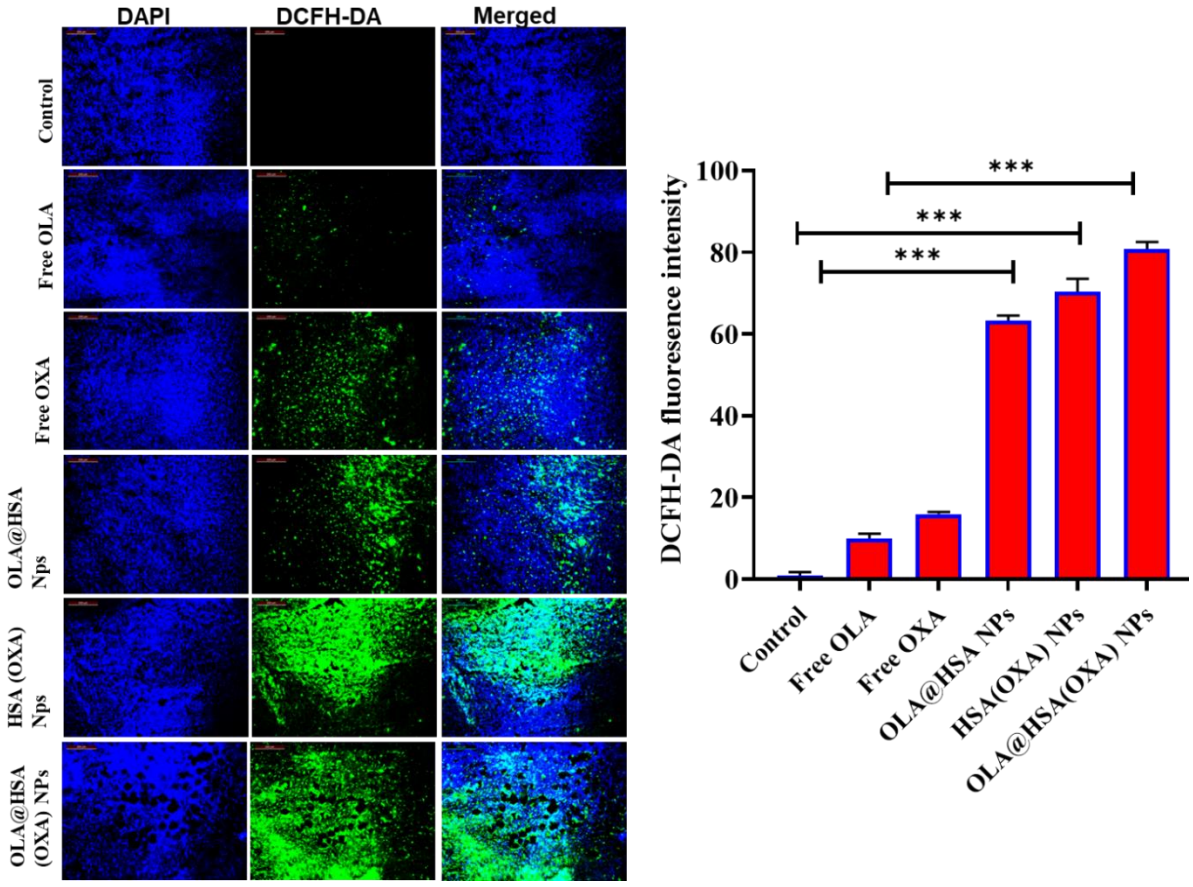

Figure 3.18: Representative images of ROS generation of Tumor tissue from Control, free Olaparib, free Oxaliplatin, OLA@HSA NPs, HSA(OXA) NPs, OLA@HSA(OXA)NPs

3.5.4.Ki-67 assay of tumor tissue:

Another assay performed on the tumor sections was for the detection of KI-67, a cell proliferative marker. The tumor sections were incubated with the KI-67 antibody, which further interacted with the fluorescence-tagged secondary antibody (Alexa flour 488) and visualized under the fluorescence microscope. It was observed that the group treated with OLA@HSA(OXA) NPs demonstrated the least green fluorescence, while the control group had the highest intensity indicating a decrease in the proliferative marker in the treatment group (Figure 3.19). As KI67 is a nuclear protein, in cancer cells, they overexpress, hence forming

an essential biomarker of tumor tissues. Following treatment, as the tumor growth is alleviated, the expression of KI-67 is subsequently decreased, leading to a reduction in the fluorescence intensity.

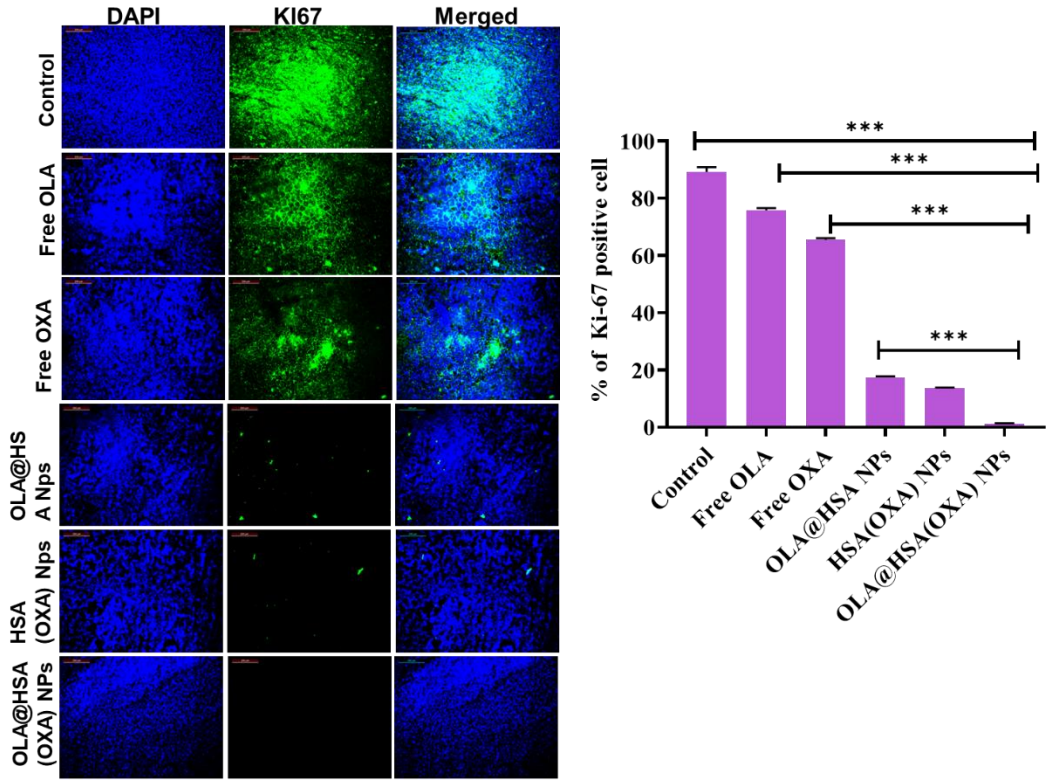

Figure 3.19: fluorescent images of tumor tissue sections of the treated mice with control, free Olaparib, free Oxaliplatin, OLA@HSA NPs, HSA(OXA) NPs, OLA@HSA(OXA)NPs for immune-histochemical analysis of Ki-67.

3.5.5. Lung Metastasis:

The histopathological observation revealed that the lung in the tumor-bearing untreated mice had a dense tissue population indicative of metastatic loci. However, lung histology of the OLA@HSA NPs-treated group was similar to the normal, non-tumor implanted mice. The property of OLA@HSA(OXA) NPs to inhibit and prevent lung metastasis was also evaluated. On day 21 of the treatment period, the tumors were excised, and the mice were kept under observation for the next 7 days. Post 7 days, the mice of all groups were sacrificed, and the

lungs were isolated and imaged for the presence of tumor nodules. In the control group, multiple such nodules were observed, while in the free OXA group, though the bioluminescence intensity decreased, it was not diminished to a great extent. On the contrary, the DTX/OA@HOP NPs group showed a significant decrease in the bioluminescence intensity, and there was negligible metastasis observed **(Figure 3.20).**

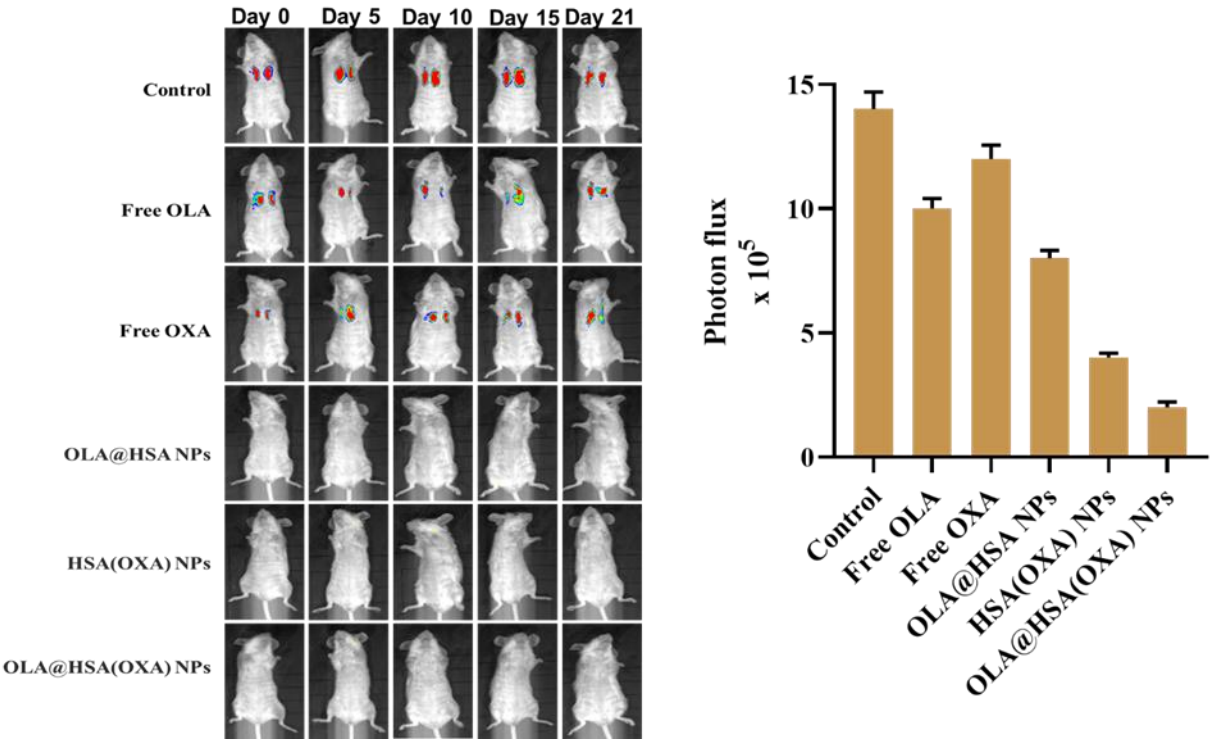

Figure 3.20: Bioluminescence imaging of lung metastatic 4T1-Luc tumors in lungs tissues of Control, free Olaparib, free Oxaliplatin, OLA@HSA, HSA(OXA)NPs and OLA@HSA(OXA)NPs -treated mice.

Chapter 4

Conclusion

Conclusion:

Breast cancer (BC) is an extremely prevalent form of cancer that affects a lot of women all over the globe, with an estimated yearly effect of ~2-2.5 million people. The prevalence of BC among women has continuously been the highest of all malignancies in both developed nations like the United States and developing nations like China. Triple-negative BC (TNBC) is a subtype of BC that only occurs in around 20 % of cases and lacks the expression of HER-2 protein, ER, and PR. As there were no proteins in the cancer cells, hormone therapy and treatment with the drugs targeting HER2 would not be useful, and the option left was chemotherapy (chemo), the option is one of the main systemic treatments. TNBC Patients will not have an option or benefit from trastuzumab-based therapy or hormonal-based therapies. The treatment options left out for the treatment of triple-negative breast cancer are surgery or chemotherapy or in combination approach that's surgery and chemotherapeutic medicines.

Different stages of triple-negative breast cancer are stage-I to stage-III triple-negative breast cancer and stage-IV TNBC and recurrent triple-negative breast cancer. Which can be called as early stage of TNBC and can be removed by surgery. Surgery first: If the tumor of larger than 2cm and smaller than 5cm and 1 to 3 lymph nodes with cancer may undergo surgery or a mastectomy. If lymph nodes are found to have cancer, then radiation is followed by surgery. There might be adjuvant chemotherapy with Olaparib to reduce the chances of Triple-negative breast cancer recurrence. Surgery second: In these cases of surgery for the second time, chemotherapy with pembrolizumab will be given to triple-negative breast cancer patients to minimize the tumor before surgery. After the second surgery, If cancer persists in the tissues, then chemotherapy with capecitabine or pembrolizumab for a period of 18 to 24 weeks to reduce the recurrence of the TNBC. Also, Olaparib oral treatment for one year will be given to patients with BRCA mutation to reduce the chances of the recurrence of TNBC. The brand name for Olaparib is Lynpazra, and this drug product was approved in 2017 by AstraZeneca

for the treatment of TNBC in the form of oral tablets in doses of 100mg and 150mg. Olaparib was approved by USFDA to treat BRCA1/2-mutated/HER-2/neu negative breast cancer at 300mg of daily dose.

As this Olaparib is an oral dosage form and not a targeted drug delivery, it may create Myelodysplastic Syndrome/Acute Myeloid Leukemia (MDS/AML) and have fatal outcomes in 1.5% of the patients. Monthly hematological toxicity monitoring is required in triple-negative breast cancer patients. During the treatment with Olaparib, 0.8% of patients got Pneumonitis, and a few cases were fatal and needed to discontinue if pneumonitis was confirmed. Also, in a few patients, it was observed that Venous thromboembolism (VTE) and fatal pulmonary embolism (PE) were observed who were taking Olaparib. Olaparib was reported to have fetal harm due to Embryo-fetal toxicity.

As a monotherapy with alone drug treatment, the most common side-effects as a single agent were anaemia, vomiting, nausea, fatigue (including asthenia), decreased appetite, diarrhoea, headache, cough, dysgeusia, dyspnoea, neutropenia, dizziness, leukopenia, dyspepsia, and thrombocytopenia. Anaemia, fatigue, nausea, diarrhoea, and decreased appetite were observed when Olaparib was given in combination with prednisone or abiraterone. Similar types of adverse effects observed when Olaparib combined with bevacizumab combination were nausea, fatigue (including asthenia), anaemia, lymphopenia, vomiting, diarrhoea, neutropenia, leukopenia, urinary tract infection, and headache.

Olaparib has low aqueous solubility and permeability due to its BCS (Biopharmaceutical Classification System) class IV drug due to its poor bioavailability of oral dosage forms, which has less sensitivity to *wild*-type *BRCA* tumor growth inhibition.

In the present research, to overcome the above challenges, Olaparib drug delivery was targeted with human serum albumin to reduce the adverse side effects of the drug. In this, Olaparib with

human serum albumin drug delivery was targeted to address the non-specificity and adverse effects. In the current research, Olaparib drug delivery with the Human serum albumin was selected as a nano-carrier to address some of the adverse effects, and the human serum albumin (HSA) is selected as a drug carrier because of its lack of toxicity, biodegradability, and immunogenicity.

Human Serum albumin has been clinically accepted and safe to use as a drug carrier in nanomedicine. Commercially Paclitaxel is available with Human serum albumin as a drug carrier under the brand name Abraxane for the treatment of cancer. The drugs with human serum albumin show the EPR effect due to its accumulation at the tumor site. The mechanism involved in this approach of transcytosis is the binding of human serum albumin with 60-kDa glycoprotein (gp60) receptor, further formation of caveolin-1 and the consequent formation of transcytosis vesicles, then internalization and reaching to the tumor tissues. This selective binding of human serum albumin with the gp-60 receptors and targeted drug delivery will reduce the side effect associated with Olaparib.

The current research was focused on the targeted delivery of Olaparib to cancer cells by reducing its unwanted side effects and with human serum albumin as a drug carrier. Nanoparticles of Olaparib with human serum albumin were prepared using the de-solvation technique; further nanoparticles were isolated and lyophilized by adding the bulking agent mannitol. The prepared NPs were evaluated for their physicochemical stability by testing the nano-particles formulation for kinetic stability, % drug loading (DL), % entrapment efficiency (EE), zeta potential, particle size, FTIR, X-ray diffraction, and biocompatibility studies. To further understand the anticancer activity of the prepared Olaparib-human serum albumin nanoparticle formulation was studied *in vitro* cell line studies in MDAMB-231 and 4T1-cell lines and *in vivo* studies in mouse models.

The prepared nanoparticles shown exhibited low polydispersity, optimal DL, entrapment, and sustained release at blood pH with accelerated release at tumor pH. The OLA@HSA NPs were stable at 4 °C, non-haemolytic, and demonstrated lower half-maximal inhibitory concentrations than free olaparib in mouse and human TNBC cell lines. The cellular uptake study indicated that the NPs were internalized with time. Compared to free drugs, OLA@HSA NPs were shown to have an increased level of mitochondrial membrane depolarization, cell cycle arrest in the G2/M phase, ROS generation, and DNA fragmentation. The *in vivo* animal study shows that the OLA@HSA NPs have shown reduced tumor volume growth significantly compared to control and free olaparib. The isolated tumors of the animal which were treated with OLA@HSA NPs show the reduced expression of PARP-1 and increased tumor proliferative marker, Ki-67, p53, γH2AX, and ROS. Overall, the OLA@HSA NPs induced a strong apoptotic response *in vitro* and *in vivo* compared to free drug and control. Further exploration is needed to evaluate their potential for successful utilization as chemotherapy in TNBC.

In this second project, combination therapy was used to develop and delivered two therapeutic agents using human serum albumin and effective against Triple-negative breast cancer with non-overlapping mechanisms which induce cell death. Combining therapeutic agents with varied mechanisms of action could produce additive or synergistic therapeutic responses, which is more beneficial than monotherapy. Here, we have studied the impact of the combination drugs that is Olaparib and Oxaliplatin with human serum albumin as a carrier for the treatment of triple-negative breast cancer and to determine whether this combination therapy has more significant biological effects together than as single agents alone in cancer cells. We have observed that the combination therapy of Olaparib with Oxaliplatin has shown improved cell cycle arrest in the G2/M phase and improved apoptosis in breast cancer cell-line models MDAMD-231 and 4T1 cell lines. These observations indicate that combination therapy

with Olaparib and Oxaliplatin shows powerful apoptotic in cancer cells and can be of potential combination therapy in clinical application.

In the first objective of the work, Olaparib was entrapped in the human serum albumin, and the preparation of OLA@HSA nanoparticles by cross-linking the OLA with HSA using the glutaraldehyde as a crosslinking agent and the nanoparticles were prepared using the de-solvation technique.

The nanosized particles, OLA@HSA NPs, were characterized to determine various physicochemical parameters. The prepared nanoparticles exhibited narrow size distribution and lower PDI with optimal drug loading and entrapment efficiency. The *in vitro* release studies it was indicating that sustained release at blood pH with a higher amount of the drug release at tumor pH, which may be helpful for the drug release as well as apoptosis of the cancer cells. The stability of the reconstituted nanoparticles OLA@HSA NPs was more stable at 4 °C compared to room temperature storage conditions. The *in vitro* non-hemolytic study demonstrated lower half-maximal inhibitory concentrations for OLA@HSA Nanoparticles compared to the free drug in mouse and human TNBC cell lines.

The OLA@HSA NPs caused the highest cell cycle arrest in the G2/M phase, DNA fragmentation, mitochondrial membrane depolarization, and ROS generation. The *in vivo* study demonstrated that the OLA@HSA NPs suppressed the tumor volume significantly compared to control and free Olaparib-treated tumors. The isolated OLA@HSA NPs-treated tumors had increased expressions of fragmented DNAs, proliferative marker, Ki-67, p53, γH2AX, and ROS and reduced expressions of PARP-1. Overall, the OLA@HSA NPs induced a strong apoptotic response *in vitro* and *in vivo*, demanding further exploration and revealing their potential for successful utilization as chemotherapy in TNBC.

In the second objective, we established the delivery using Human Serum Albumin as the carrier for Olaparib and Oxaliplatin. In the monotherapy with Olaparib, sometimes there might be recurrence which can't be addressed with Olaparib monotherapy, and it requires combination drug therapy. Hence the combination of Olaparib with Oxaliplatin was explored to meet the unmet medical need of TNBC recurrence.

Drugs were crosslinked with Human serum albumin and delivered to the tumor cells. A combination of Olaparib with Oxaliplatin was reported the in the treatment and inhibition of tumor proliferation in colorectal cancer, which has XRCC2 deficient; also, in the literature, it was reported that combining chemotherapeutic agents with gene agents for cancer treatment has an improved therapeutic effect. From the literature, it was evident that the patients treated with single-agent chemotherapy, due to its limitations on specific cancer survival pathways, showed slow response as well as relapse of tumor. Combination therapies will have the advantages of the synergistic effect; it overcomes the MDR and will have reduced toxicity.

The current combination drug delivery of Olaparib and Oxaliplatin delivery was targeted to reduce drug resistance and improve synergistic effects in the treatment of triple-negative breast cancer. A combination of Olaparib with Oxaliplatin and using human serum albumin as a carrier was not explored in the literature to date for the treatment of triple-negative breast cancer. Hence the current research was focused on this approach.

Combined drug loading (Olaparib and Oxaliplatin) was done onto the human serum albumin by using the conjugating agent with CO-NH bond formation between the drugs and HSA using the glutaraldehyde as a crosslinking agent using the de-solvation technique. The prepared combination nano-particles of OLA@HSA(OXA) NPs were characterized using various physicochemical evaluations. *In vitro* release of the prepared nanoparticle of OLA@HSA(OXA) NPs found to be higher in the pH 5.5, which will be of tumor pH. From

the reconstitution stability studies OLA@HSA(OXA), NPs were comparatively more stable at 4 °C than controlled room temperature conditions. Form the non-hemolytic studies demonstrated that lower half-maximal inhibitory concentrations with OLA@HSA(OXA) NPs than free drugs and the individually prepared nanoparticle formulations. The increased expression level of the apoptotic marker phosphatidylserine was observed for the OLA@HSA(OXA) NP compared to the other free drug as well as the formulations prepared individual drugs with the Human Serum Albumin. The OLA@HSA(OXA) NPs enhanced DNA fragmentation, mitochondrial membrane depolarization, and ROS generation and resulted in the highest cell cycle arrest in the G2/M phase. Tumor volume was smallest with OLA@HSA(OXA) NPs compared to all other formulations, which were individually made with Human serum albumin and free drugs Olaparib and Oxaliplatin. Overall, the OLA@HSA(OXA) NPs showed the highest *in vitro* and *in vivo* apoptosis, demanding further exploration and can be future combination drug therapy of Olaparib with Oxaliplatin for the in the drug-resistant and recurrent cases of the triple-negative breast cancer TNBC.

Chapter 5

Future scope of work

Future scope of work

Huma Serum albumin drug delivery has been explored in the last decade after the first commercial success for the nano-paclitaxel using the nab technology. Currently, different drugs are under exploration, and various stages of clinical trials with human serum albumin as a carrier were nab-Docetaxel (ABI-008), (nab-rapamycin) ABI-009, ABI-010(nab-17AAG) and ABI-011(Dual Microtubule and Topoisomerase-1 inhibitor solid tumors). The current research was studied for Olaparib and Oxaliplatin using the human Serum Albumin carrier for the treatment of Triple-negative breast cancer as a monotherapy as well as combination therapy for recurrent TNBC. Optimization and usage of the advanced approaches will increase the drug loading to the nanoparticle and which will have improved drug-loading capacity, tumor-specific uptake as well as anti-cancer effect. To enhance the drug-loading capacity, many methods have been developed to improve the interaction between the drug and the carrier in polymeric nanocarrier. To enhance the anticancer effect, numerous biologically active carriers have been developed as dual-functional carriers.

Different anti-cancer drugs can be explored with human serum albumin as a carrier that connects easily with gp-60 receptors on the cancer cells and releases the SPARC protein, which internalizes easily and is delivered to the target site, which will have minimal side effects. Albumin-based drug delivery is free from solvents, and side effects with solvent-based formulations can be avoidable. The developed delivery with human serum albumin can be explored by combining therapeutics with molecularly targeted biologics, gene therapeutics as well with anti-cancer drugs can be explored. However, optimization and development of combination drug delivery with human serum albumin are quite more challenging, and the monotherapies require an improved optimization skill set to arrive at stable formulations which can treat cancer and Olaparib and Oxaliplatin drug delivery with Human serum albumin needs further exploration.

Chapter 6

References

References

1. Jain, V., Kumar, H., Anod, H.V., Chand, P., Gupta, N.V., Dey, S. and Kesharwani, S.S., 2020. A review of nanotechnology-based approaches for breast cancer and triple-negative breast cancer. Journal of Controlled Release, 326, pp.628-647.
2. Fang, X., Cao, J. and Shen, A., 2020. Advances in anti-breast cancer drugs and the application of nano-drug delivery systems in breast cancer therapy. Journal of Drug Delivery Science and Technology, 57, p.101662.
3. Bray, F., Ferlay, J., Soerjomataram, I., Siegel, R.L., Torre, L.A. and Jemal, A., 2018. Global cancer statistics 2018: GLOBOCAN estimates of incidence and mortality worldwide for 36 cancers in 185 countries. CA: a cancer journal for clinicians, 68(6), pp.394-424.
4. Saraiva, D., Cabral, M.G., Jacinto, A. and Braga, S., 2017. How many diseases is triple-negative breast cancer: the protagonism of the immune microenvironment. Esmo Open, 2(4), p.e000208.
5. Xiong, G., Stewart, R.L., Chen, J., Gao, T., Scott, T.L., Samayoa, L.M., O'Connor, K., Lane, A.N. and Xu, R., 2018. Collagen prolyl 4-hydroxylase 1 is essential for HIF-1α stabilization and TNBC chemoresistance. Nature communications, 9(1), p.4456.
6. Chalakur-Ramireddy, N.K. and Pakala, S.B., 2018. Combined drug therapeutic strategies for the effective treatment of Triple Negative Breast Cancer. Bioscience reports, 38(1), p.BSR20171357.
7. Thakur, K.K., Bordoloi, D. and Kunnumakkara, A.B., 2018. The alarming burden of triple-negative breast cancer in India. Clinical breast cancer, 18(3), pp.e393-e399.
8. Maaren, M.C., Munck, L., Strobbe, L.J., Sonke, G.S., Westenend, P.J., Smidt, M.L., Poortmans, P.M. and Siesling, S., 2019. Ten-year recurrence rates for breast cancer

subtypes in the Netherlands: a large population-based study. International journal of cancer, 144(2), pp.263-272.

9. Massagué, J. and Obenauf, A.C., 2016. Metastatic colonization by circulating tumour cells. Nature, 529(7586), pp.298-306.
10. Chaffer, C.L. and Weinberg, R.A., 2011. A perspective on cancer cell metastasis. science, 331(6024), pp.1559-1564.
11. DeSantis, C.E., Ma, J., Goding Sauer, A., Newman, L.A. and Jemal, A., 2017. Breast cancer statistics, 2017, racial disparity in mortality by state. CA: a cancer journal for clinicians, 67(6), pp.439-448.
12. Elgebaly, H.A., Mosa, N.M., Allach, M., El-Massry, K.F., El-Ghorab, A.H., Al Hroob, A.M. and Mahmoud, A.M., 2018. Olive oil and leaf extract prevent fluoxetine-induced hepatotoxicity by attenuating oxidative stress, inflammation and apoptosis. Biomedicine & Pharmacotherapy, 98, pp.446-453.
13. Smith, R.A., Andrews, K.S., Brooks, D., Fedewa, S.A., Manassaram-Baptiste, D., Saslow, D. and Wender, R.C., 2019. Cancer screening in the United States, 2019: A review of current American Cancer Society guidelines and current issues in cancer screening. CA: a cancer journal for clinicians, 69(3), pp.184-210.
14. Berrino, F., Bellati, C., Secreto, G., Camerini, E., Pala, V., Panico, S., Allegro, G. and Kaaks, R., 2001. Reducing bioavailable sex hormones through a comprehensive change in diet: the diet and androgens (DIANA) randomized trial. Cancer Epidemiology Biomarkers & Prevention, 10(1), pp.25-33.
15. Lahmann, P.H., Lissner, L., Gullberg, B., Olsson, H. and Berglund, G., 2003. A prospective study of adiposity and postmenopausal breast cancer risk: the Malmö Diet and Cancer Study. International Journal of Cancer, 103(2), pp.246-252.

16. Lauby-Secretan, B., Scoccianti, C., Loomis, D., Benbrahim-Tallaa, L., Bouvard, V., Bianchini, F. and Straif, K., 2015. Breast-cancer screening—viewpoint of the IARC Working Group. New England journal of medicine, 372(24), pp.2353-2358.
17. Vogel, V.G., 2008. Epidemiology, genetics, and risk evaluation of postmenopausal women at risk of breast cancer. Menopause, 15(4), pp.782-789.
18. Maffini, M.V., Soto, A.M., Calabro, J.M., Ucci, A.A. and Sonnenschein, C., 2004. The stroma as a crucial target in rat mammary gland carcinogenesis. Journal of cell science, 117(8), pp.1495-1502.
19. Sonnenschein, C. and Soto, A.M., 2016. Carcinogenesis explained within the context of a theory of organisms. Progress in biophysics and molecular biology, 122(1), pp.70-76.
20. Qian, B.Z. and Pollard, J.W., 2010. Macrophage diversity enhances tumor progression and metastasis. Cell, 141(1), pp.39-51.
21. Dumars, C., Ngyuen, J.M., Gaultier, A., Lanel, R., Corradini, N., Gouin, F., Heymann, D. and Heymann, M.F., 2016. Dysregulation of macrophage polarization is associated with the metastatic process in osteosarcoma. Oncotarget, 7(48), p.78343.
22. Polyak, K., 2007. Breast cancer: origins and evolution. The Journal of clinical investigation, 117(11), pp.3155-3163.
23. Basse, C. and Arock, M., 2015. The increasing roles of epigenetics in breast cancer: Implications for pathogenicity, biomarkers, prevention and treatment. International journal of cancer, 137(12), pp.2785-2794.
24. Baumann, M., Krause, M. and Hill, R., 2008. Exploring the role of cancer stem cells in radioresistance. Nature Reviews Cancer, 8(7), pp.545-554.

25. Zhang, M., Lee, A.V. and Rosen, J.M., 2017. The cellular origin and evolution of breast cancer. Cold Spring Harbor perspectives in medicine, 7(3), p.a027128.
26. Al-Hajj, M., Wicha, M.S., Benito-Hernandez, A., Morrison, S.J. and Clarke, M.F., 2003. Prospective identification of tumorigenic breast cancer cells. Proceedings of the National Academy of Sciences, 100(7), pp.3983-3988.
27. Molyneux, G., Geyer, F.C., Magnay, F.A., McCarthy, A., Kendrick, H., Natrajan, R., MacKay, A., Grigoriadis, A., Tutt, A., Ashworth, A. and Reis-Filho, J.S., 2010. BRCA1 basal-like breast cancers originate from luminal epithelial progenitors and not from basal stem cells. Cell stem cell, 7(3), pp.403-417.
28. Sun, Y.S., Zhao, Z., Yang, Z.N., Xu, F., Lu, H.J., Zhu, Z.Y., Shi, W., Jiang, J., Yao, P.P. and Zhu, H.P., 2017. Risk factors and preventions of breast cancer. International journal of biological sciences, 13(11), p.1387.
29. Sgroi, D.C., 2010. Preinvasive breast cancer. Annual Review of Pathology: Mechanisms of Disease, 5, pp.193-221.
30. Siegel, R.L., Miller, K.D. and Jemal, A., 2018. Cancer statistics, 2018. CA: a cancer journal for clinicians, 68(1), pp.7-30.
31. Brewer, H.R., Jones, M.E., Schoemaker, M.J., Ashworth, A. and Swerdlow, A.J., 2017. Family history and risk of breast cancer: an analysis accounting for family structure. Breast cancer research and treatment, 165, pp.193-200.
32. Rosato, V., Bosetti, C., Negri, E., Talamini, R., Dal Maso, L., Malvezzi, M., Falcini, F., Montella, M. and La Vecchia, C., 2014. Reproductive and hormonal factors, family history, and breast cancer according to the hormonal receptor status. European journal of cancer prevention, 23(5), pp.412-417.
33. Hormones, E. and Breast Cancer Collaborative Group, 2013. Sex hormones and risk of breast cancer in premenopausal women: a collaborative reanalysis of individual

participant data from seven prospective studies. The lancet oncology, 14(10), pp.1009-1019.

34. Soroush, A., Farshchian, N., Komasi, S., Izadi, N., Amirifard, N. and Shahmohammadi, A., 2016. The role of oral contraceptive pills on increased risk of breast cancer in Iranian populations: a meta-analysis. Journal of cancer prevention, 21(4), p.294.
35. Coombs, N.J., Cronin, K.A., Taylor, R.J., Freedman, A.N. and Boyages, J., 2010. The impact of changes in hormone therapy on breast cancer incidence in the US population. Cancer Causes & Control, 21, pp.83-90.
36. Liu, J.Y., Chen, T.J. and Hwang, S.J., 2016. The risk of breast cancer in women using menopausal hormone replacement therapy in Taiwan. International journal of environmental research and public health, 13(5), p.482.
37. Fahlén, M., Fornander, T., Johansson, H., Johansson, U., Rutqvist, L.E., Wilking, N. and von Schoultz, E., 2013. Hormone replacement therapy after breast cancer: 10 year follow up of the Stockholm randomised trial. European journal of cancer, 49(1), pp.52-59.
38. Ravdin, P.M., Cronin, K.A., Howlader, N., Berg, C.D., Chlebowski, R.T., Feuer, E.J., Edwards, B.K. and Berry, D.A., 2007. The decrease in breast-cancer incidence in 2003 in the United States. New England Journal of Medicine, 356(16), pp.1670-1674.
39. Kungu, A., Hamajima, N. and Hirose, K., 2002. Alcohol, tobacco and breast cancer--collaborative reanalysis of individual data from 53 epidemiological studies, including 58,515 women with breast cancer and 95,067 women without the disease. British Journal of Cancer, 87(11),pp.1234–1245.

40. Jung, S., Wang, M., Anderson, K., Baglietto, L., Bergkvist, L., Bernstein, L., van den Brandt, P.A., Brinton, L., Buring, J.E., Heather Eliassen, A. and Falk, R., 2016. Alcohol consumption and breast cancer risk by estrogen receptor status: in a pooled analysis of 20 studies. International journal of epidemiology, 45(3), pp.916-928.
41. Makarem, N., Chandran, U., Bandera, E.V. and Parekh, N., 2013. Dietary fat in breast cancer survival. Annual review of nutrition, 33, pp.319-348.
42. Knight, J.A., Fan, J., Malone, K.E., John, E.M., Lynch, C.F., Langballe, R., Bernstein, L., Shore, R.E., Brooks, J.D., Reiner, A.S. and Woods, M., 2017. Alcohol consumption and cigarette smoking in combination: A predictor of contralateral breast cancer risk in the WECARE study. International journal of cancer, 141(5), pp.916-924.
43. Catsburg, C., Miller, A.B. and Rohan, T.E., 2015. Active cigarette smoking and risk of breast cancer. International journal of cancer, 136(9), pp.2204-2209.
44. Kispert, S. and McHowat, J., 2017. Recent insights into cigarette smoking as a lifestyle risk factor for breast cancer. Breast Cancer: Targets and Therapy, pp.127-132.
45. Inoue, K. and Fry, E.A., 2015. Aberrant expression of cyclin D1 in cancer. Signal transduction insights, 4, pp.STI-S30306.
46. Lefebvre, C., Bachelot, T., Filleron, T., Pedrero, M., Campone, M., Soria, J.C., Massard, C., Levy, C., Arnedos, M., Lacroix-Triki, M. and Garrabey, J., 2016. Mutational profile of metastatic breast cancers: a retrospective analysis. PLoS medicine, 13(12), p.e1002201.
47. Berardi, R., Morgese, F., Onofri, A., Mazzanti, P., Pistelli, M., Ballatore, Z., Savini, A., De Lisa, M., Caramanti, M., Rinaldi, S. and Pagliaretta, S., 2013. Role of maspin in cancer. Clinical and translational medicine, 2(1), pp.1-19.

48. Su, Y., Wang, X., Li, J., Xu, J. and Xu, L., 2015. The clinicopathological significance and drug target potential of FHIT in breast cancer, a meta-analysis and literature review. Drug design, development and therapy, pp.5439-5445.

49. Desmedt, C., Zoppoli, G., Gundem, G., Pruneri, G., Larsimont, D., Fornili, M., Fumagalli, D., Brown, D., Rothé, F., Vincent, D. and Kheddoumi, N., 2016. Genomic characterization of primary invasive lobular breast cancer. Journal of clinical oncology, 34(16), pp.1872-1881.

50. Choi, M., Kipps, T. and Kurzrock, R., 2016. ATM mutations in cancer: therapeutic implications. Molecular cancer therapeutics, 15(8), pp.1781-1791.

51. Loibl, S., Darb-Esfahani, S., Huober, J., Klimowicz, A., Furlanetto, J., Lederer, B., Hartmann, A., Eidtmann, H., Pfitzner, B., Fasching, P.A. and Tiemann, K., 2016. Integrated analysis of PTEN and p4EBP1 protein expression as predictors for pCR in HER2-positive breast cancer. Clinical Cancer Research, 22(11), pp.2675-2683.

52. Cheng, L., Zhou, Z., Flesken-Nikitin, A., Toshkov, I.A., Wang, W., Camps, J., Ried, T. and Nikitin, A.Y., 2010. Rb inactivation accelerates neoplastic growth and substitutes for recurrent amplification of cIAP1, cIAP2 and Yap1 in sporadic mammary carcinoma associated with p53 deficiency. Oncogene, 29(42), pp.5700-5711.

53. Roberts, M.R., Sucheston-Campbell, L.E., Zirpoli, G.R., Higgins, M., Freudenheim, J.L., Bandera, E.V., Ambrosone, C.B. and Yao, S., 2017. Single nucleotide variants in metastasis-related genes are associated with breast cancer risk, by lymph node involvement and estrogen receptor status, in women with European and African ancestry. Molecular carcinogenesis, 56(3), pp.1000-1009.

54. Hientz, K., Mohr, A., Bhakta-Guha, D. and Efferth, T., 2017. The role of p53 in cancer drug resistance and targeted chemotherapy. Oncotarget, 8(5), p.8921.

55. Singh, S.K., Singh, S., Lillard Jr, J.W. and Singh, R., 2017. Drug delivery approaches for breast cancer. International journal of nanomedicine, pp.6205-6218.

56. Kang, D.I., Kang, H.K., Gwak, H.S., Han, H.K. and Lim, S.J., 2009. Liposome composition is important for retention of liposomal rhodamine in P-glycoprotein-overexpressing cancer cells. Drug delivery, 16(5), pp.261-267.

57. Jain, V., Kumar, H., Anod, H.V., Chand, P., Gupta, N.V., Dey, S. and Kesharwani, S.S., 2020. A review of nanotechnology-based approaches for breast cancer and triple-negative breast cancer. Journal of Controlled Release, 326, pp.628-647.

58. Tran, P., Lee, S.E., Kim, D.H., Pyo, Y.C. and Park, J.S., 2020. Recent advances of nanotechnology for the delivery of anticancer drugs for breast cancer treatment. Journal of Pharmaceutical Investigation, 50, pp.261-270.

59. Xing, H., Tang, L., Yang, X., Hwang, K., Wang, W., Yin, Q., Wong, N.Y., Dobrucki, L.W., Yasui, N., Katzenellenbogen, J.A. and Helferich, W.G., 2013. Selective delivery of an anticancer drug with aptamer-functionalized liposomes to breast cancer cells in vitro and in vivo. Journal of materials chemistry B, 1(39), pp.5288-5297.

60. Cao, H., Dan, Z., He, X., Zhang, Z., Yu, H., Yin, Q. and Li, Y., 2016. Liposomes coated with isolated macrophage membrane can target lung metastasis of breast cancer. ACS nano, 10(8), pp.7738-7748.

61. Fu, M., Tang, W., Liu, J.J., Gong, X.Q., Kong, L., Yao, X.M., Jing, M., Cai, F.Y., Li, X.T. and Ju, R.J., 2020. Combination of targeted daunorubicin liposomes and targeted emodin liposomes for treatment of invasive breast cancer. Journal of drug targeting, 28(3), pp.245-258.

62. Itoo, A.M., Paul, M., Ghosh, B. and Biswas, S., 2022. Oxaliplatin delivery via chitosan/vitamin E conjugate micelles for improved efficacy and MDR-reversal in breast cancer. Carbohydrate Polymers, 282, p.119108.
63. Gong, Z., Chen, M., Ren, Q., Yue, X. and Dai, Z., 2020. Fibronectin-targeted dual-acting micelles for combination therapy of metastatic breast cancer. Signal Transduction and Targeted Therapy, 5(1), p.12.
64. Katiyar, S.S., Muntimadugu, E., Rafeeqi, T.A., Domb, A.J. and Khan, W., 2016. Co-delivery of rapamycin-and piperine-loaded polymeric nanoparticles for breast cancer treatment. Drug delivery, 23(7), pp.2608-2616.
65. Xiong, K., Zhang, Y., Wen, Q., Luo, J., Lu, Y., Wu, Z., Wang, B., Chen, Y., Zhao, L. and Fu, S., 2020. Co-delivery of paclitaxel and curcumin by biodegradable polymeric nanoparticles for breast cancer chemotherapy. International journal of pharmaceutics, 589, p.119875.
66. Mehnert, W. and Mäder, K., 2012. Solid lipid nanoparticles: production, characterization and applications. Advanced drug delivery reviews, 64, pp.83-101.
67. Akter, Z., Khan, F.Z. and Khan, M.A., 2023. Gold nanoparticles in triple-negative breast cancer therapeutics. Current Medicinal Chemistry, 30(3), pp.316-334.
68. Wong, F., 2007. Drug insight: the role of albumin in the management of chronic liver disease. Nature Clinical Practice Gastroenterology & Hepatology, 4(1), pp.43-51.
69. Divsalar, A., Saboury, A.A., Ahadi, L., Zemanatiyar, E., Mansouri-Torshizi, H., Ajloo, D. and Sarma, R.H., 2011. Biological evaluation and interaction of a newly designed anti-cancer Pd (II) complex and human serum albumin. Journal of Biomolecular Structure and Dynamics, 29(2), pp.283-296.

70. Sudlow, G.D.J.B., Birkett, D.J. and Wade, D.N., 1975. The characterization of two specific drug binding sites on human serum albumin. Molecular pharmacology, 11(6), pp.824-832.
71. Kratz, F., Müller-Driver, R., Hofmann, I., Drevs, J. and Unger, C., 2000. A novel macromolecular prodrug concept exploiting endogenous serum albumin as a drug carrier for cancer chemotherapy. Journal of medicinal chemistry, 43(7), pp.1253-1256.
72. Pignatta, S., Orienti, I., Falconi, M., Teti, G., Arienti, C., Medri, L., Zanoni, M., Carloni, S., Zoli, W., Amadori, D. and Tesei, A., 2015. Albumin nanocapsules containing fenretinide: pre-clinical evaluation of cytotoxic activity in experimental models of human non-small cell lung cancer. Nanomedicine: Nanotechnology, Biology and Medicine, 11(2), pp.263-273.
73. Kumari, P., Paul, M., Bobde, Y., Soniya, K., Kiran Rompicharla, S.V., Ghosh, B. and Biswas, S., 2020. Albumin-based lipoprotein nanoparticles for improved delivery and anticancer activity of curcumin for cancer treatment. Nanomedicine, 15(29), pp.2851-2869.
74. Nano-emulsions. Elsevier [Internet] Available from: https://www.sciencedirect.com/science/article/pii/S1359029405000348. Accessed on Jun 24 2023
75. Miele, E., Spinelli, G.P., Miele, E., Tomao, F. and Tomao, S., 2009. Albumin-bound formulation of paclitaxel (Abraxane® ABI-007) in the treatment of breast cancer. International journal of nanomedicine, pp.99-105.
76. Miele, E., Spinelli, G.P., Miele, E., Tomao, F. and Tomao, S., 2009. Albumin-bound formulation of paclitaxel (Abraxane® ABI-007) in the treatment of breast cancer. International journal of nanomedicine, pp.99-105.

77. Guney Eskiler, G., Cecener, G., Egeli, U. and Tunca, B., 2018. Triple negative breast cancer: new therapeutic approaches and BRCA status. Apmis, 126(5), pp.371-379.

78. Gerratana, L., Basile, D., Buono, G., De Placido, S., Giuliano, M., Minichillo, S., Coinu, A., Martorana, F., De Santo, I., Del Mastro, L. and De Laurentiis, M., 2018. Androgen receptor in triple negative breast cancer: A potential target for the targetless subtype. Cancer treatment reviews, 68, pp.102-110.

79. Le, D. and Gelmon, K.A., 2018. Olaparib tablets for the treatment of germ line BRCA-mutated metastatic breast cancer. Expert review of clinical pharmacology, 11(9), pp.833-839.

80. Belli, C., Duso, B.A., Ferraro, E. and Curigliano, G., 2019. Homologous recombination deficiency in triple negative breast cancer. The Breast, 45, pp.15-21.

81. Bianchini, G., Balko, J.M., Mayer, I.A., Sanders, M.E. and Gianni, L., 2016. Triple-negative breast cancer: challenges and opportunities of a heterogeneous disease. Nature reviews Clinical oncology, 13(11), pp.674-690.

82. Hongthong, K. and Ratanaphan, A., 2016. BRCA1-associated triple-negative breast cancer and potential treatment for ruthenium-based compounds. Current cancer drug targets, 16(7), pp.606-617.

83. Rivero, J. and Kohn, E.C., 2017. PARP Inhibitors: The Cornerstone of DNA Repair-Targeted Therapies. Oncology (Williston Park, NY), 31(4), pp.265-273.

84. D'Andrea, A.D., 2018. Mechanisms of PARP inhibitor sensitivity and resistance. DNA repair, 71, pp.172-176.

85. Murai, J., Huang, S.Y.N., Das, B.B., Renaud, A., Zhang, Y., Doroshow, J.H., Ji, J., Takeda, S. and Pommier, Y., 2012. Trapping of PARP1 and PARP2 by clinical PARP inhibitors. Cancer research, 72(21), pp.5588-5599.

86. Arun, B., Akar, U., Gutierrez-Barrera, A.M., Hortobagyi, G.N. and Ozpolat, B., 2015. The PARP inhibitor AZD2281 (Olaparib) induces autophagy/mitophagy in BRCA1 and BRCA2 mutant breast cancer cells. International journal of oncology, 47(1), pp.262-268.
87. Mao, Y., Huang, X., Shuang, Z., Lin, G., Wang, J., Duan, F., Chen, J. and Li, S., 2018. PARP inhibitor olaparib sensitizes cholangiocarcinoma cells to radiation. Cancer medicine, 7(4), pp.1285-1296.
88. Robson, M., Im, S.A., Senkus, E., Xu, B., Domchek, S.M., Masuda, N., Delaloge, S., Li, W., Tung, N., Armstrong, A. and Wu, W., 2017. Olaparib for metastatic breast cancer in patients with a germline BRCA mutation. New England Journal of Medicine, 377(6), pp.523-533.
89. Griguolo, G., Dieci, M.V., Guarneri, V. and Conte, P., 2018. Olaparib for the treatment of breast cancer. Expert review of anticancer therapy, 18(6), pp.519-530.
90. Robson, M.E., Tung, N., Conte, P., Im, S.A., Senkus, E., Xu, B., Masuda, N., Delaloge, S., Li, W., Armstrong, A. and Wu, W., 2019. OlympiAD final overall survival and tolerability results: Olaparib versus chemotherapy treatment of physician's choice in patients with a germline BRCA mutation and HER2-negative metastatic breast cancer. Annals of Oncology, 30(4), pp.558-566.
91. Pop, L., Suciu, I., Ionescu, O., Bacalbasa, N. and Ionescu, P., 2021. The role of novel poly (ADP-ribose) inhibitors in the treatment of locally advanced and metastatic Her-2/neu negative breast cancer with inherited germline BRCA1/2 mutations. A review of the literature. Journal of Medicine and Life, 14(1), p.17.
92. Du, C., Qi, Y., Zhang, Y., Wang, Y., Zhao, X., Min, H., Han, X., Lang, J., Qin, H., Shi, Q. and Zhang, Z., 2018. Epidermal growth factor receptor-targeting peptide

nanoparticles simultaneously deliver gemcitabine and olaparib to treat pancreatic cancer with breast cancer 2 (BRCA2) mutation. ACS nano, 12(11), pp.10785-10796.

93. Zhang, Y., Hu, H., Tang, W., Zhang, Q., Li, M., Jin, H., Huang, Z., Cui, Z., Xu, J., Wang, K. and Shi, C., 2020. A multifunctional magnetic nanosystem based on "two strikes" effect for synergistic anticancer therapy in triple-negative breast cancer. Journal of controlled release, 322, pp.401-415.
94. Bono, J., Mateo, J., Fizazi, K., Saad, F., Shore, N., Sandhu, S., Chi, K.N., Sartor, O., Agarwal, N., Olmos, D. and Thiery-Vuillemin, A., 2020. Olaparib for metastatic castration-resistant prostate cancer. New England Journal of Medicine, 382(22), pp.2091-2102.
95. Ven, A.L., Tangutoori, S., Baldwin, P., Qiao, J., Gharagouzloo, C., Seitzer, N., Clohessy, J.G., Makrigiorgos, G.M., Cormack, R., Pandolfi, P.P. and Sridhar, S., 2017. Nanoformulation of olaparib amplifies PARP inhibition and sensitizes PTEN/TP53-deficient prostate cancer to radiation. Molecular cancer therapeutics, 16(7), pp.1279-1289.
96. Wu, M., Liu, J., Hu, C., Li, D., Yang, J., Wu, Z., Yang, L., Chen, Y., Fu, S. and Wu, J., 2018. Olaparib nanoparticles potentiated radiosensitization effects on lung cancer. International journal of nanomedicine, pp.8461-8472.
97. Li, D., Hu, C., Yang, J., Liao, Y., Chen, Y., Fu, S.Z. and Wu, J.B., 2020. Enhanced Anti-Cancer Effect of Folate-Conjugated Olaparib Nanoparticles Combined with Radiotherapy in Cervical Carcinoma. International Journal of Nanomedicine, pp.10045-10058.
98. McCrorie, P., Mistry, J., Taresco, V., Lovato, T., Fay, M., Ward, I., Ritchie, A.A., Clarke, P.A., Smith, S.J., Marlow, M. and Rahman, R., 2020. Etoposide and olaparib polymer-coated nanoparticles within a bioadhesive sprayable hydrogel for post-

surgical localised delivery to brain tumours. European Journal of Pharmaceutics and Biopharmaceutics, 157, pp.108-120.

99. Novohradsky, V., Zajac, J., Vrana, O., Kasparkova, J. and Brabec, V., 2018. Simultaneous delivery of olaparib and carboplatin in PEGylated liposomes imparts this drug combination hypersensitivity and selectivity for breast tumor cells. Oncotarget, 9(47), p.28456.

100. Kratz, F., 2008. Albumin as a drug carrier: design of prodrugs, drug conjugates and nanoparticles. Journal of controlled release, 132(3), pp.171-183

101. Hoogenboezem, E.N. and Duvall, C.L., 2018. Harnessing albumin as a carrier for cancer therapies. Advanced drug delivery reviews, 130, pp.73-89.

102. Kumari, P., Rompicharla, S.V.K., Muddineti, O.S., Ghosh, B. and Biswas, S., 2018. Transferrin-anchored poly (lactide) based micelles to improve anticancer activity of curcumin in hepatic and cervical cancer cell monolayers and 3D spheroids. International journal of biological macromolecules, 116, pp.1196-1213.

103. Kumari, P., Paul, M., Bhatt, H., Rompicharla, S.V.K., Sarkar, D., Ghosh, B. and Biswas, S., 2020. Chlorin e6 conjugated methoxy-poly (ethylene glycol)-poly (d, l-lactide) glutathione sensitive micelles for photodynamic therapy. Pharmaceutical Research, 37, pp.1-17.

104. Muddineti, O.S., Kumari, P., Ajjarapu, S., Lakhani, P.M., Bahl, R., Ghosh, B. and Biswas, S., 2016. Xanthan gum stabilized PEGylated gold nanoparticles for improved delivery of curcumin in cancer. Nanotechnology, 27(32), p.325101.

105. Varlan, A. and Hillebrand, M., 2010. Bovine and human serum albumin interactions with 3-carboxyphenoxathiin studied by fluorescence and circular dichroism spectroscopy. Molecules, 15(6), pp.3905-3919.

106. Muddineti, O.S., Kumari, P., Ghosh, B., Torchilin, V.P. and Biswas, S., 2017. d-α-Tocopheryl succinate/phosphatidyl ethanolamine conjugated amphiphilic polymer-based nanomicellar system for the efficient delivery of curcumin and to overcome multiple drug resistance in cancer. ACS Applied Materials & Interfaces, 9(20), pp.16778-16792.

107. Kumari, P., Rompicharla, S.V.K., Bhatt, H., Ghosh, B. and Biswas, S., 2019. Development of chlorin e6-conjugated poly (ethylene glycol)-poly (d, l-lactide) nanoparticles for photodynamic therapy. Nanomedicine, 14(7), pp.819-834.

108. Muddineti, O.S., Kumari, P., Ray, E., Ghosh, B. and Biswas, S., 2017. Curcumin-loaded chitosan–cholesterol micelles: evaluation in monolayers and 3D cancer spheroid model. Nanomedicine, 12(12), pp.1435-1453.

109. Gong, G., Zhi, F., Wang, K., Tang, X., Yuan, A., Zhao, L., Ding, D. and Hu, Y., 2011. Fabrication of a nanocarrier system through self-assembly of plasma protein and its tumor targeting. Nanotechnology, 22(29), p.295603.

110. Taheri, A., Atyabi, F., Nouri, F.S., Ahadi, F., Derakhshan, M.A., Amini, M., Ghahremani, M.H., Ostad, S.N., Mansoori, P. and Dinarvand, R., 2011. Nanoparticles of conjugated methotrexate-human serum albumin: preparation and cytotoxicity evaluations. Journal of nanomaterials, 2011, pp.1-7.

111. Paul, S., Sepay, N., Sarkar, S., Roy, P., Dasgupta, S., Sardar, P.S. and Majhi, A., 2017. Interaction of serum albumins with fluorescent ligand 4-azido coumarin: spectroscopic analysis and molecular docking studies. New Journal of Chemistry, 41(24), pp.15392-15404.

112. Capomaccio, R., Osório, I., Ojea-Jiménez, I., Ceccone, G., Colpo, P., Gilliland, D., Hussain, R., Siligardi, G., Rossi, F., Ricard-Blum, S. and Calzolai, L., 2016. Gold

nanoparticles increases UV and thermal stability of human serum albumin. Biointerphases, 11(4).

113. Luna-Vázquez-Gómez, R., Arellano-García, M.E., García-Ramos, J.C., Radilla-Chávez, P., Salas-Vargas, D.S., Casillas-Figueroa, F., Ruiz-Ruiz, B., Bogdanchikova, N. and Pestryakov, A., 2021. Hemolysis of human erythrocytes by Argovit™ AgNPs from healthy and diabetic donors: An in vitro study. Materials, 14(11), p.2792.

114. Choi, J., Reipa, V., Hitchins, V.M., Goering, P.L. and Malinauskas, R.A., 2011. Physicochemical characterization and in V itro hemolysis evaluation of silver nanoparticles. Toxicological Sciences, 123(1), pp.133-143.

115. Hu, H., Zhang, Y., Ji, W., Mei, H., Wu, T., He, Z., Wang, K. and Shi, C., 2022. Hyaluronic acid-coated and Olaparib-loaded PEI− PLGA nanoparticles for the targeted therapy of triple negative breast cancer. Journal of Microencapsulation, 39(1), pp.25-36.

116. Misra, R., Patra, B., Varadharaj, S. and Verma, R.S., 2021. Establishing the promising role of novel combination of triple therapeutics delivery using polymeric nanoparticles for Triple negative breast cancer therapy. BioImpacts: BI, 11(3), p.199.

117. Lee, J.H., Moon, H., Han, H., Lee, I.J., Kim, D., Lee, H.J., Ha, S.W., Kim, H. and Chung, J.W., 2019. Antitumor effects of intra-arterial delivery of albumin-doxorubicin nanoparticle conjugated microbubbles combined with ultrasound-targeted microbubble activation on VX2 rabbit liver tumors. Cancers, 11(4), p.581.

118. Yang, X., Ndawula, C., Zhou, H., Gong, X. and Jin, J., 2015. JF-305, a pancreatic cancer cell line is highly sensitive to the PARP inhibitor olaparib. Oncology letters, 9(2), pp.757-761.

119. Itoo, A.M., Paul, M., Ghosh, B. and Biswas, S., 2022. Oxaliplatin delivery via chitosan/vitamin E conjugate micelles for improved efficacy and MDR-reversal in breast cancer. Carbohydrate Polymers, 282, p.119108.

120. Liu, W.B., Zhou, J., Qu, Y., Li, X., Lu, C.T., Xie, K.L., Sun, X.L. and Fei, Z., 2010. Neuroprotective effect of osthole on MPP+-induced cytotoxicity in PC12 cells via inhibition of mitochondrial dysfunction and ROS production. Neurochemistry International, 57(3), pp.206-215.

121. Jiang, S., Zhu, R., He, X., Wang, J., Wang, M., Qian, Y. and Wang, S., 2017. Enhanced photocytotoxicity of curcumin delivered by solid lipid nanoparticles. International Journal of Nanomedicine, pp.167-178.

122. Kumari, P., Jain, S., Ghosh, B., Zorin, V. and Biswas, S., 2017. Polylactide-based block copolymeric micelles loaded with chlorin e6 for photodynamic therapy: in vitro evaluation in monolayer and 3D spheroid models. Molecular Pharmaceutics, 14(11), pp.3789-3800.

123. Bhatt, H., Ghosh, B. and Biswas, S., 2020. Cell-penetrating peptide and α-tocopherol-conjugated poly (amidoamine) dendrimers for improved delivery and anticancer activity of loaded paclitaxel. ACS Applied Bio Materials, 3(5), pp.3157-3169.

124. Marcucci, F. and Corti, A., 2012. How to improve exposure of tumor cells to drugs—Promoter drugs increase tumor uptake and penetration of effector drugs. Advanced drug delivery reviews, 64(1), pp.53-68.

125. Atiya, H.I., Dvorkin-Gheva, A., Hassell, J., Patel, S., Parker, R.L., Hartstone-Rose, A., Hodge, J., Fan, D. and Ramsdell, A.F., 2019. Intraductal adaptation of the 4T1 mouse model of breast cancer reveals effects of the epithelial microenvironment on tumor progression and metastasis. Anticancer research, 39(5), pp.2277-2287.

126. Li, W., Li, X., Liu, S., Yang, W., Pan, F., Yang, X.Y., Du, B., Qin, L. and Pan, Y., 2017. Gold nanoparticles attenuate metastasis by tumor vasculature normalization and epithelial–mesenchymal transition inhibition. International journal of nanomedicine, pp.3509-3520.

127. Li, W., Li, X., Liu, S., Yang, W., Pan, F., Yang, X.Y., Du, B., Qin, L. and Pan, Y., 2017. Gold nanoparticles attenuate metastasis by tumor vasculature normalization and epithelial–mesenchymal transition inhibition. International journal of nanomedicine, pp.3509-3520.

128. Kalyane, D., Raval, N., Maheshwari, R., Tambe, V., Kalia, K. and Tekade, R.K., 2019. Employment of enhanced permeability and retention effect (EPR): Nanoparticle-based precision tools for targeting of therapeutic and diagnostic agent in cancer. Materials Science and Engineering: C, 98, pp.1252-1276.

129. Kumbham, S., Paul, M., Itoo, A., Ghosh, B. and Biswas, S., 2022. Oleanolic acid-conjugated human serum albumin nanoparticles encapsulating doxorubicin as synergistic combination chemotherapy in oropharyngeal carcinoma and melanoma. International journal of pharmaceutics, 614, p.121479.

130. Yin, L., Duan, J.J., Bian, X.W. and Yu, S.C., 2020. Triple-negative breast cancer molecular subtyping and treatment progress. Breast Cancer Research, 22, pp.1-13.

131. Abotaleb, M., Kubatka, P., Caprnda, M., Varghese, E., Zolakova, B., Zubor, P., Opatrilova, R., Kruzliak, P., Stefanicka, P. and Büsselberg, D., 2018. Chemotherapeutic agents for the treatment of metastatic breast cancer: An update. Biomedicine & pharmacotherapy, 101, pp.458-477.

132. Oberoi, H.S., Nukolova, N.V., Kabanov, A.V. and Bronich, T.K., 2013. Nanocarriers for delivery of platinum anticancer drugs. Advanced drug delivery reviews, 65(13-14), pp.1667-1685.

133. Omarini, C., Guaitoli, G., Pipitone, S., Moscetti, L., Cortesi, L., Cascinu, S. and Piacentini, F., 2018. Neoadjuvant treatments in triple-negative breast cancer patients: where we are now and where we are going. Cancer management and research, pp.91-103.

134. Rose, M., Burgess, J.T., O'Byrne, K., Richard, D.J. and Bolderson, E., 2020. PARP inhibitors: clinical relevance, mechanisms of action and tumor resistance. Frontiers in cell and developmental biology, 8, p.564601

135. Tang, Y., Yu, Z., Lu, X., Fan, Q. and Huang, W., 2022. Overcoming vascular barriers to improve the theranostic outcomes of nanomedicines. Advanced Science, 9(13), p.2103148.promisin

136. Hassanin, I. and Elzoghby, A., 2020. Albumin-based nanoparticles: A promising strategy to overcome cancer drug resistance. Cancer Drug Resistance, 3(4), p.930.

Publications and Presentations

Publications and Presentations

Publications

1. **Nageswara Rao Vysyaraju,** Milan Paul, Sanjay Ch, Balaram Ghosh & Swati Biswas Olaparib@ human serum albumin nanoparticles.as sustained drug-releasing tumour-targeting nanomedicine to inhibit growth and metastasis in the mouse model of triple-negative breast cancer. Journal of Drug Targeting, 2022 Jul 03:2092623.

Manuscripts under process

1. Combination drug delivery of Olaparib and Oxaliplatin using human serum albumin for the treatment of triple negative breast cancer with synergistic effect in the mouse model. Manuscript is under communication.

Presentations

1. **Nageswara Rao Vysyaraju,** Milan Paul, Sanjay Ch, Balaram Ghosh & Swati Biswas Olaparib@ human serum albumin nanoparticles.as sustained drug-releasing tumour-targeting nanomedicine to inhibit growth and metastasis in the mouse model of triple-negative breast cancer -Poster presentation, at the 20th International e Symposium on Advances in Technology and Business Potential of New Drug Delivery Systems organized by Controlled Release Society –Indian Chapter held from February 24-26, 2022.

Biography

Biography of Nageswara Rao Vysyaraju

Mr Nageswara Rao Vysyaraju has completed his Diploma in Pharmacy from Govt Polytechnic College, Visakhapatnam, Andhra Pradesh, India in 2003. He pursued his Bachelor's of Pharmacy from Sri Vishnu College of Pharmacy, Bhimavaram, affiliated to Andhra University, Andhra Pradesh, Indian in 2006. He completed his Masters in Pharmaceutical Sciences from BITS Pilani, Rajasthan Campus, India. Mr Nageswara Rao worked in formulation development as a Tech Lead in Dr. Reddy's Laboratories Ltd, Eskayef Pharmaceuticals Ltd and currently working as a Principal Scientist in Sandoz Ltd. As a part of research interest Mr. Nageswara Rao joined as part-time Ph.D. scholar under Prof. Swati Biswas's lab at BITS Pilani Hyderabad Campus to pursue his doctoral research. Mr Nageswara Rao Vysyaraju worked on "Targeted delivery of chemotherapeutic agents using Human Serum albumin for the treatment of Cancer". As part of his research work he has worked on the "Olaparib loaded human serum albumin nanoparticles as sustained drug-releasing tumour-targeting nanomedicine to inhibit growth and metastasis of triple-negative breast cancer in mouse model and also on the Combination drug delivery of Olaparib and Oxaliplatin with human serum albumin for the treatment of triple negative breast cancer and synergistic effect of combination therapy". He has presented his research in CRS 2022 Annual Meeting and Expo on Advanced delivery science by the Controlled Release Society and selected his poster as one of the best posters in CRS. He has published one peer-reviewed scientific publications in reputed international journals, another one in the under review and presented papers at various international conferences.

Biography of Prof. Swati Biswas

Prof. Swati Biswas is presently working as Professor, in Department of Pharmacy, Birla Institute of Technology and Science, Pilani, Hyderabad Campus. She received her B. Pharm degree (1998) and M. Pharm (2000) from Jadavpur University, India. She was awarded her Ph.D. in Pharmaceutical Sciences in the year 2008 from Wayne State University, USA. After completion of doctoral studies, she pursued her postdoctoral studies in North eastern University, USA (2013). She has been involved in research for the last 15 years. She is the editorial advisory board member for the journal ACS publications, molecular pharmaceutics for the tenure 2021-2023, and associate editor for the journal, frontiers in biomaterials Sciences in the specialty section of delivery systems and controlled release (since 2021). She has been featured among the world's top 2 % scientists in the single year 2019 in pharmacology and pharmacy/nanoscience & nanotechnology/ clinical medicine. She has to her credit more than 90 research publications, two US patents and three Indian Patents. She has authored 4 book chapters in "Dendrimers: Synthesis, Applications and Role in Nanotechnology", "Drug Delivery Strategies for Poorly Water-Soluble Drugs", "Handbook of Polymers for Pharmaceutical technologies, Volume 2: Processing and Applications" and "**RNA imaging"**. She has successfully completed many sponsored projects and currently handling projects sponsored by DST and ICMR. She has guided four Ph.D student and currently four students are pursuing their Ph.D. work under her guidance.